TECHNICAL REPORT STANDARD TITLE PAGE

1. Report No.	2. Government Accession No.	3. Recipient's Catalog No.
FHWA/TX-88+350-4F		

4. Title and Subtitle
BEHAVIOR OF ONTARIO-TYPE BRIDGE DECKS ON STEEL GIRDERS

5. Report Date
January 1988

6. Performing Organization Code

7. Author(s)
K. H. Kim, J. M. Dominguez, R. E. Klingner, and N. H. Burns

8. Performing Organization Report No.
Research Report 350-4F

9. Performing Organization Name and Address
Center for Transportation Research
The University of Texas at Austin
Austin, Texas 78712-1075

10. Work Unit No.

11. Contract or Grant No.
Research Study 3-5-83-350

12. Sponsoring Agency Name and Address
Texas State Department of Highways and Public Transportation; Transportation Planning Division
P. O. Box 5051
Austin, Texas 78763-5051

13. Type of Report and Period Covered
Final

14. Sponsoring Agency Code

15. Supplementary Notes
Study conducted in cooperation with the U. S. Department of Transportation, Federal Highway Administration. Research Study Title: "Behavior of Ontario-Type Bridge Decks, With and Without Skew"

16. Abstract

An experimental and analytical investigation was conducted regarding the behavior of reinforced concrete skew bridge decks with Ontario-type reinforcement. A series of parametric studies was also conducted to investigate the effect on bridge performance of some design variables which were not studied experimentally.

In the experimental part of the investigation, a full-scale model representing the essential behavior of a full skew bridge was built and tested in the Ferguson Structural Engineering Laboratory of The University of Texas at Austin. Using a finite element analysis program, the skew bridge test specimen was developed to behave like the full skew bridge. The test specimen had details similar to those required by the Ontario Highway Bridge Design Code, modified as recommended by the Texas SDHPT.

Three series of tests were conducted: two at the skew edges, and one at the center. At each test location, the skew bridge specimen was first loaded statically to approximately 60 kips (about 3 times the current AASHTO HS20 truck load, including impact factor). The specimen was then tested to failure at each test location, using monotonically increasing load.

17. Key Words	18. Distribution Statement
skew decks, reinforced concrete, Ontario-type reinforcement, full-scale model, finite element analysis, tests	No restrictions. This document is available to the public through the National Technical Information Service, Springfield, Virginia 22161.

19. Security Classif. (of this report)	20. Security Classif. (of this page)	21. No. of Pages	22. Price
Unclassified	Unclassified	174	

Form DOT F 1700.7 (8-69)

BEHAVIOR OF ONTARIO-TYPE BRIDGE DECKS ON STEEL GIRDERS

by

K. H. KIM, J.M. DOMINQUEZ, R. E. KLINGNER, AND N. H. BURNS

Research Report No. 350-4F

Research Project 3-5-83-350

"Behavior of Ontario-Type Bridge Decks,
With and Without Skew"

Conducted for

Texas

State Department of Highways and Public Transportation

In Cooperation with the
U.S. Department of Transportation
Federal Highway Administration

by

CENTER FOR TRANSPORTATION RESEARCH
BUREAU OF ENGINEERING RESEARCH
THE UNIVERSITY OF TEXAS AT AUSTIN

January 1988

The contents of this report reflect the views of the authors, who are responsible for the facts and accuracy of the data presented herein. The contents do not necessarily reflect the official views or policies of the Federal Highway Administration. This report does not constitute a standard, specification, or regulation.

There was no invention or discovery conceived or first actually reduced to practice in the course of or under this contract, including any art, method, process, machine, manufacture, design or composition of matter, or any new and useful improvement thereof, or any variety of plant which is or may be patentable under the patent laws of the United States of America or any foreign country.

PREFACE

Recent research in the U.S. and Canada has suggested that the flexural capacity of bridge decks is increased by in-plane compressive membrane forces, created when the cracked deck is restrained by supports that cannot move laterally. This phenomenon, commonly referred to as "arching action," is the basis for the semi-empirical design provisions of the current Ontario (Canada) Bridge Design Code. That code permits the use of less flexural steel than required by current AASHTO Specifications, resulting in bridge decks which are generally economical and resistant to corrosion.

The research described here is a continuation of Research Project 3-5-83-350, of which the overall objective was to study the performance of full-scale bridge decks designed taking arching action into account. Three reports have been published dealing with previous phases of this project: Report 350-1, Report 350-2, and Report 350-3. The specific objectives addressed in Report 350-4 were:

1) To verify, analytically and experimentally, the effects of skew on the performance of Ontario-type bridge decks.

2) To verify analytically the effects on bridge performance, of the following design variables:

   a) span-to-depth ratio of deck,
   b) longitudinal spacing of live loads,
   c) width of cantilever overhang, and
   d) presence of integral barriers.

3) Based on those analytical and experimental results, to verify the acceptability of Ontario-type bridge decks involving the above design variables.

4) To suggest modifications, if Ontario-type decks do not perform acceptably with respect to any of the above variables.

SUMMARY

An experimental and analytical investigation was conducted regarding the behavior of reinforced concrete skew bridge decks with Ontario-type reinforcement. A series of parametric studies was also conducted to investigate the effect on bridge performance, of some design variables which were not studied experimentally.

In the experimental part of the investigation, a full- scale model representing the essential behavior of a full skew bridge was built and tested in the Ferguson Structural Engineering Laboratory of The University of Texas at Austin. Using a finite element analysis program, the skew bridge test specimen was developed to behave like the full skew bridge. The test specimen had details similar to those required by the Ontario Highway Bridge Design Code, modified as recommended by the Texas SDHPT.

Three series of tests were conducted: two at the skew edges, and one at the center. At each test location, the skew bridge specimen was first loaded statically to approximately 60 kips (about 3 times the current AASHTO HS20 truck load, including impact factor). The specimen was then tested to failure at each test location, using monotonically increasing load.

The skew bridge deck performed satisfactorily under the current AASHTO design load levels as well as the overload conditions (about three times the current AASHTO design wheel load). The skew edges failed by shear; the center, by punching shear. The calculated flexural capacity considering arching action always far exceeded the actual failure load (shear or punching shear) at each test location.

To check the experimental results and permit their extension to bridge decks other than the one studied experimentally, a detailed finite element model of the specimen was developed using a general-purpose structural analysis program. A sequence of linear analyses was used to predict the nonlinear behavior of the deck. This approach was checked using a nonlinear analysis program, and found to be accurate and economical. Analytical predictions and experimental results agreed closely.

Using a rectangular bridge model, parametric studies were conducted to determine the effects on bridge deck performance, of design variables such as span-to-depth ratio of deck, width of cantilever overhang, presence of integral barriers, and longitudinal spacing of live loads. Membrane forces were not significantly affected by these variables except in the case of very closely spaced loads with total loaded length longer than half the length of the bridge.

IMPLEMENTATION

Skew bridge decks similar to the one tested in this study, and detailed in accordance with the Texas SDHPT recommendations for Ontario-type decks, can perform satisfactorily. Such decks should be constructed in the field, and their field performance should be monitored.

Flexural capacity of a reinforced bridge deck far exceeds its shear capacity, even at an edge with a large skew angle. Therefore, the factor of safety of a reinforced concrete bridge deck should be evaluated based on the shear capacity of the edge, considering the skew angle. The precise prediction of the shear capacity at the edge can be obtained by further research as recommended in this report.

TABLE OF CONTENTS

TABLE OF CONTENTS

TABLE OF CONTENTS

TABLE OF CONTENTS

LIST OF FIGURES

LIST OF FIGURES (continued)

LIST OF FIGURES (continued)

LIST OF FIGURES (continued)

LIST OF FIGURES (continued)

LIST OF FIGURES (continued)

LIST OF TABLES

CHAPTER 1

INTRODUCTION

1.1 General

A current trend in the design of reinforced concrete bridge decks is to consider the effect of in-plane membrane forces, which significantly increase the flexural capacity of the deck. This phenomenon, referred to as "arching action" in much of the literature, is the basis for the semi-empirical design provisions of the current Ontario (Canada) Bridge Design Code [26]. According to that code, arching action permits the use of less flexural steel than that required by current AASHTO specifications [1]. Reduced flexural reinforcement can lead to reduced construction as well as maintenance costs, because the reduced steel area has less tendency to cause popouts and spalling of the deck surface.

The research described here is a continuation of Texas State Department of Highways and Public Transportation (SDHPT) Project 350, which concerns the investigation of the performance of Ontario-type bridge decks. Three reports have been published dealing with previous phases of Project 350 [13, 14, 36]. Results of the previous research are reviewed in Chapter 2. Some of that review material is adapted from those three reports.

1.2 Objectives and Scope

Previous results of Project 350, discussed in Chapter 2, have demonstrated satisfactory performance of Ontario-type decks for non-skew bridge decks, continuous as well as simply supported. Ontario-type decks offer simpler and cheaper bridge deck designs. However, very little information is available concerning the behavior of Ontario-type bridge decks with skew.

The general objective of this research is to study the behavior of Ontario-type decks in a wider variety of applications. Specific objectives are:

1) To verify, analytically and experimentally, the effects of skew on bridge performance.

2) To verify analytically the effects on bridge performance, of the following design variables:

a) span-to-depth ratio of deck;

b) longitudinal spacing of live loads;

c) width of cantilever overhang; and

d) presence of integral barriers.

3) Based on those analytical and experimental results, to verify the acceptability of Ontario-type bridge decks involving the above design variables; and

4) To suggest modifications, if Ontario-type decks do not perform acceptably with respect to any of the above variables.

1.3 Empirical Provisions of Current Ontario Bridge Design Code

The current Ontario Highway Bridge Design Code [26] provides an empirical design method for bridge decks. This empirical method is based mainly on the presumption of significant compressive membrane action in the deck slab. Design of the deck slab involves prescribing 0.3 % reinforcement in each direction at the top and bottom of the deck. Slabs designed using these provisions are assumed adequate for crack control and shear resistance.

Conditions for the empirical method are as follows:

1) The transverse span length of the deck should not exceed 3.7 m (12.1 ft). Also, the cantilever portion of the deck should extend at least 1.0 m (3.3 ft) from the center of the exterior girder.

2) The span length to thickness ratio of the deck should not exceed 15. For skew slabs, the skew span length shall be used in calculating the ratio.

3) For skew angles greater than 20 degrees, the end portion of the deck slab shall be provided with at least 0.6 % isotropic reinforcement.

4) The slab thickness shall not be less than 225 mm (9 in.), and spacing of the reinforcement in each face shall not exceed 300 mm (12 in.).

5) Diaphragms shall extend throughout the transverse cross section of the bridge between external girders, and the

maximum spacing of such diaphragms shall be 8 m (26 ft) for steel-beams and box girders. Diaphragms shall be provided at supports for concrete girders.

6) Edge stiffening shall be provided in accordance with the Code provisions.

Design of bridge decks with skew angles less than or equal to 20 degrees is identical to that of non-skew bridge decks, except that the skew span length should be used in calculations. As shown in Fig. 1.1, for skew angles greater than 20 degrees, the end portions of the deck slab shall be provided with 0.6 % isotropic reinforcement.

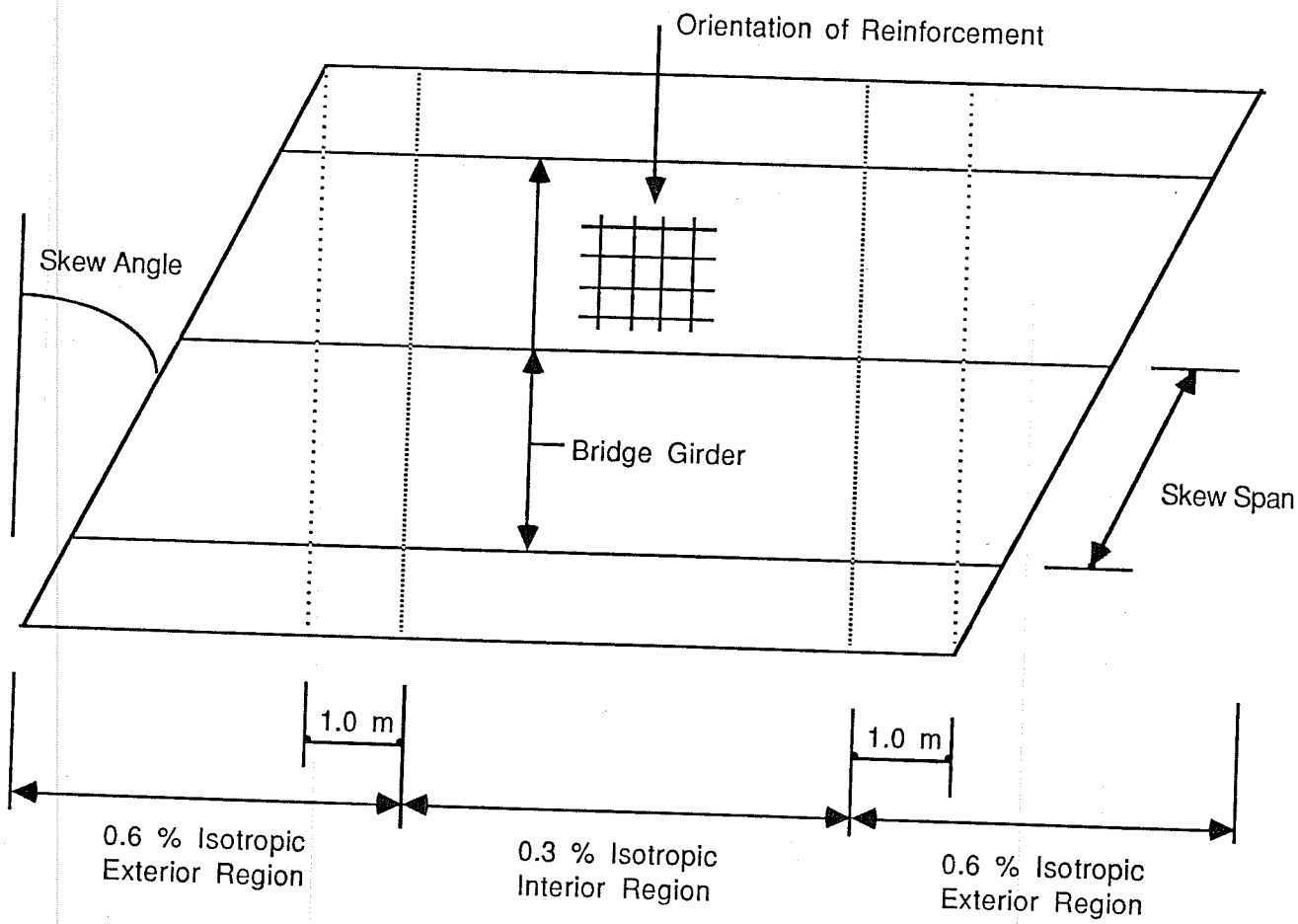

Fig. 1.1 Reinforcement of Ontario-type skew bridge deck

CHAPTER 2

BACKGROUND

2.1 General

The theoretical background of the "arching action" concept, and also a historical review of related research, are presented in this chapter. Results of the previous research of Project 350 are also discussed. Much of the material reviewed in this chapter is adapted from a previous report of Project 350 [14].

2.2 Theoretical Background

A simply supported beam subjected to vertical loads is normally analyzed as a line member deforming in flexure and shear (Fig. 2.1). No axial restraint force is developed in such a beam if there is no horizontal restraint at the supports.

Even with restraining supports (Fig. 2.2(a)), no axial restraint force is developed in the beam as long as small- deflection theory is applied and the depth of the member is neglected. However, if the bottom fiber of the beam is restrained against elongation by horizontal supports and the depth of the member is considered, compressive axial force will be present along with flexure and shear, as shown in Fig. 2.2(b). This axial compression is commonly referred as "arching action" in most of the literature on this subject.

After flexural cracking, arching action can also be developed in a reinforced concrete beam with fixed supports at both ends. The neutral axis of the cracked beam is shifted toward the bottom fiber at the supports, and toward the top fiber at midspan. Under vertical loads, each uncracked portion of the beam rotates about the point where its neutral axis intersects the support (Fig. 2.3). Because of the eccentric location of the neutral axis, compressive membrane forces are developed even with small deflections of the beam.

As shown in Fig. 2.4, bridge decks, which span transversely and are supported by longitudinal girders, are analogous to the cracked beam discussed above. Flexural cracking causes the neutral planes of the deck to shift, producing transverse and longitudinal compressive membrane forces in the cracked deck.

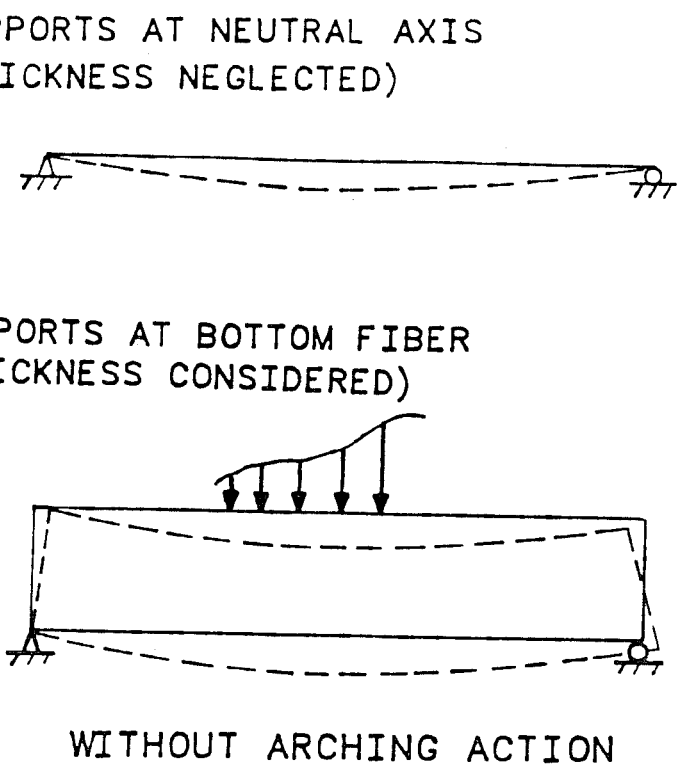

Fig. 2.1 Simply supported beam, no horizontal restraint at supports

A) SUPPORTS AT NEUTRAL AXIS
(THICKNESS NEGLECTED)

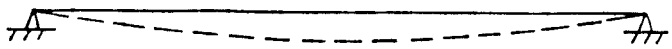

B) SUPPORTS AT BOTTOM FIBER
(THICKNESS CONSIDERED)

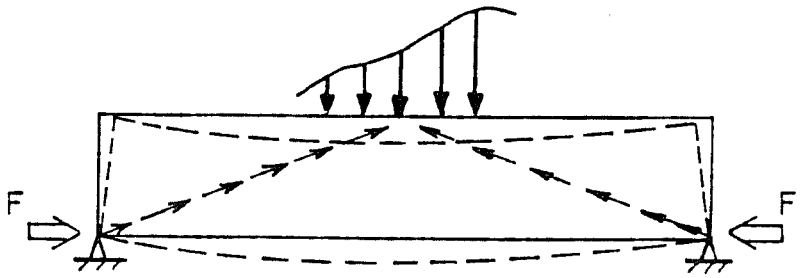

WITH ARCHING ACTION

Fig. 2.2 Simply supported beam with horizontal restraint at supports

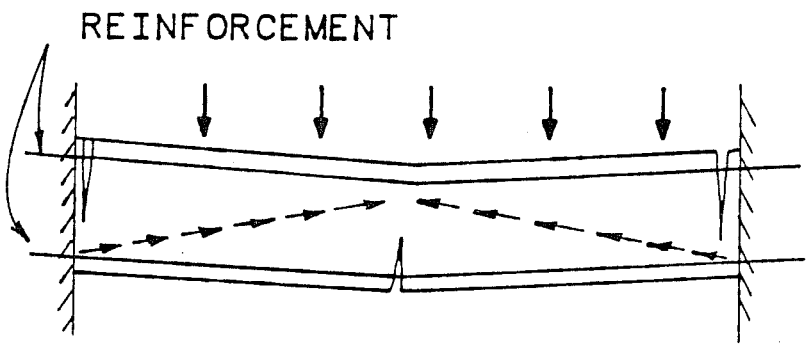

Fig. 2.3 Arching action in cracked beam

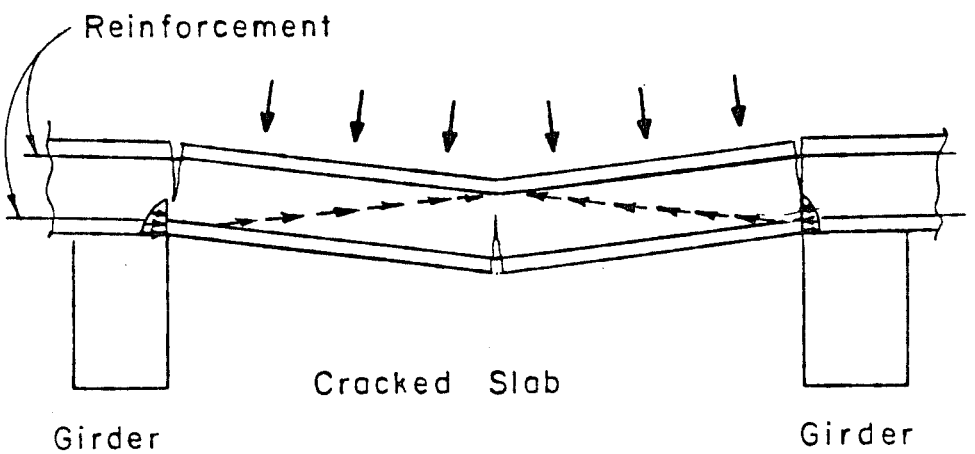

Fig. 2.4 Arching action in cracked slab

2.3 Historical Review

The effect of in-plane membrane forces on the load- carrying capacity of reinforced concrete slabs has been investigated for several decades. In 1957, Liesenberg, Robertson, and McGraw [24] tested 50 slab panels in an old building prior to its demolition. Test results showed the existence of compressive membrane action, and its beneficial effects on the load-carrying capacity of the slabs. After a study of the behavior of continuous prestressed concrete slabs, Guyon suggested that arching action should be taken into account in designing such slabs subjected to concentrated loads [17]. Other experimental verifications were also performed by Christiansen [9], Fredericksen [10], and Park [27, 28, 29, 30, 31]. In the late 1950's, single panels were tested by Sozen and Gamble [15, 16] at the University of Illinois. The panels, bounded by horizontal restraining members, were found to have flexural capacities considerably in excess of the load-carrying capacity predicted by yield-line theory.

Since 1969, many field tests have been conducted by the Structural Research Section of the Ontario Ministry of Transportation and Communications [26]. It was found that the reinforced concrete deck slabs carried loads much greater than the loads predicted by traditional analysis methods, even if the deck had considerably deteriorated, or if a large percentage of the reinforcing steel had been lost due to corrosion. Using 1/8- scale models [6, 18, 19], a series of studies was conducted at Queen's University, under the sponsorship of the Ontario Ministry of Transportation and Communications. Results showed that large reserves of strength existed in deck slabs under static and fatigue loadings. Actual bridge tests proved that arching action contributed significantly to the flexural capacity of bridge decks [4, 11, 12].

Based on these studies, an empirical design method was proposed, involving the use of an isotropic reinforcement layout in the deck [26]. The required reinforcement is considerably less than that required by the current AASHTO design code [1].

In the United States, the New York Highway Department recently conducted a study of the strength of highway bridge decks [7] using reduced-scale models. Under design load, the stress in reinforcement was found not to exceed 12 ksi. The deck slabs bounded by girders carried at least six times the design wheel load, and always failed by punching shear.

2.4 Previous Research of Project 350

2.4.1 Tests. In the first phase of this project, a 20- by 50-ft full-scale composite bridge was built and tested in the Ferguson Structural Engineering Laboratory of The University of Texas at Austin (Figs. 2.5 and 2.6). Half of the bridge deck was made of cast-in-place concrete, and the other half, of precast prestressed concrete panels with cast-in-place concrete topping. The bridge was loaded at four locations (Fig. 2.7). Test loadings were developed based on standard AASHTO truck loadings. An HS20 truck produces a design service wheel load of 16 kips. When multiplied by the maximum AASHTO impact factor of 1.30, this results in a maximum service wheel load of 20.8 kips. Double tandem wheels used frequently in practical cases are not considered in this study, since they occupy more loaded area than a single wheel with the same total load, resulting in less bending moments and shear forces in the deck.

The bridge was first loaded statically up to 60 kips per ram (about three times the current AASHTO design wheel load) to study its response to loads at service and overload levels. It was then subjected to sinusoidal fatigue loading to a maximum of 26 kips per ram. After 5 million cycles of fatigue loading, the bridge was statically loaded to a maximum of 40 kips per ram to study its behavior after fatigue cracking. After these tests, concentrated load tests to failure were conducted both for the cast-in-place deck, and for the deck constructed with precast prestressed panels and cast-in-place concrete topping.

2.4.2 Analysis. Finite element models of the test specimen were developed using an existing structural analysis program (SAP4), to check the experimental results and permit their extension to bridge decks other than the one studied experimentally [14].

The bridge deck was modeled using two layers of 16-node thick shell elements (Fig. 2.8). As shown schematically in Fig. 2.9, composite action of the deck slab and the girder was modeled using a combination of thick shell elements and three-dimensional beam elements. The bridge steel girder was discretized using a series of three-dimensional beam elements with the same properties as the girder, and located at the girder midheight. The beam elements were then connected using rigid links to the thick shell elements at the corresponding nodal points, satisfying typical assumptions for plane sections.

Since one of the primary objectives of the research was to study the effect of the compressive membrane action developed in the deck after cracking, a good representation of deck cracking was

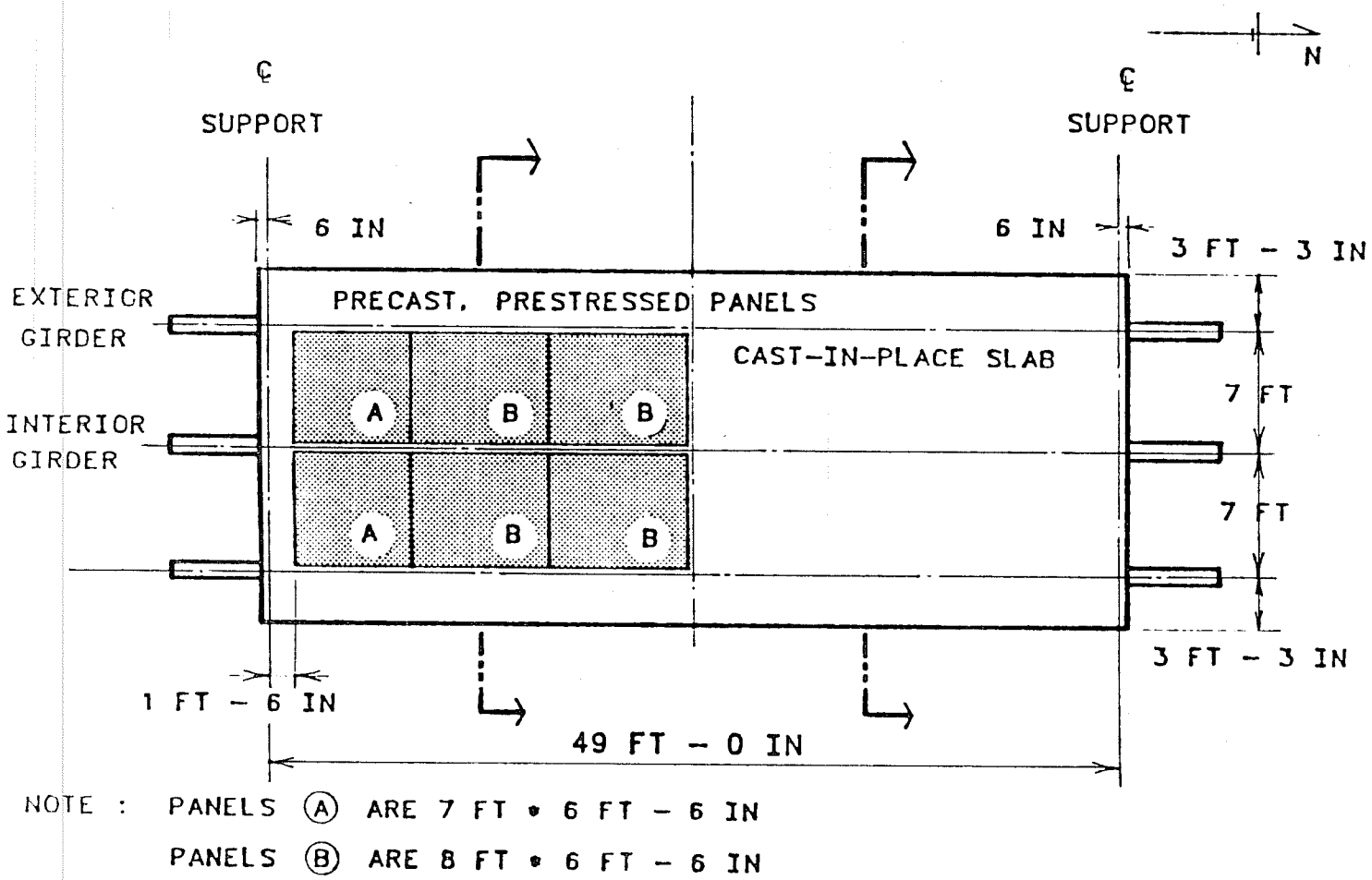

Fig. 2.5 Plan view of previous test specimen

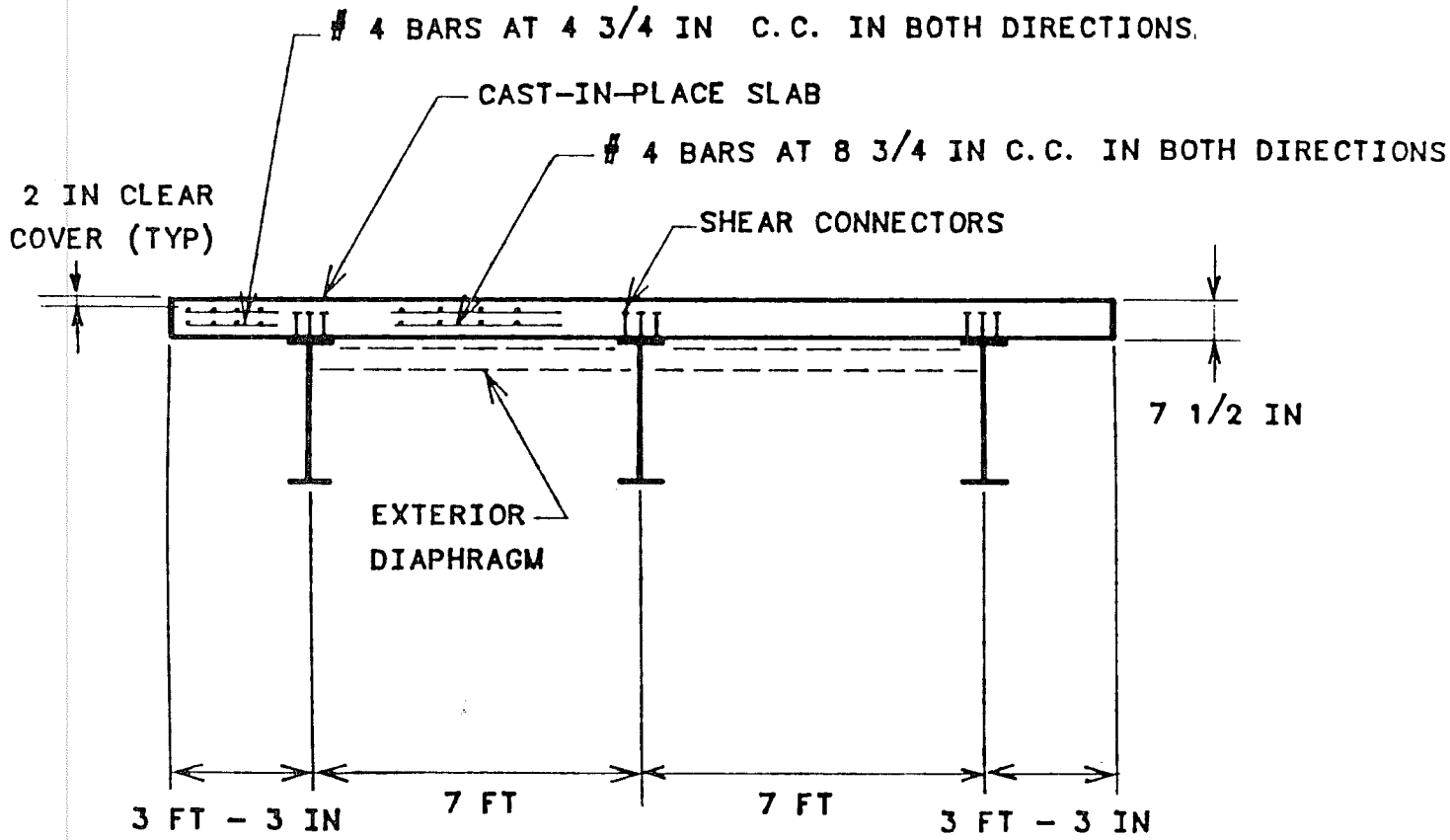

Fig. 2.6 Cross section of previous test specimen showing cast-in-place deck

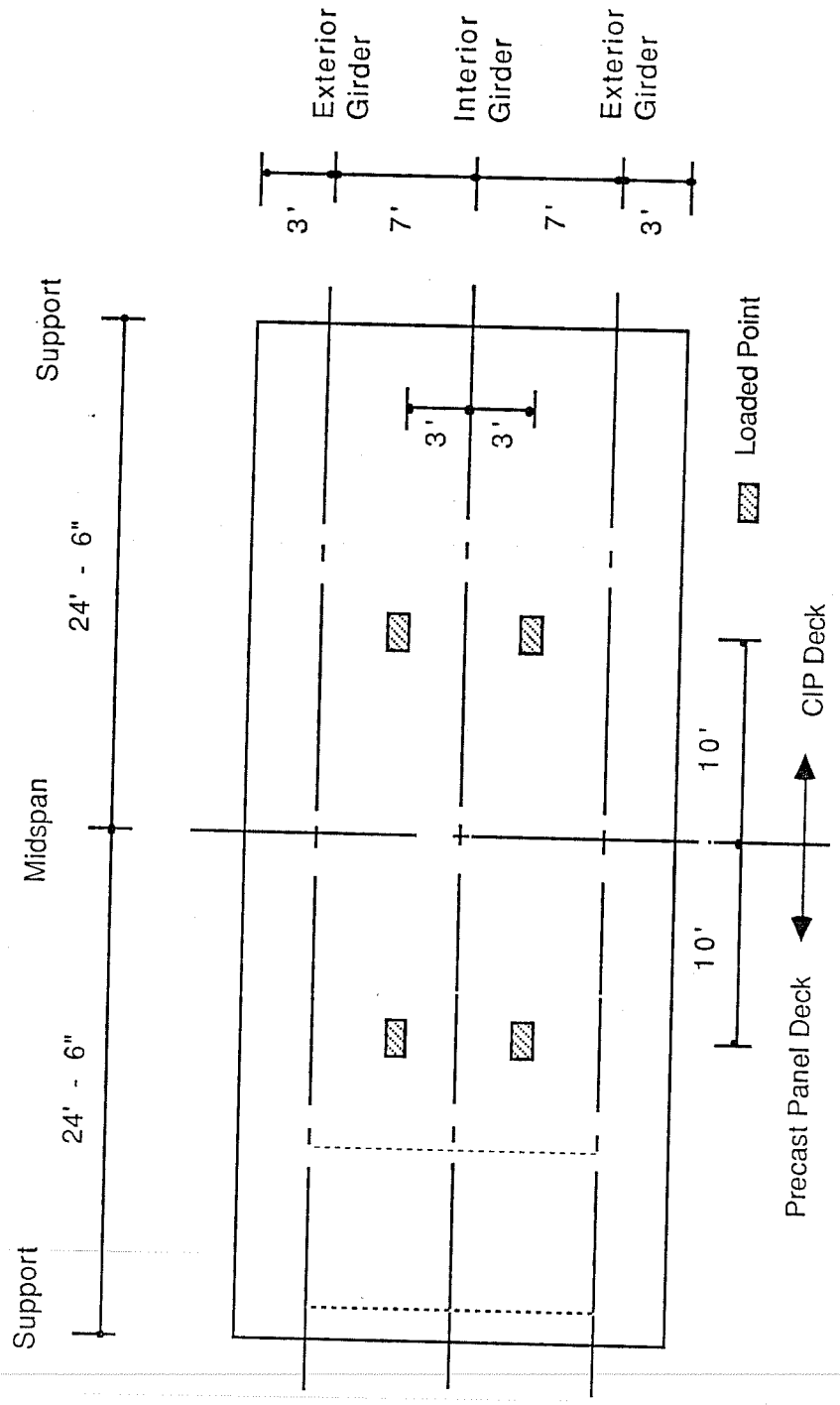

Fig. 2.7 Placement of load on previous test specimen

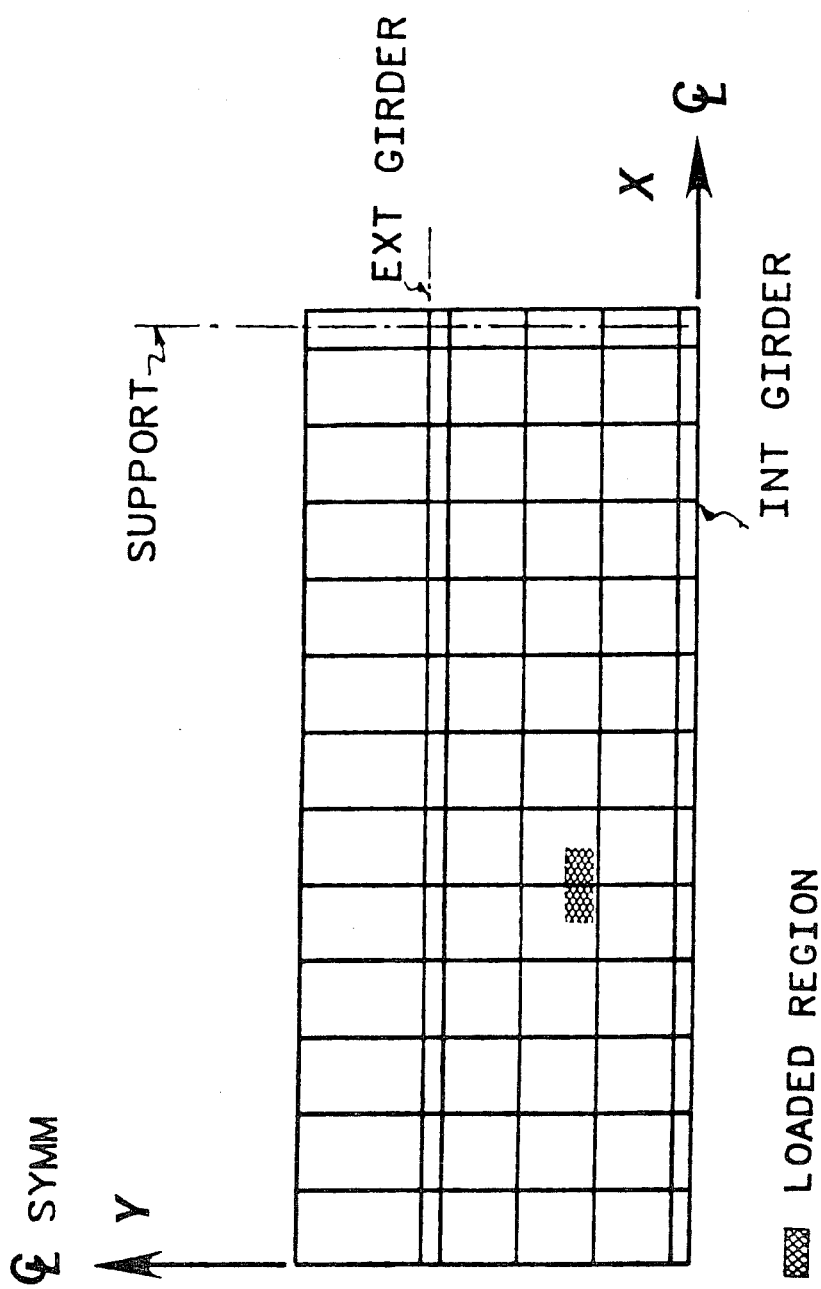

Fig. 2.8 Finite element mesh of quarter bridge model

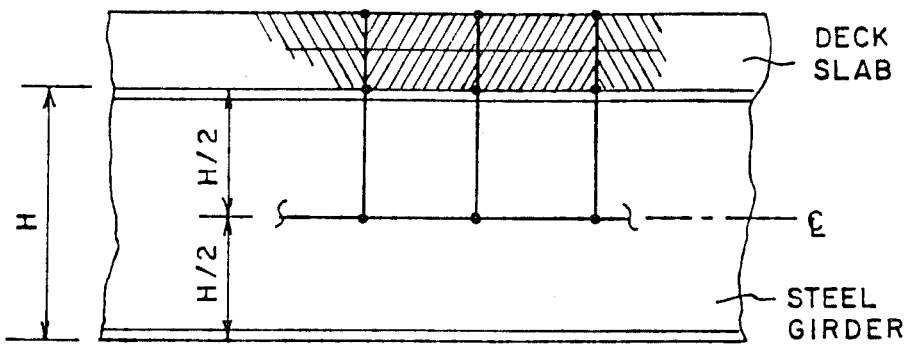

ACTUAL COMPOSITE GIRDER

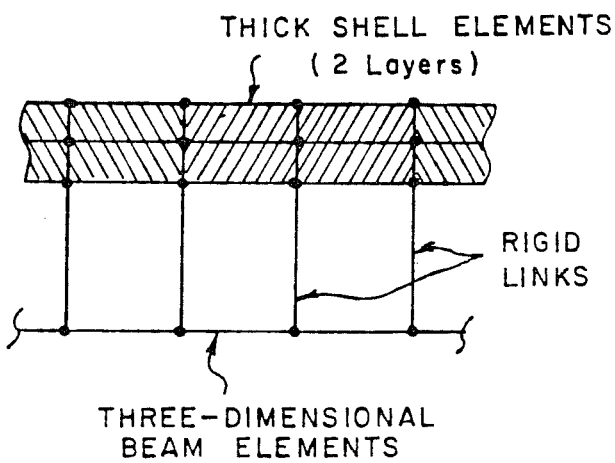

FINITE ELEMENT MODEL

Fig. 2.9 Schematic representation of finite element model of composite girder

necessary. Modeling of cracking using the finite element method has been studied by many researchers [3]. Each proposed model has three distinguishing features: 1) crack initiation criteria; 2) crack representation; and 3) representation of crack propagation.

A strength criterion is generally used for determining crack initiation. Cracking of concrete can be predicted by various measures of its tensile strength, such as split cylinder tests, modulus of rupture tests, and biaxial stress tests. Analytical solutions of the bridge model showed that the deck was essentially in a state of plane stress. Therefore, Kupfer's biaxial failure envelope [23] was used to detect cracking in the deck. At each load level, the maximum principal stress at the center of each element is computed and compared with the biaxial cracking criterion proposed by Kupfer as shown in Fig. 2.10. Once the maximum principal tensile stress in any element exceeds the failure value, the entire element is treated as cracked perpendicular to the direction of that stress.

For crack representation, two methods are generally used: discrete crack models and smeared crack models. In the discrete crack model, cracks are modeled by separating nodal points as shown in Fig. 2.11. Some difficulties are encountered with this approach in the analysis of bridge deck. First, the location and orientation of the cracks are not known in advance. Although this model can be improved to some extent by refining the element nodes, it is still complex and time-consuming to refine the structural topology following the formation of a crack. Therefore, smeared crack models were employed to predict the deck behavior after cracking (Fig. 2.12). The smeared crack model was first introduced by Rashid [32], and modified by many investigators [5, 8, 25, 33, 37, 38]. In this model, the modulus of elasticity in the direction parallel to the principal tensile stress is reduced to the effective tensile stiffness of reinforcement crossing the smeared crack plane. The shear modulus was reduced by a factor of 0.5 in the cracking direction, representing the shear stiffness along the cracked plane due to aggregate interlock and dowel action [14].

Nonlinear behavior due to cracking was modeled using a sequence of linear elastic analyses. A schematic representation of this sequential approach is presented in Fig. 2.13. The bridge model was first subjected to a given load and deflected linearly along Path 1 (Fig. 2.13). The maximum principal stress in each element was compared with the biaxial tensile strength. Elements having maximum ratios of calculated stress to strength greater than unity were regarded as cracked. The first cracking load P1 was then calculated by scaling the load to give a maximum ratio of unity (one cracked element) or slightly greater than unity (possibly more than one

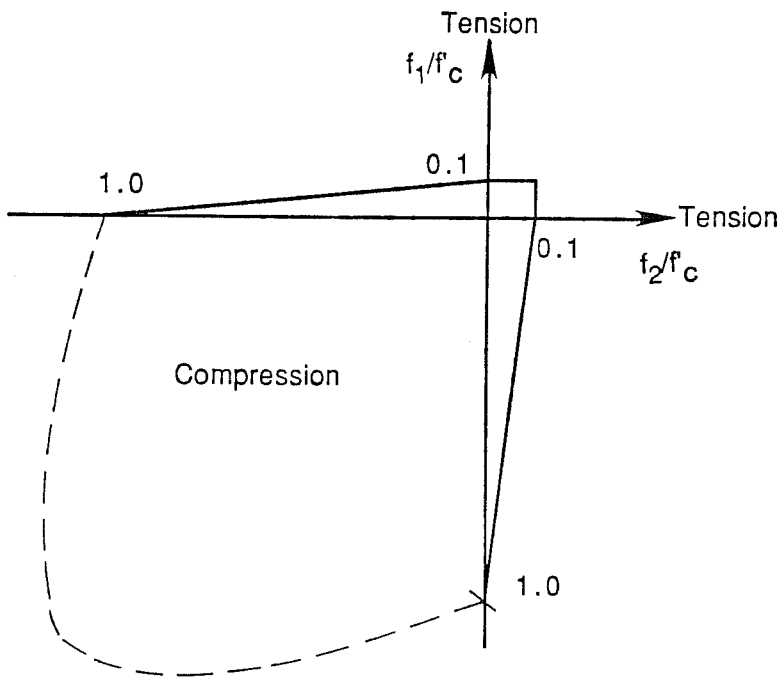

Fig. 2.10 Kupfer's biaxial stress criterion

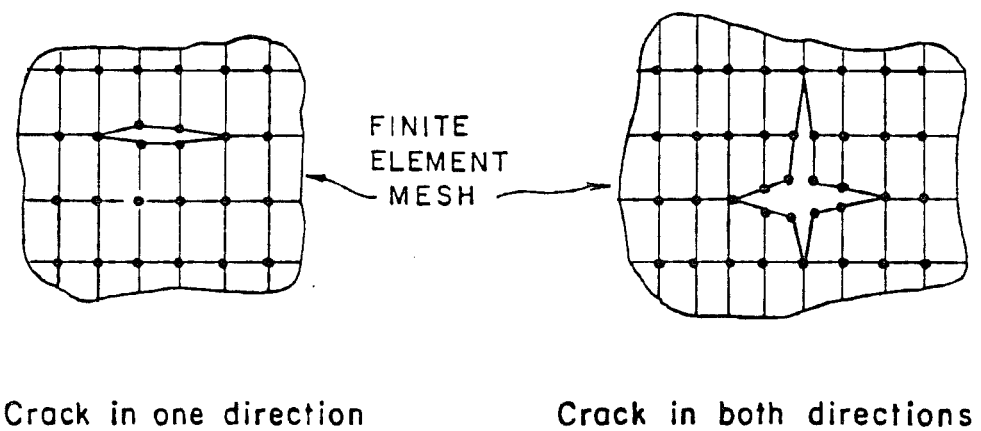

Fig. 2.11 Schematic representation of discrete crack model

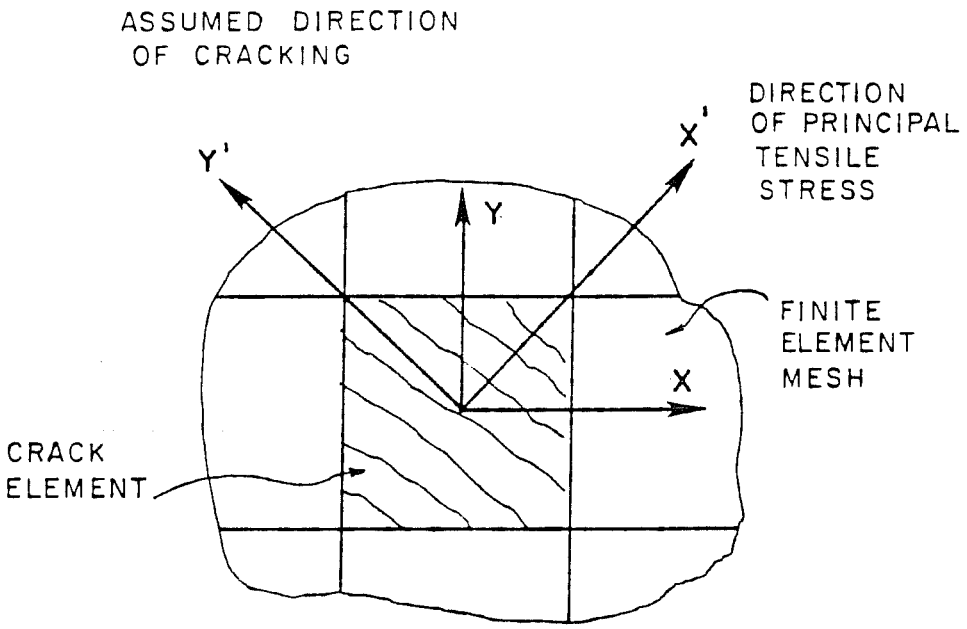

Fig. 2.12 Schematic representation of smeared crack model

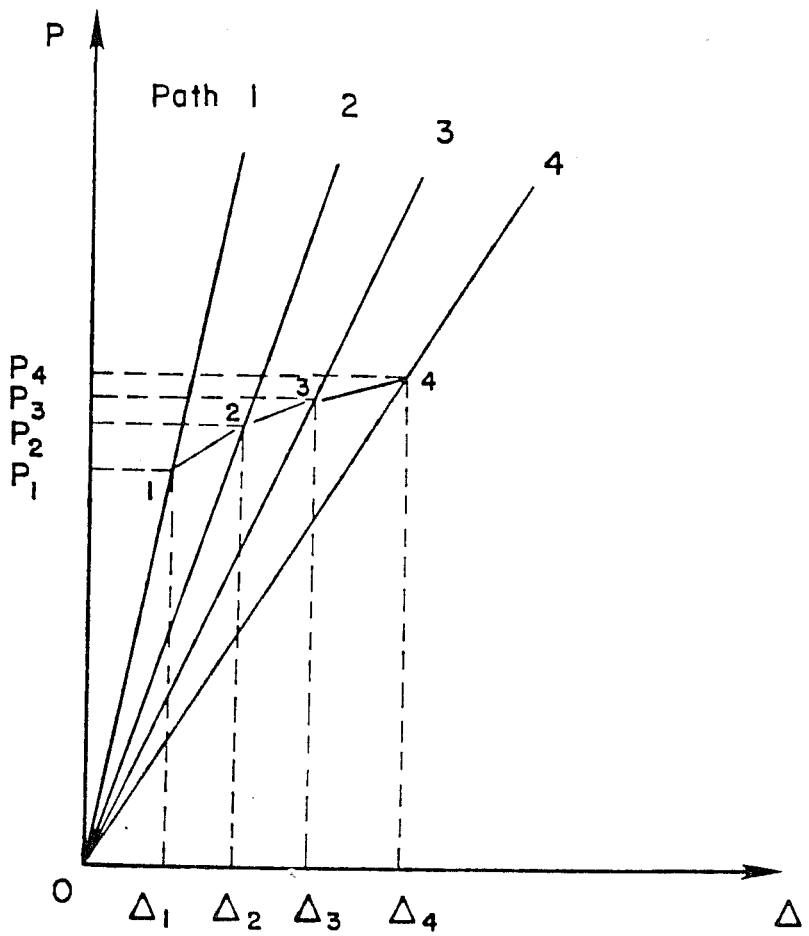

Fig. 2.13 Schematic representation of sequential linear approach

cracked element). The crack orientation within each cracked element was computed, and the element stiffnesses were reformed using a smeared cracking model. The analytical model was then unloaded to the origin. Upon re-loading, since the model stiffness was reduced due to cracking, it would deflect linearly along Path 2 of Fig. 2.13. The ratio of maximum principal stress to maximum tensile strength was again calculated and was used to predict the next cracking load P2 and its corresponding deflection. After unloading back to the origin, this procedure was repeated to obtain Paths 3, 4 and so forth (Fig. 2.13). Points 1, 2, 3 and 4 then represent a series of accurate load-deflection combinations with loading and unloading as described above. If the specimen were loaded monotonically, the load-deflection curve would go from the origin through points 1, 2, 3 and so forth, assuming path-independent behavior. This path represents a close approximation to the actual nonlinear behavior. It is much faster and cheaper in terms of computer time, but less so in terms of human effort. The latter, however, can be reduced by selecting the cracking loads to allow simultaneous cracking of elements with similar stress magnitudes.

The modeling concept and analytical approach described above were verified by analyses and tests [14], and are further verified as described in Chapter 3 of this report.

2.4.3 Results of Previous Research of Project 350. The bridge deck designed in accordance with the Ontario Bridge Design provisions performed satisfactorily before and after cracking, under current AASHTO design load levels as well as overload conditions (about three times the current AASHTO design load). After 5 million cycles of fatigue loading, some crack extensions were found at the bottom of the deck, but no crack propagation was found at the top. Load-deflection relationships before and after fatigue loading were almost identical, implying that cracking of the deck did not significantly change the stiffness of the deck even after fatigue loading.

Significant arching action developed in the deck after cracking, and increased the flexural capacity of the deck slab. The deck slab failed by punching shear, not by flexure.

Analytical predictions and experimental results agreed well, showing that the analytical models of the specimen were satisfactory and could be extended to other bridge configurations.

CHAPTER 3

FURTHER VERIFICATION OF ANALYTICAL PROCEDURES

3.1 General

As discussed in Section 2.4, finite element models of the test specimen were developed in previous phases of Project 350, and were used to check the experimental results and permit their extension to bridge decks other than the one studied experimentally. Performance of the analytical models was verified by comparing the analytical results to solutions based on beam theory [14]. This chapter is intended to describe further verification of the analytical models, particularly with regard to verification of the sequential linear analysis approach. This verification was conducted by comparing the results of a sequential linear analysis, with those from an existing nonlinear analysis program.

Nonlinear analyses were conducted using ABAQUS, a general-purpose nonlinear analysis package available to the University of Texas at Austin through a special academic license [20, 21, 22]. Using ABAQUS as well as SAP4, a portion of the rectangular bridge deck which had been studied in previous phases of Project 350 was modeled and analyzed (Fig. 3.1). To simplify the modeling, the bridge's steel girders were not included in the analysis, and the continuous deck was assumed to be simply supported at the girders. These simplifications were justified by the fact that the purpose of this verification was to compare results for a model embodying only the essential features of bridge specimens studied in this project. Verification did not require modeling of a complete bridge.

3.2 Analysis Using SAP4

The finite element mesh used in the SAP4 analysis is shown in Fig. 3.2. The bridge deck was modeled using two layers of 16-node thick shell elements. Modeling and analysis techniques are identical to those reviewed in Section 2.4, and will not be presented here.

3.3 Analysis Using ABAQUS

The finite element mesh used in the ABAQUS analysis was identical to that used in the SAP4 analysis (Fig. 3.2), and involved

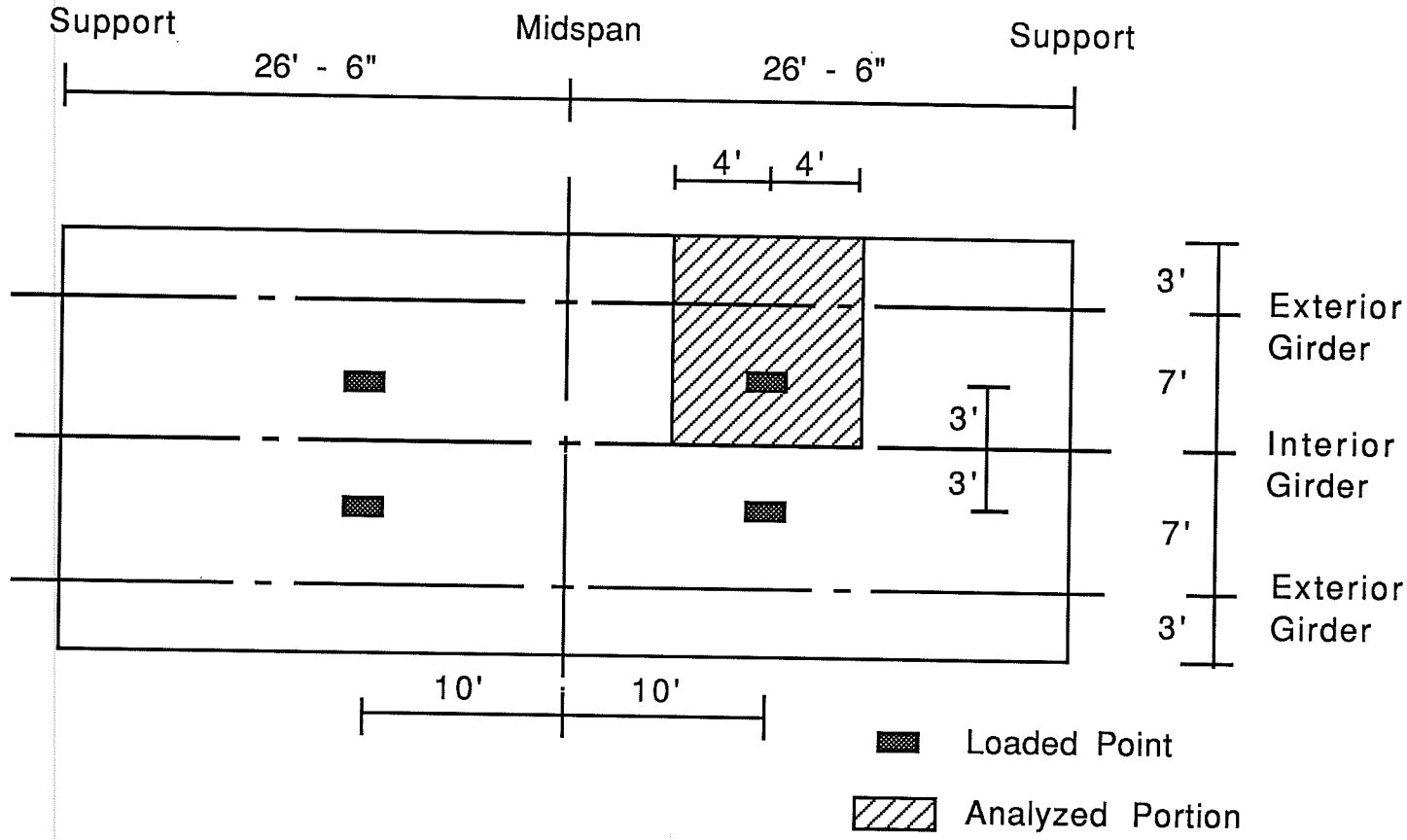

Fig. 3.1 Portion of full bridge used in verification of analytical model

8-node rectangular shell elements (SR8). To model adequately the development of plasticity and cracking, 5 integration points were used through the thickness of the deck. The modified Riks method [20, 21, 22] was chosen to maintain solution stability after concrete cracking.

3.4 Comparison of Results from SAP4 and ABAQUS Analyses

3.4.1 Load-Deflection Relationships. The relationships between applied load and vertical deflection at the loaded point as computed by the SAP4 and ABAQUS analyses are shown in Fig. 3.3. The results generally agree. The load- deflection relationships differ somewhat after first cracking. This is possibly due to the following:

1) The effects of tension stiffening were included in the ABAQUS analysis, but not in the SAP4 analysis. Tension stiffening is an indirect way to model the interaction of concrete and reinforcement after cracking. Using ABAQUS, concrete strength after cracking is assumed to decrease linearly to zero at a strain ϵo (Fig. 3.4). Tension stiffening is a mandatory option. The strain ϵo may be set to the default value of 0.0002 (used in this analysis), or to any user-specified value. With a very small value of ϵo (simulating no tension stiffening), the response of the ABAQUS model was very unstable after cracking, and the load-deflection behavior could not be followed.

   In the SAP4 analyses, however, a cracked element was assumed to lose all tensile stiffness perpendicular to the crack direction, except for the stiffness of the deck reinforcement.

2) In the ABAQUS analysis, stiffness of cracked elements are evaluated at integration points, permitting an element to be considered as partially cracked. In the SAP4 analysis, however, the entire element is assumed to be cracked, if the stress at the center of the element exceeds the tensile strength of concrete.

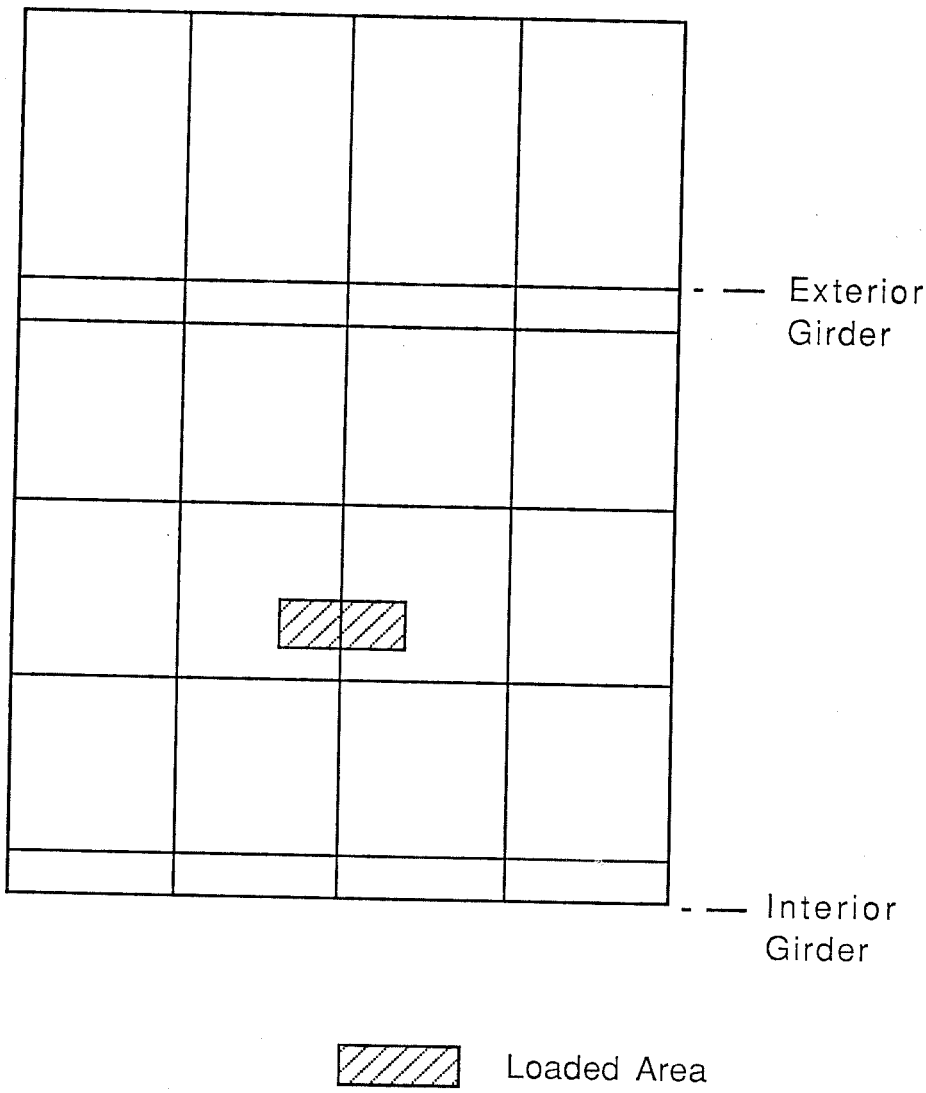

Fig. 3.2 Finite elment mesh of bridge deck used in verification of analytical model

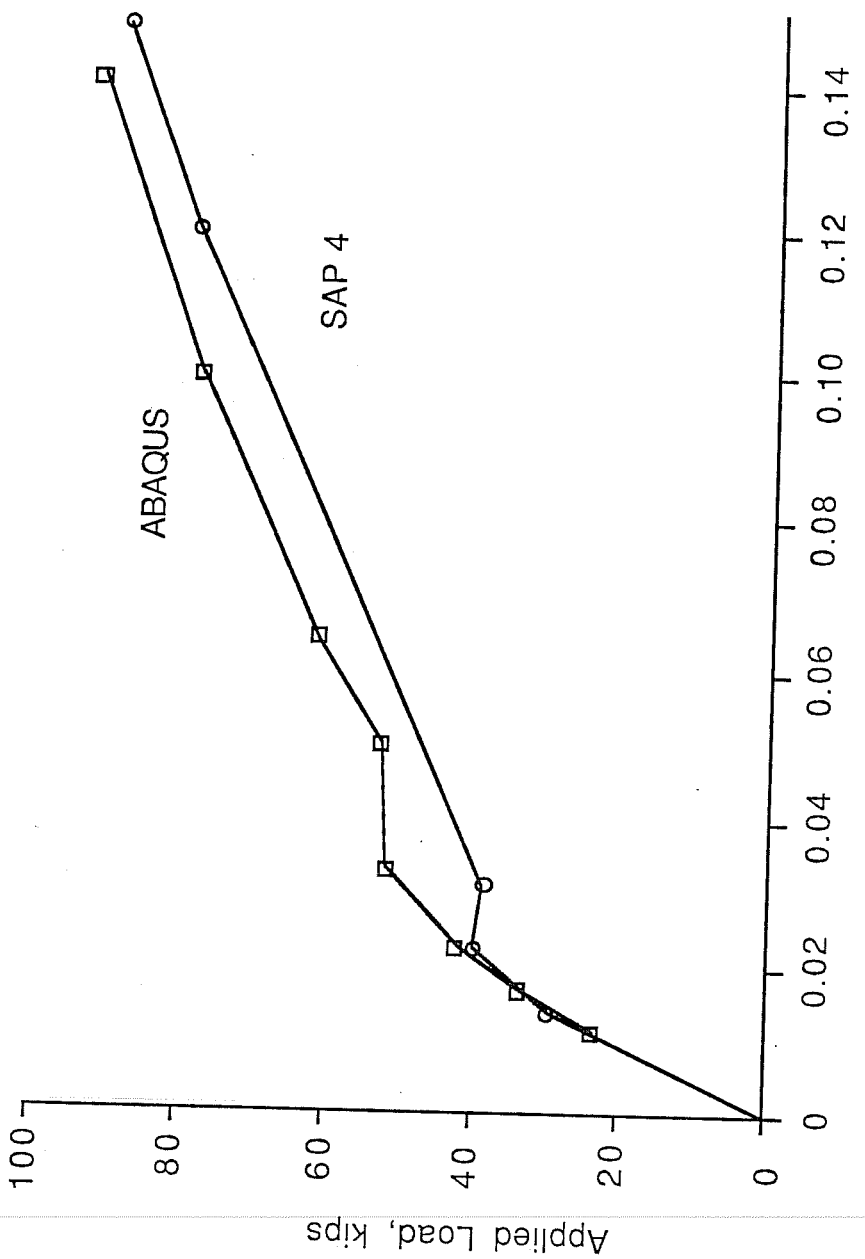

Fig. 3.3 Load-deflection relationships at loading point (SAP 4 vs. ABAQUS)

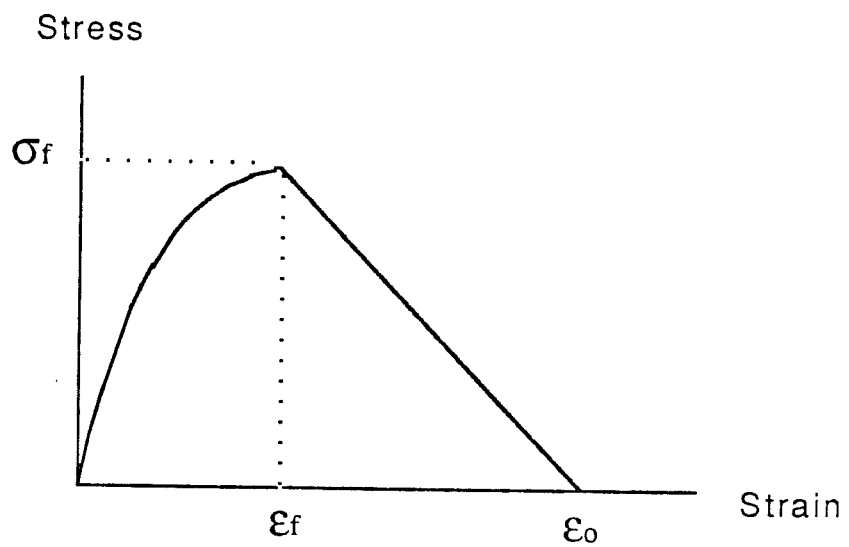

ε_f = Tensile Strain at Failure

ε_o = Tensile Strain at Zero Tensile Strength

Fig. 3.4 Modeling of tension stiffening effect used in ABAQUS

As a result, cracked elements appear to lose stiffness more rapidly in the SAP4 analysis, than in the ABAQUS analysis.

3.4.2 Transverse Moment and Membrane Force. Transverse moments and transverse membrane forces are compared in Figs. 3.5 and 3.6 respectively. Analytical results agreed quite well in both cases.

3.4.3 Computation Time and Cost. Total solution times required in the SAP4 and ABAQUS analyses are compared in Table 3.1. The estimated total solution time of 14,350 seconds to analyze the full bridge model by ABAQUS was arrived at by assuming the same relative time as for other SAP4 analyses. The nonlinear analysis required much more computation time than the sequential linear analysis (about 3.8 times for this studied case).

Using the CDC Dual Cyber 175/750 system of The University of Texas at Austin, estimated costs for the SAP4 and ABAQUS analyses are presented in Table 3.2.

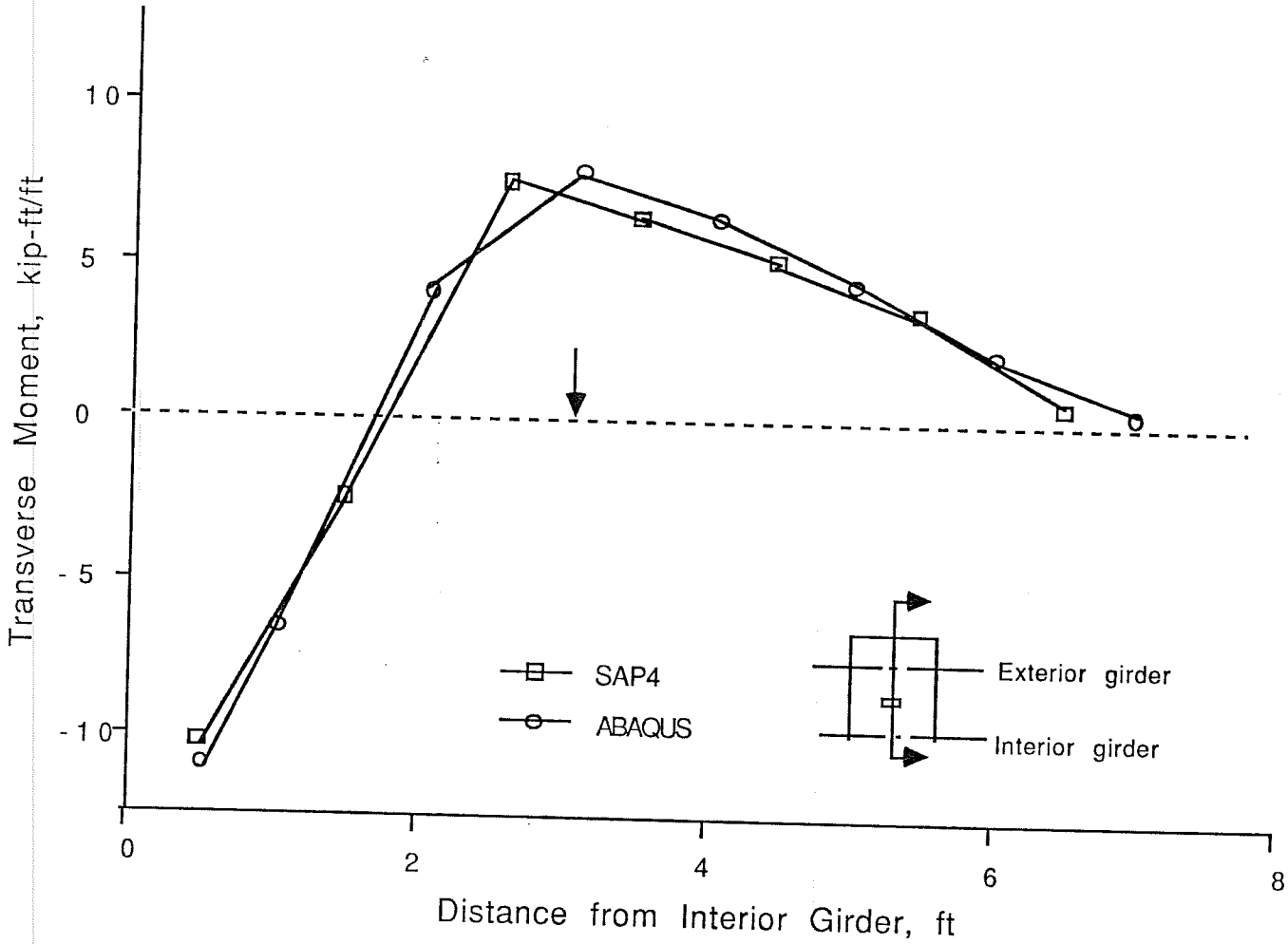

Fig. 3.5 Calculated transverse moment along line through loading point, P = 60 kips (SAP 4 vs. ABAQUS)

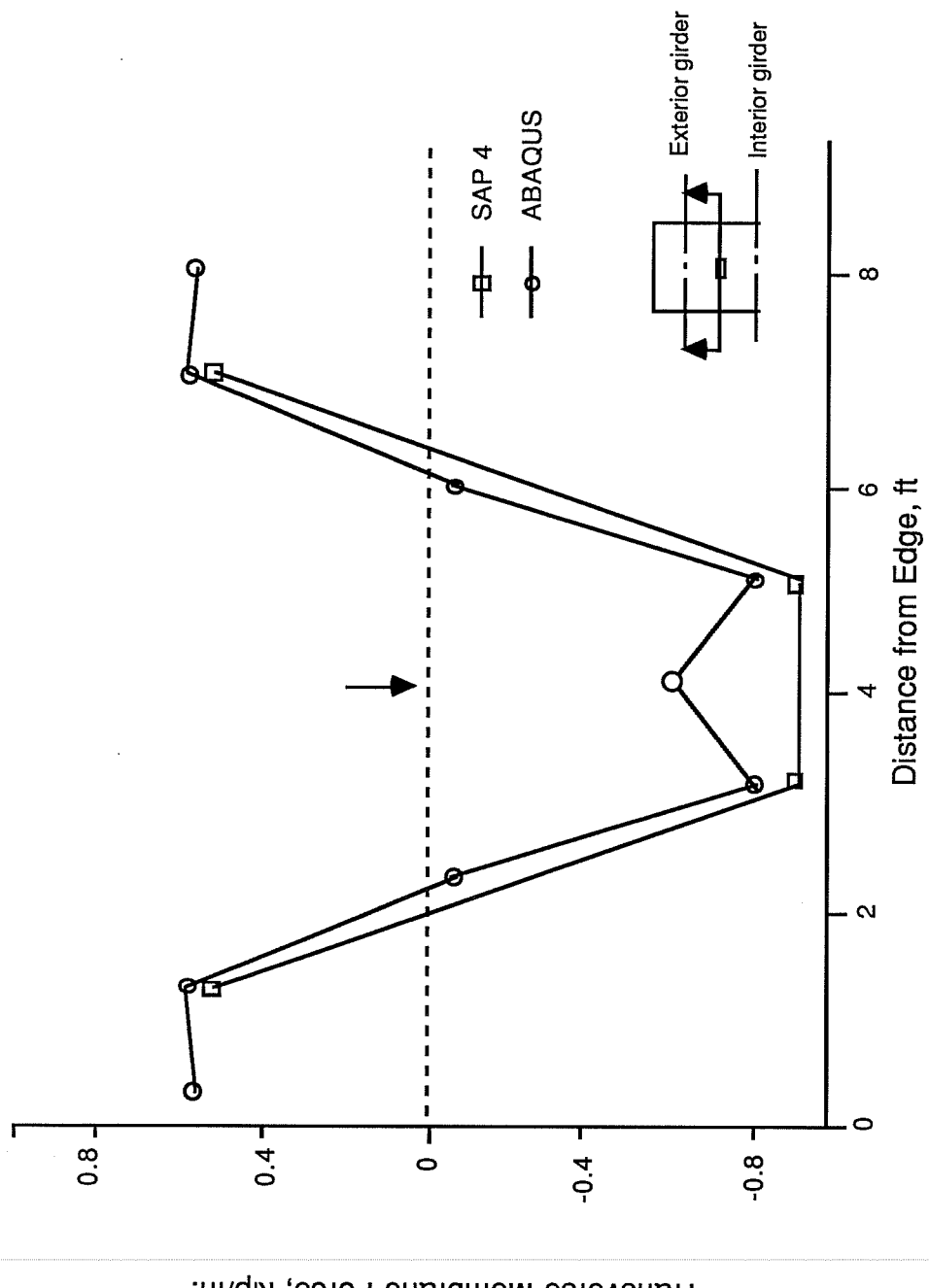

Fig. 3.6 Calculated transverse membrane force at interior girder, P = 60 kips (SAP 4 vs. ABAQUS)

Table 3.1 Computation Times for SAP4 and ABAQUS Analyses

Analyses by	Time for analysis of studied model (seconds)	Time for analysis of full bridge (seconds)
SAP4	650	4750
ABAQUS	2870	14,350 (estimated)

Table 3.2 Computation Costs for SAP4 and ABAQUS Analyses

Analyses by	Cost for analysis of studied model	Cost for analysis of full bridge
SAP4	$ 41.53	$ 303.47
ABAQUS	$ 183.36	$ 916.80 (estimated)

CHAPTER 4

DEVELOPMENT OF SKEW BRIDGE SPECIMEN

4.1 General

In this chapter, the methods used to develop the skew bridge test specimen are presented. In previous phases of Project 350, it was found that when a concentrated load is applied to a cracked bridge deck, significant transverse and longitudinal membrane forces exist only within about 10 ft of the loaded point (Fig. 4.1). The length within which full membrane action is developed is therefore about 20 ft, or approximately half a typical bridge girder span. Assuming transverse symmetry about the bridge's longitudinal centerline, it was decided to use a test specimen representing one-quarter of a full-scale skew bridge. Because the test specimen had to replicate the behavior of a complete bridge, it was necessary to adjust its configuration and support conditions carefully. This process is now described. It was made possible owing to the degree of confidence which had been developed in the finite element analytical procedures SAP4 described previously.

Using the analytical techniques described in Section 2.3.3, a series of trial specimens were developed, modeled analytically, and analyzed. These trial specimens were modified to arrive at a skew bridge specimen that would behave like the full skew bridge.

4.2 Comparison of Full Rectangular and Quarter Rectangular Bridges

The first step in developing a skew quarter bridge model was to find whether a rectangular quarter bridge could be modeled to behave like a full rectangular bridge. The full rectangular bridge (Fig. 4.2) was first studied using the same analytical model developed in the previous phases of Project 350 [14].

As the first trial, one quarter of the full bridge was modeled as shown in Fig. 4.3. The interior girder was modeled as a beam fixed along its lower edge. As shown in Fig. 4.4, the trial quarter bridge specimen had larger negative transverse moments and smaller positive transverse moments than the full bridge. The larger negative moments were caused by the vertical restraint of the interior girder. The full bridge has three identical steel girders. Under the loading

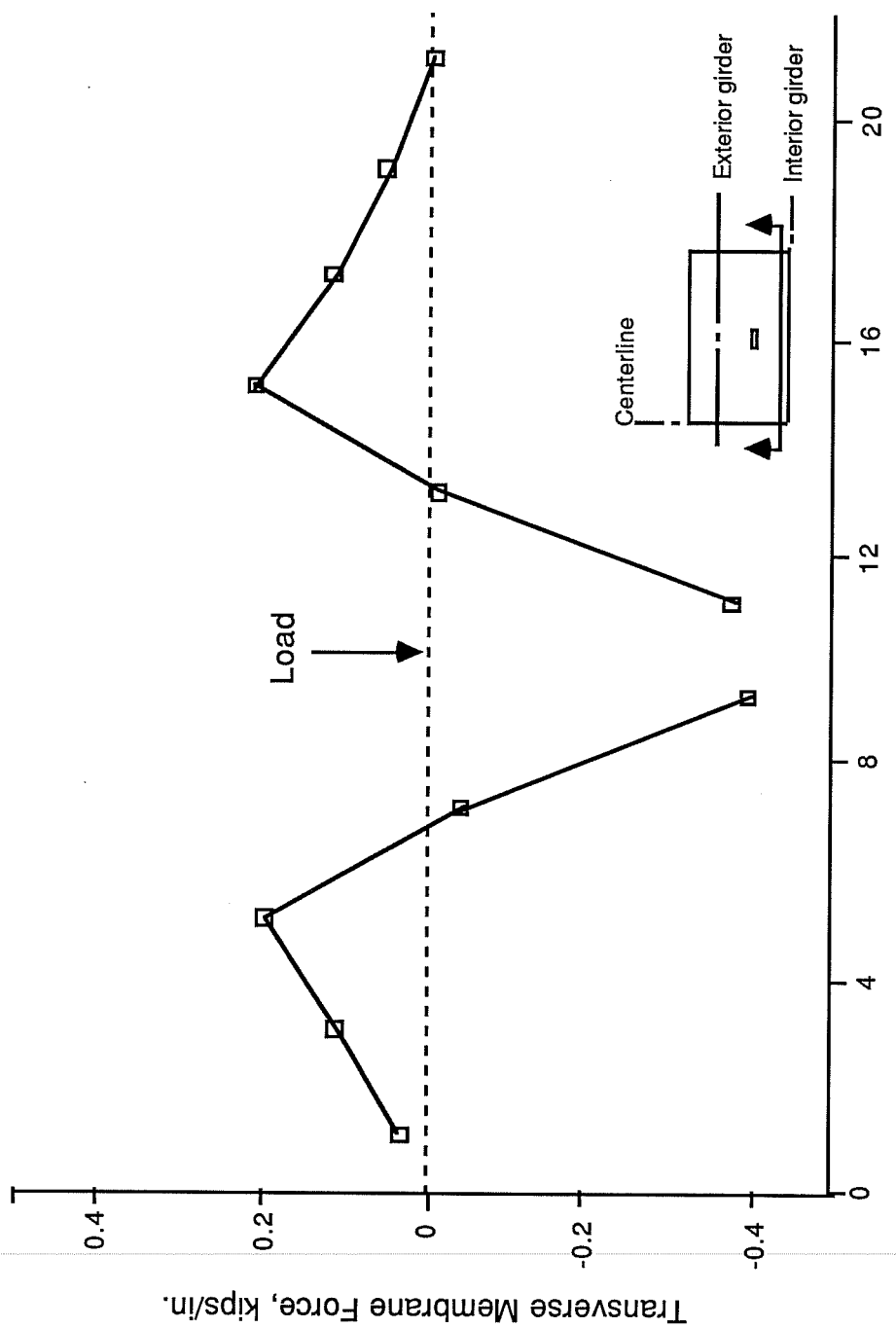

Fig. 4.1 Distribution of transverse membrane force at interior girder

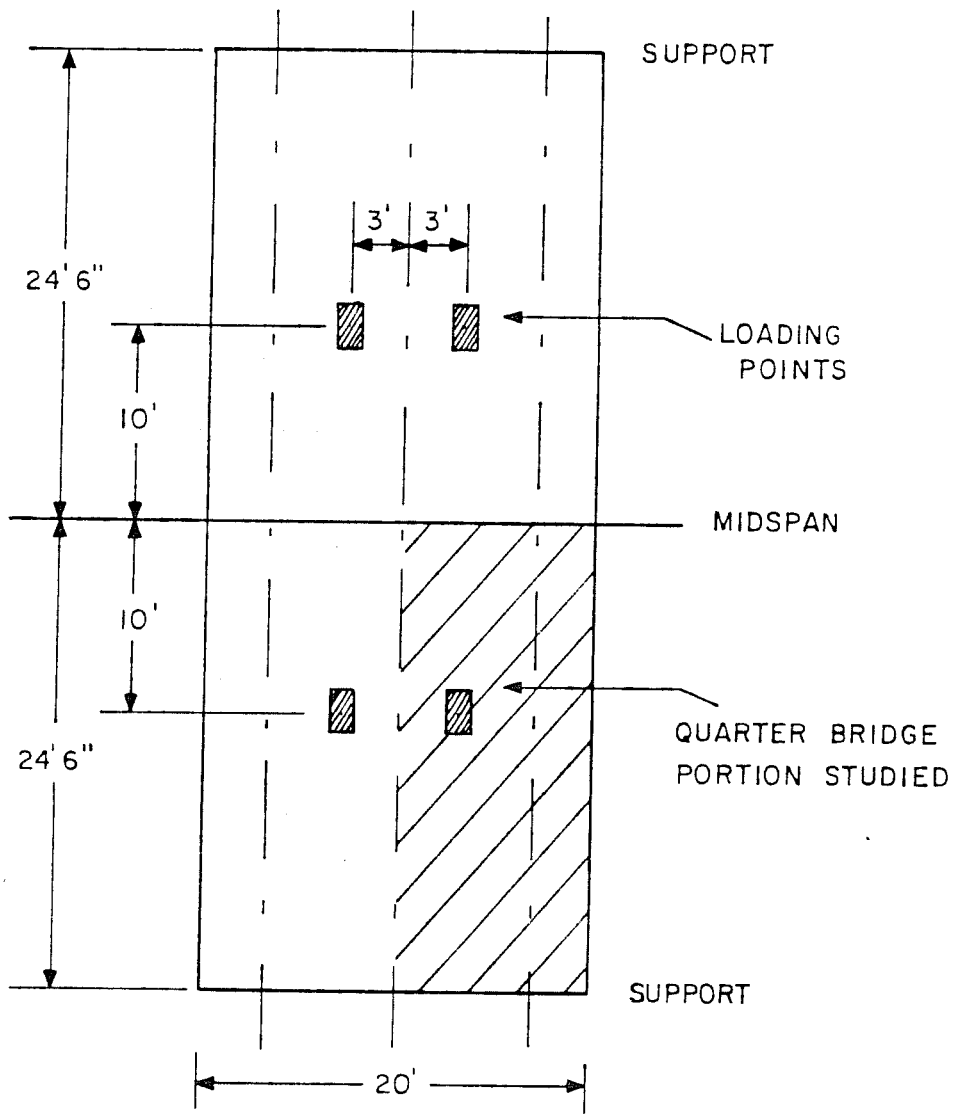

Fig. 4.2 Full and quarter rectangular bridge models

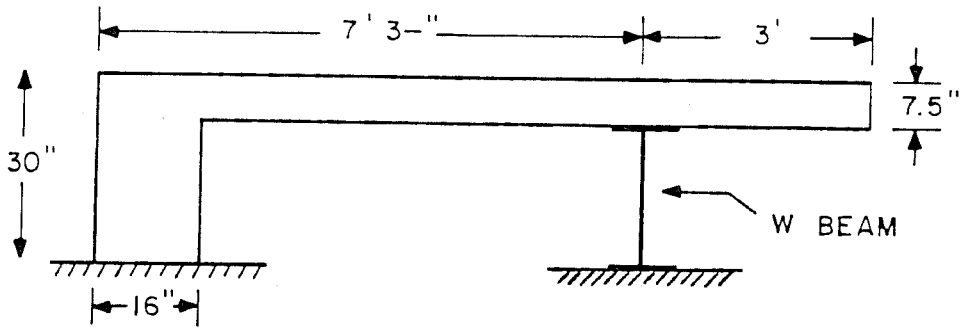

a) Transverse Section A-A

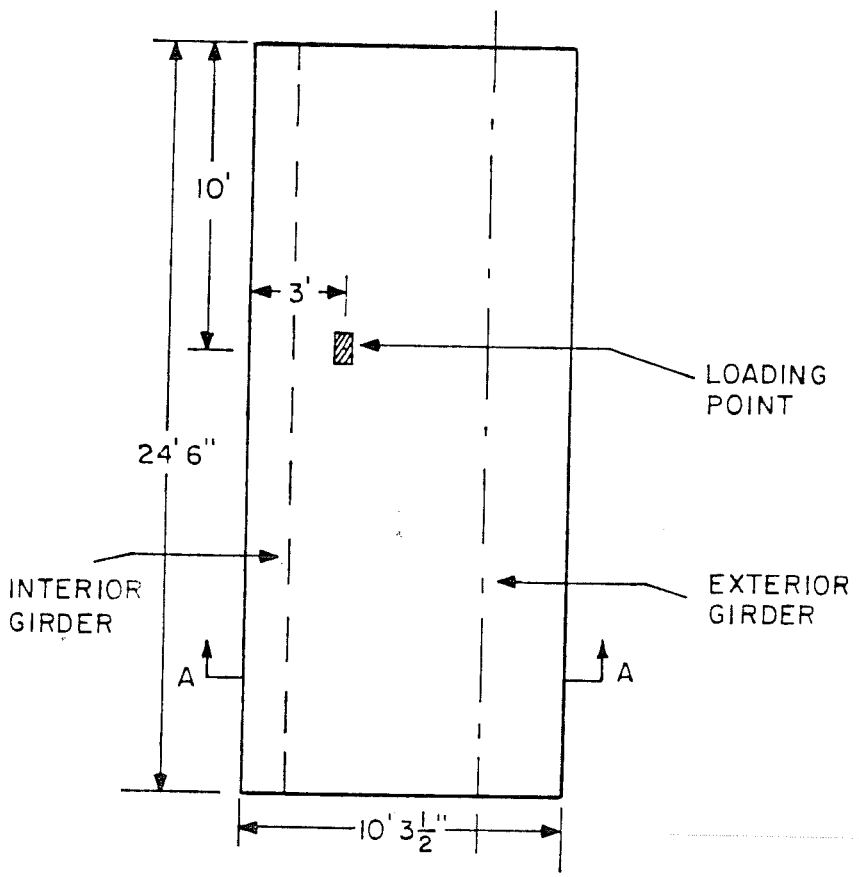

b) Plan View

Fig. 4.3 Quarter rectangular bridge model
(Trial rectangular specimen No. 1)

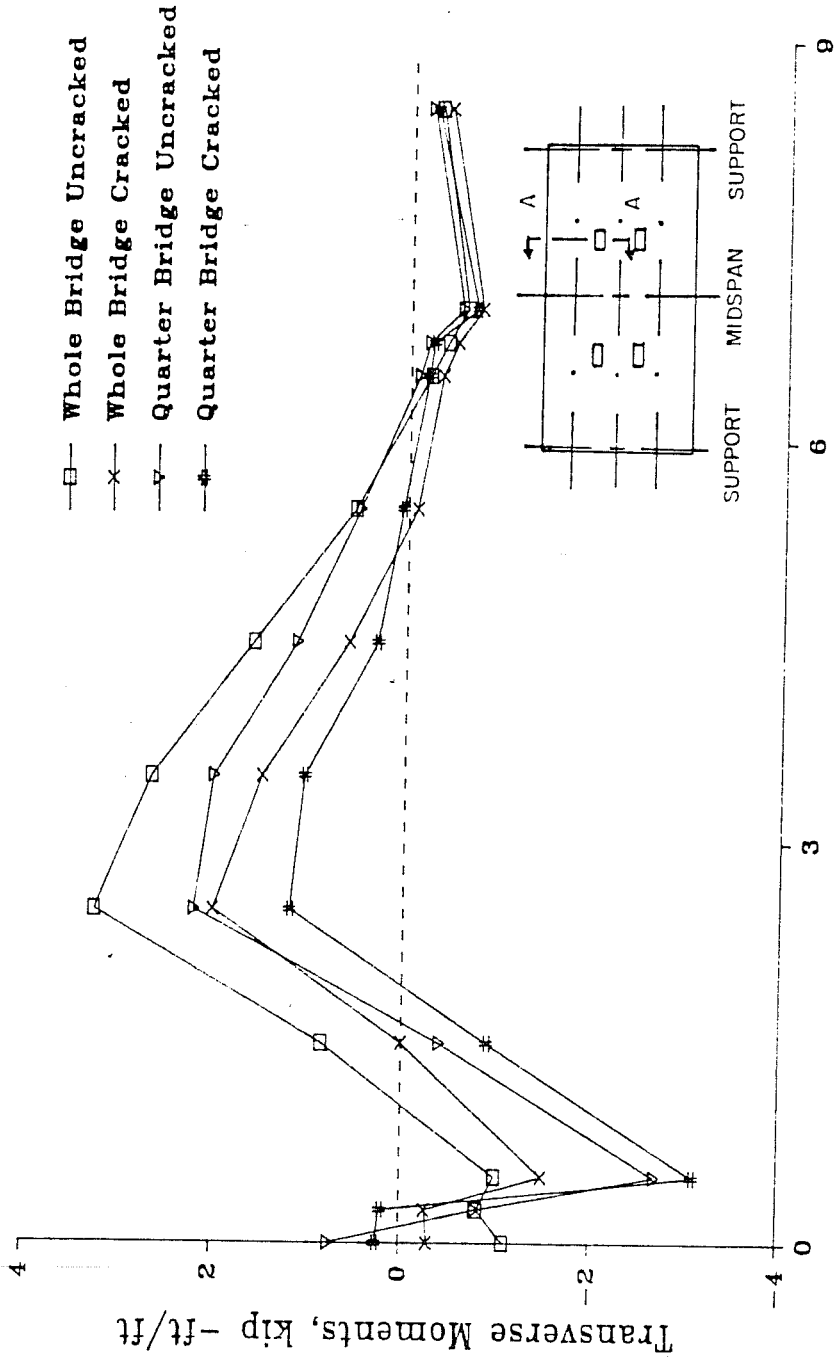

Fig. 4.4 Calculated transverse moments in full and quarter rectangular bridge models (Trial rectangular specimen No. 1)

condition of Fig. 4.2, the interior girder deflects more than the exterior ones, reducing the negative moment in the deck at the interior support. Also, as shown in Fig. 4.5, the transverse membrane forces are smaller after cracking, in the trial quarter bridge specimen than in the full bridge. This implies that this trial quarter bridge model has less in-plane stiffness than the full bridge. Furthermore, some lateral movement of the interior girder is permitted in the trial quarter bridge specimen, while none is allowed for the full bridge.

As shown in Fig. 4.6, a second trial specimen was then proposed in which vertical movement of the interior girder was permitted by introducing vertical springs underneath the girder at both ends, and lateral movement was prevented by lateral supports at the side. After several trials with different vertical spring stiffnesses, the calculated performance of the trial quarter bridge specimen became quite similar to that of the full bridge. Comparison of transverse moments and transverse membrane forces are presented in Figs. 4.7 and 4.8 respectively. Thus, the quarter bridge model was considered to simulate adequately the behavior of the full bridge. A skew quarter bridge model was then examined using the same boundary conditions.

4.3 Development of Skew Quarter Bridge Model

In the development of skew quarter bridge specimen, a arbitrary skew tangent of 0.5 was selected, corresponding to a skew angle of 26.57 degrees. This was modified as discussed subsequently. Two different locations for loading points were investigated, one away from the skew edge of the deck, and the other, very close to the edge. The first trial skew bridge model, shown in Fig. 4.9, is the same as the second rectangular quarter bridge model described in Section 4.2 (Fig. 4.6), except for the presence of skew. When the loading point is located far from the skew edge of the deck, skew does not significantly affect the behavior of the deck slab. As shown in Fig. 4.10, the full rectangular bridge, the full skew bridge, and the quarter skew bridge model all behave very similarly under this loading condition.

Two edge loading cases were studied. The first involved free skew edges, and the second, skew edges stiffened with transverse beams. The shape of the specimen was chosen to allow these two loading cases to be examined using a single test specimen. The relationship between loading points of the quarter skew bridges and of the test model skew bridge is shown in Fig. 4.11. Based on the

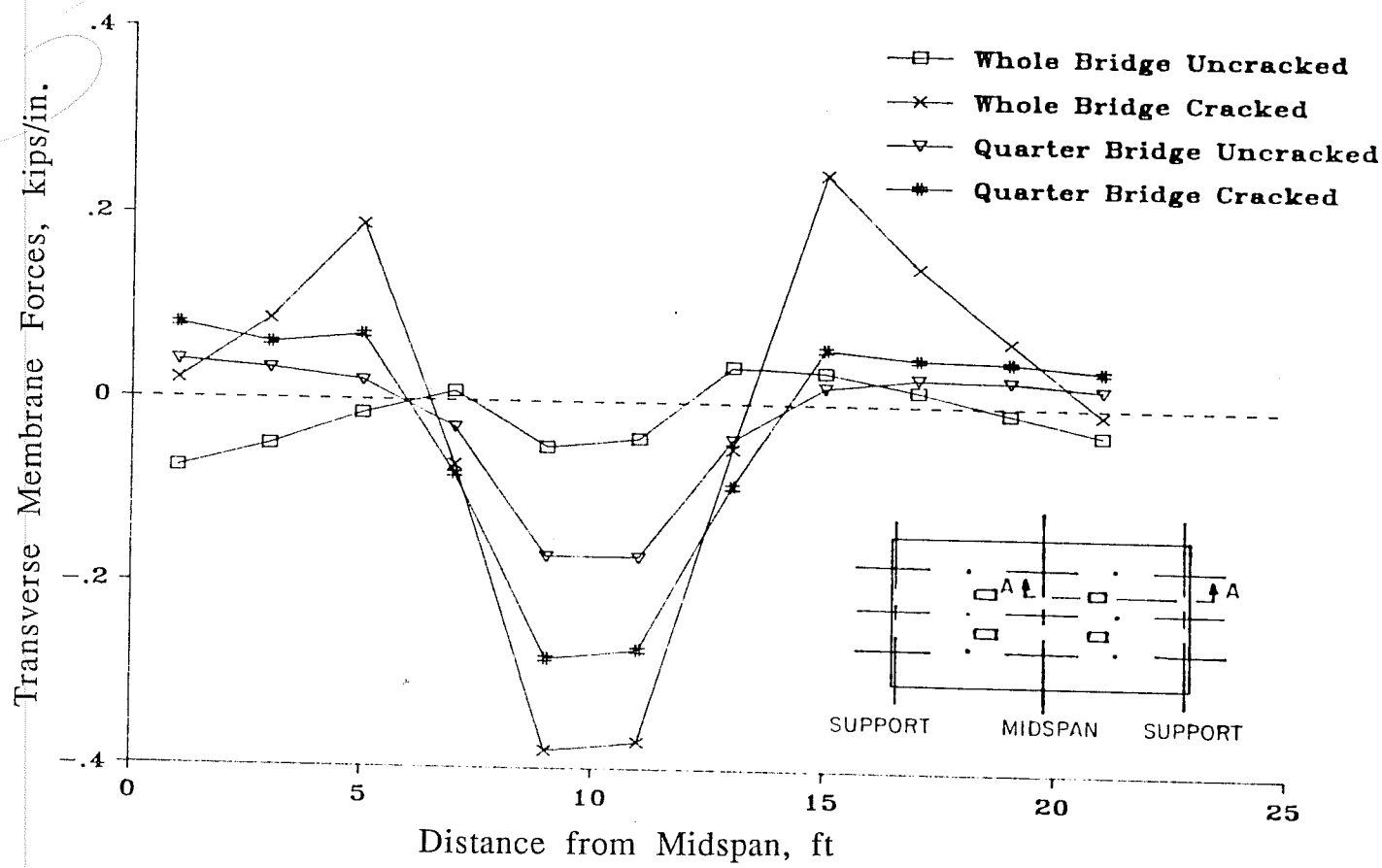

Fig. 4.5 Calculated transverse membrane forces in full and quarter rectangular bridge models (Trial rectangular specimen No. 1)

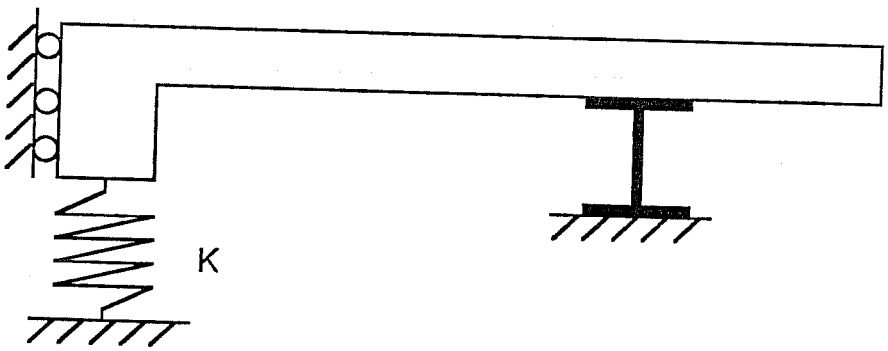

Fig. 4.6 Boundary conditions for trial rectangular specimen No. 2 (springs at the supports of the interior beam)

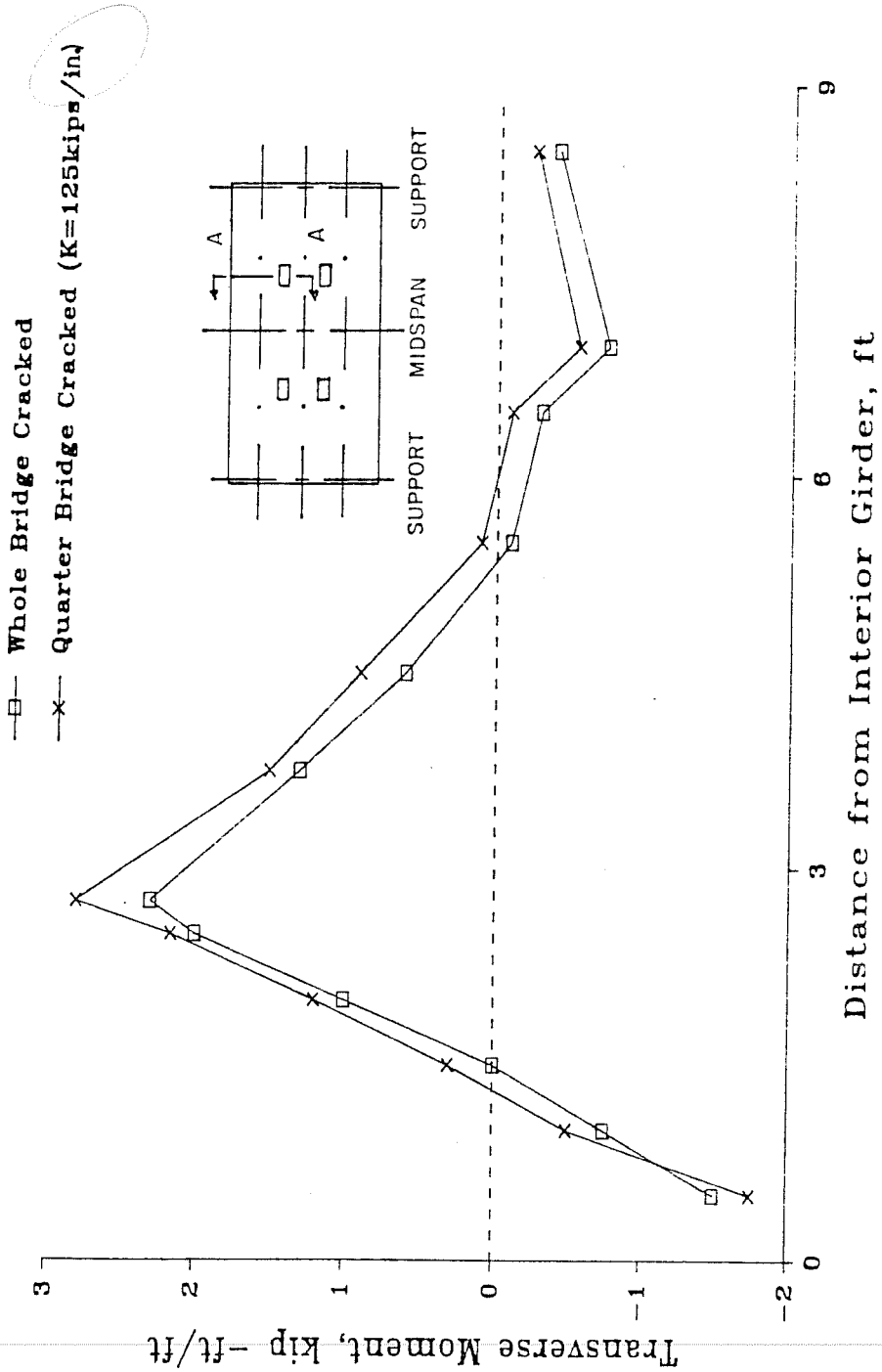

Fig. 4.7 Calculated transverse moments in full and quarter rectangular bridge models (Trial rectangular specimen No. 2)

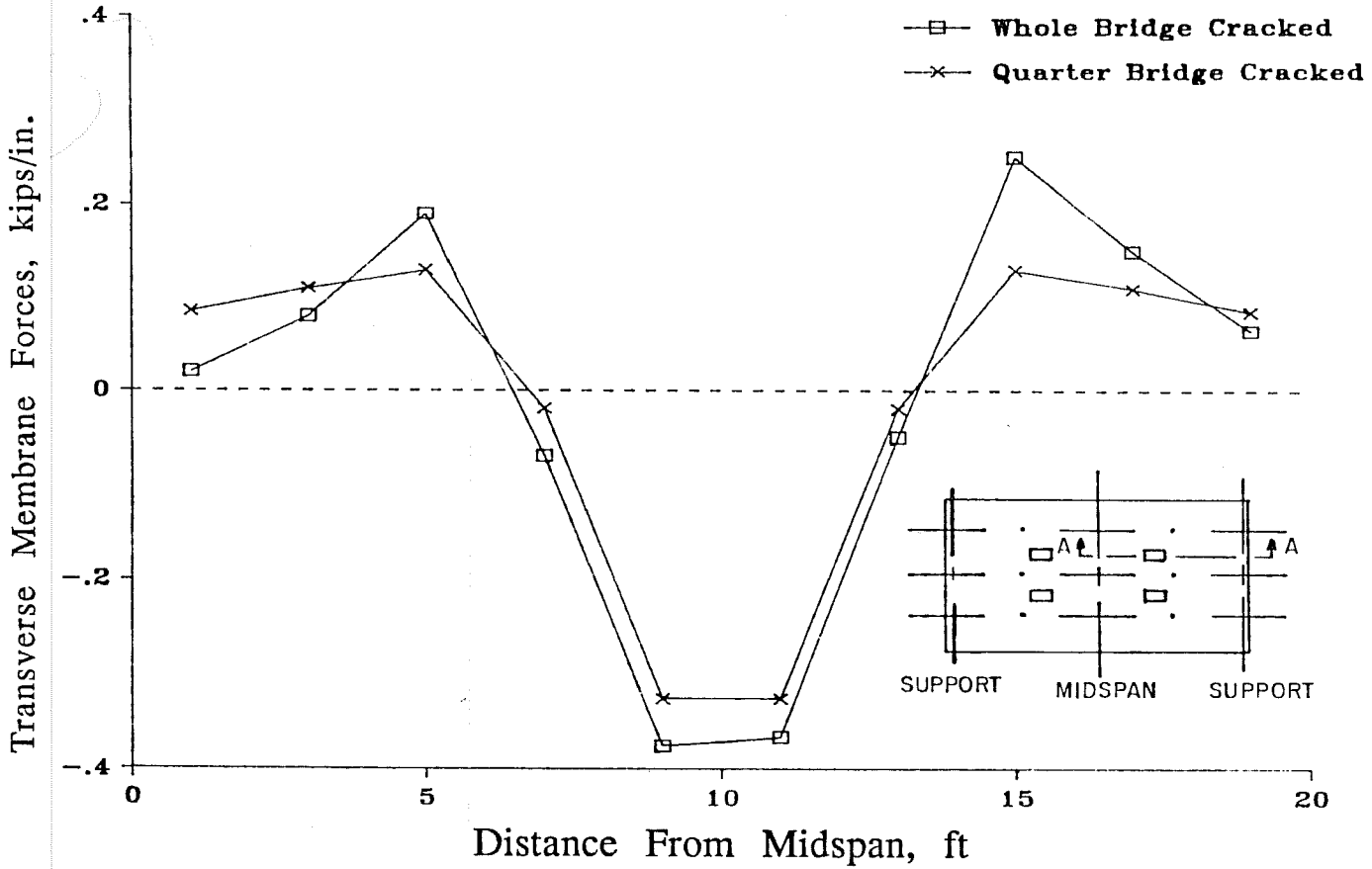

Fig. 4.8 Calculated transverse membrane forces in full and quarter rectangular bridge models (Trial rectangular specimen No. 2)

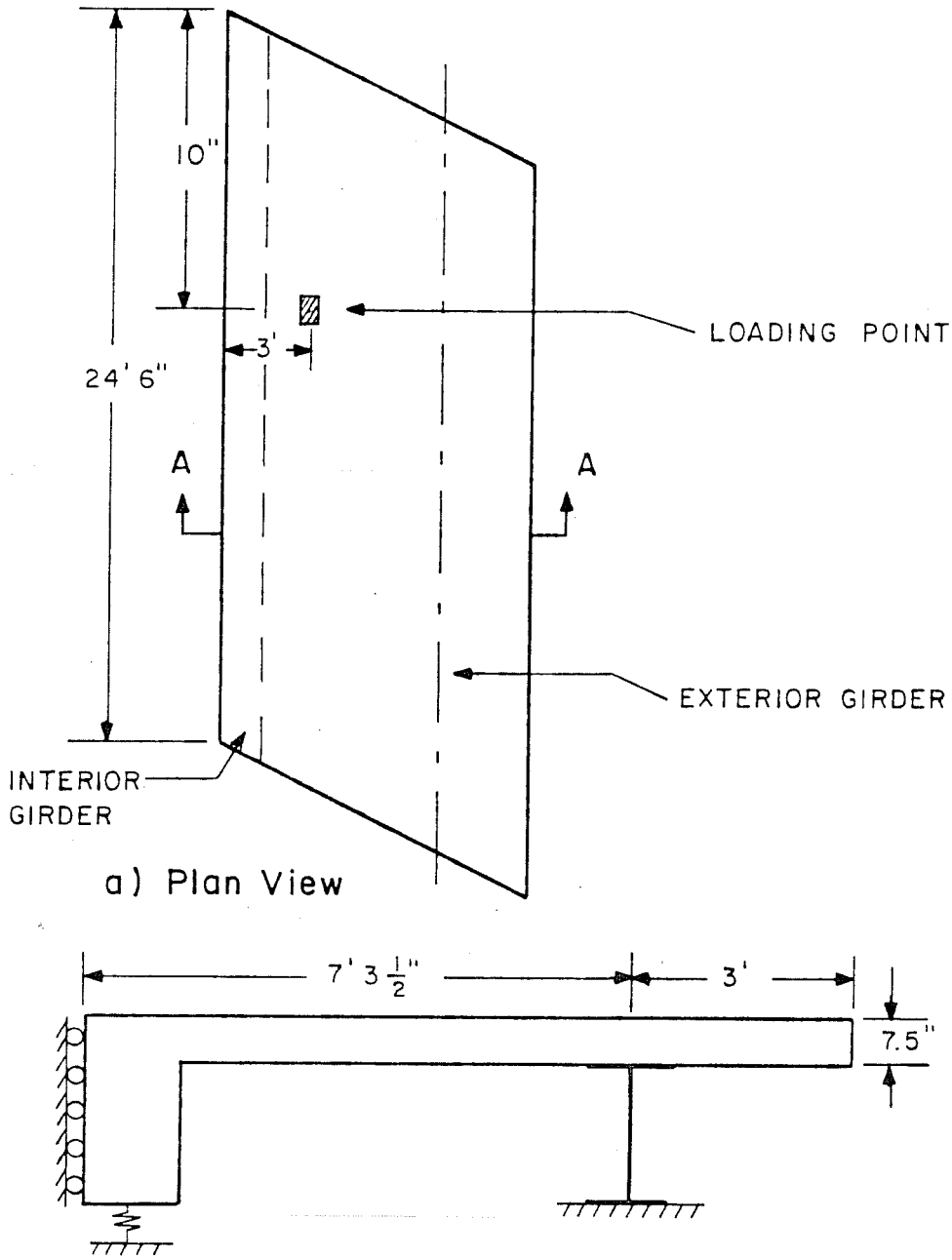

Fig. 4.9 Quarter skew bridge model for interior loading

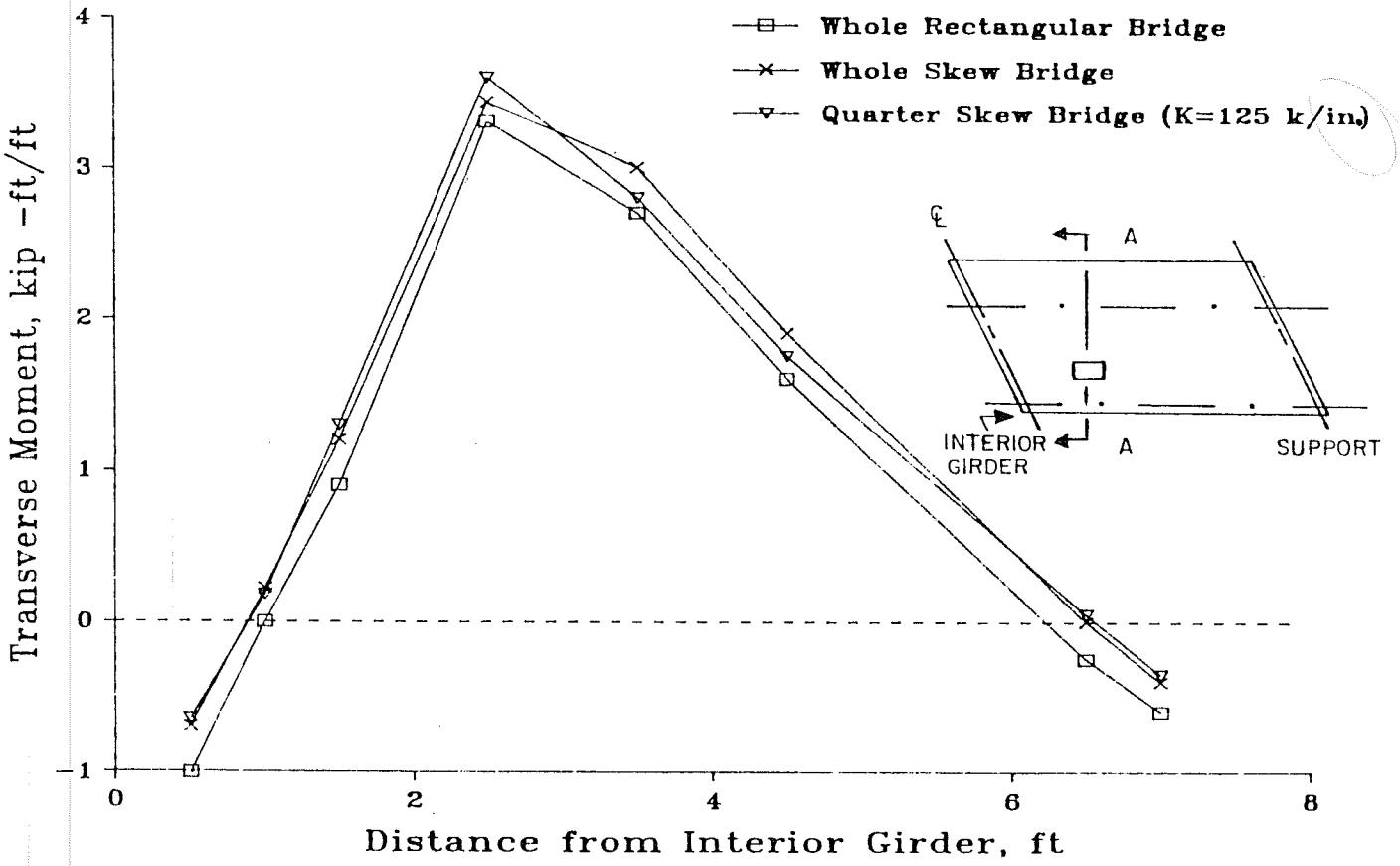

Fig. 4.10 Calculated transverse moments for skew and rectangular bridges with an interior loading condition

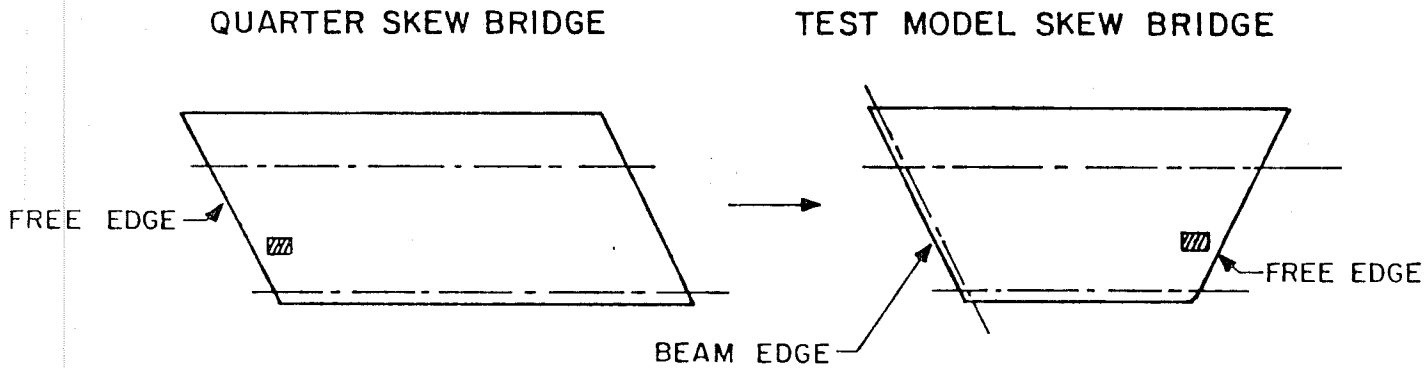

a) One edge loaded

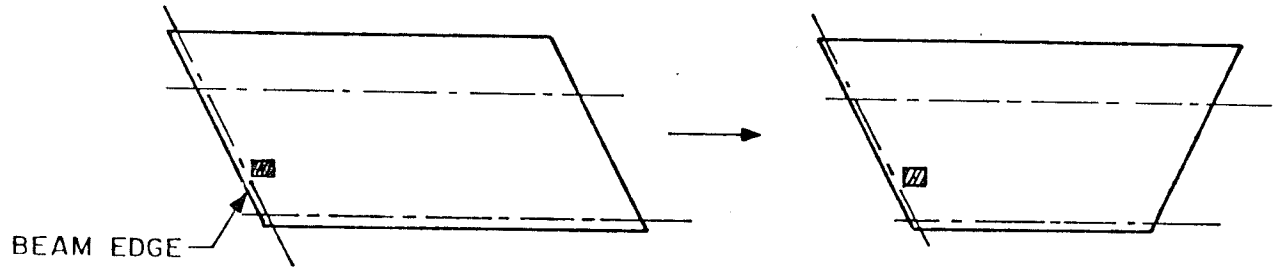

b) Other edge loaded

Fig. 4.11 Equivalent edge loadings for quarter skew bridge and test model skew bridge

concept that full membrane action could be developed within a longitudinal distance of 20 ft (Section 4.1), the test bridge specimen was made 20 ft long from edge to edge on a longitudinal line through the loading points. Detailed dimensions of the proposed test model skew bridge are shown in Fig. 4.12.

Calculated transverse moments for the full skew bridge, the quarter skew bridge, and trial skew specimen No. 1, along the free edge or along the beam edge, are shown in Figs. 4.13 and 4.14. The behavior of trial skew specimen No. 1 is almost identical to that of the skew quarter bridge. However, their performance does not agree with that of the full skew bridge. Trial skew specimen No. 1 and the quarter skew bridge have higher negative moments at the interior girder than the full skew bridge does. This implies that the interior girder of the trial specimen and the quarter bridge, which is fixed rotationally at the bottom, is too stiff rotationally.

When these rotational degrees of freedom were released, the transverse moments approached those of the full bridge demonstrating that by adjusting the torsional stiffness of the interior girder, a quarter skew bridge can be modeled to behave flexurally like the full skew bridge (Figs. 4.13 and 4.14). After several trials with different sizes of the interior girder, it was found that much better agreement with full bridge behavior was obtained when the beam was replaced by a vertical wall simulating the rotational stiffness of the other portion of the deck (Fig. 4.15). However, some problems were encountered in using this wall. First, the wall is too stiff in the longitudinal direction of the deck, which might affect deck behavior. Second, it is hard to provide spring supports underneath the wall. However, it was found that the longitudinal flexural behavior of the bridge was very little affected by the vertical stiffness of the interior girder (wall). It was also found that with a loading point near the edge, the vertical springs at the interior girder have little influence, because there is little differential displacement between the interior and the exterior girder in this case. After a few more trials, each end of the wall was given at the same angle as the skew angle in the deck, to better simulate the rotational stiffness of the adjoining deck. In a sense, this was as though the skew slab had been folded down to form the wall.

The wall height used in the analysis was based on the need to allow enough room under the deck slab for the test setup. To make the rotational stiffness of the wall equal that of the adjoining deck, the following relationship was satisfied:

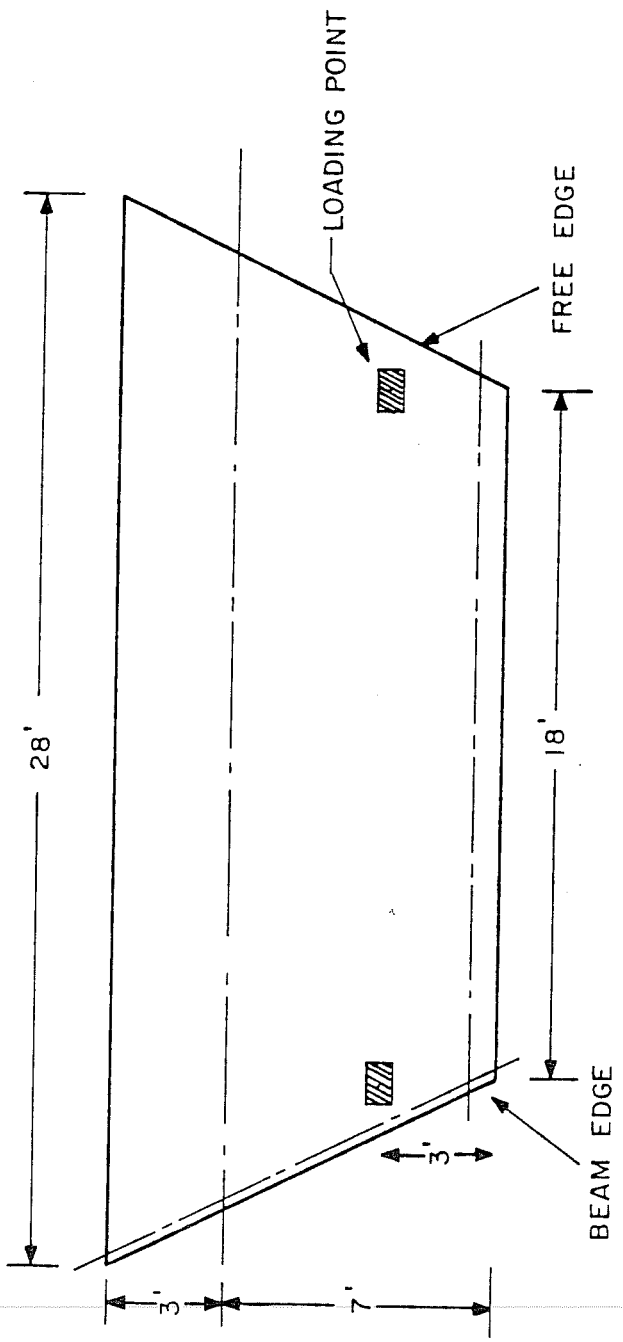

Fig. 4.12 Proposed quarter skew bridge test model 1

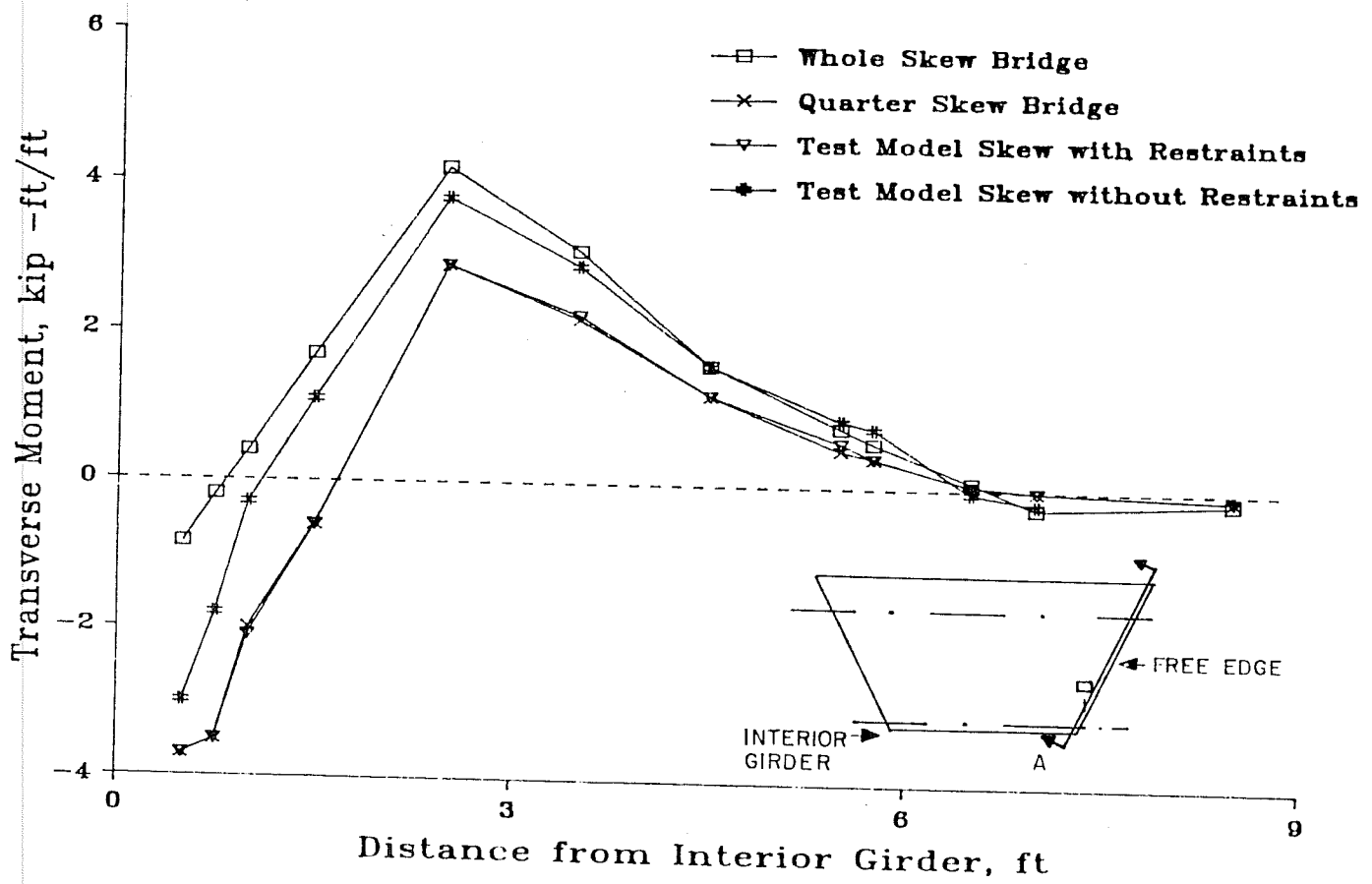

Fig. 4.13 Calculated transverse moments in skew bridge models with free edge

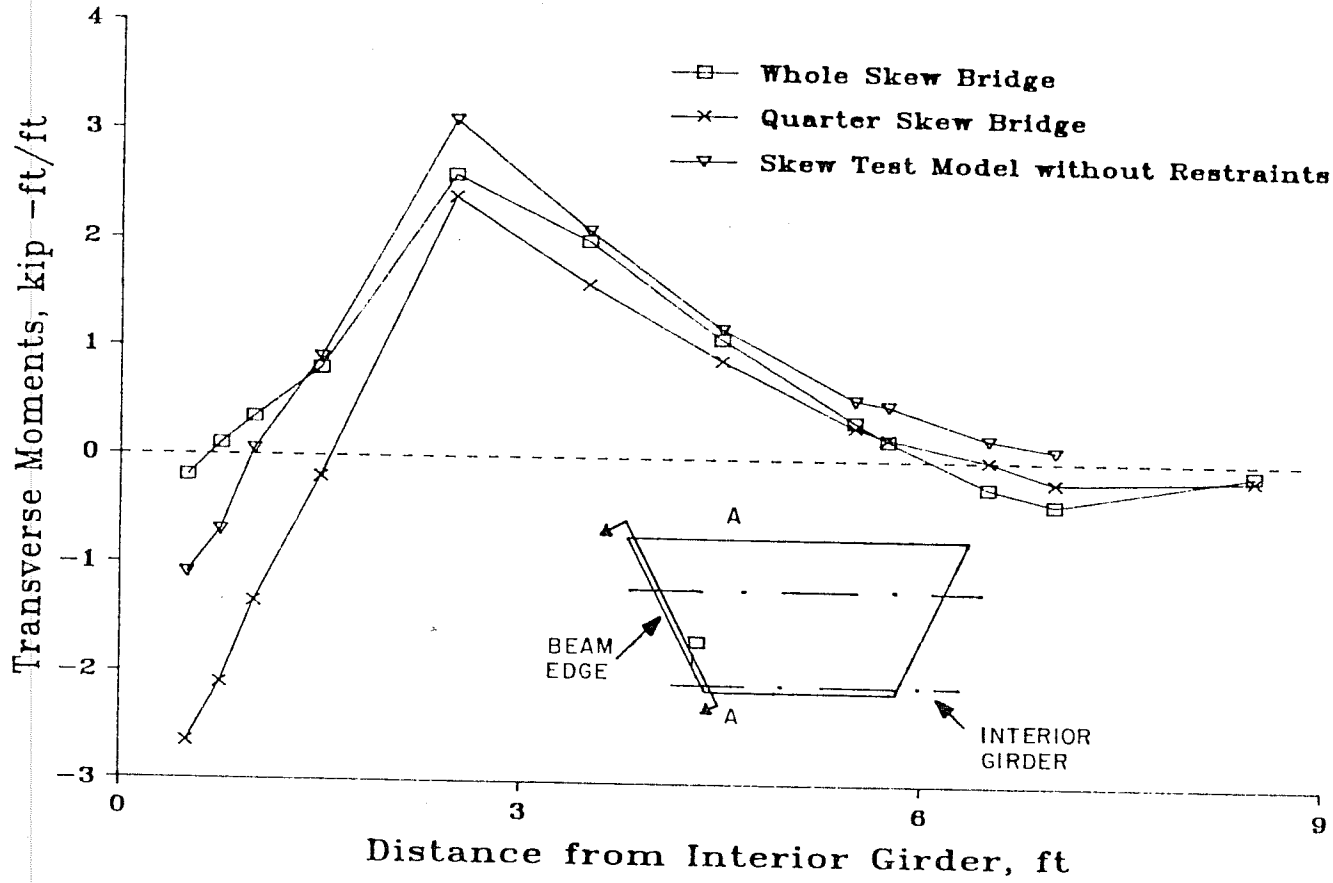

Fig. 4.14 Calculated transverse moments in skew bridge models with beam edge

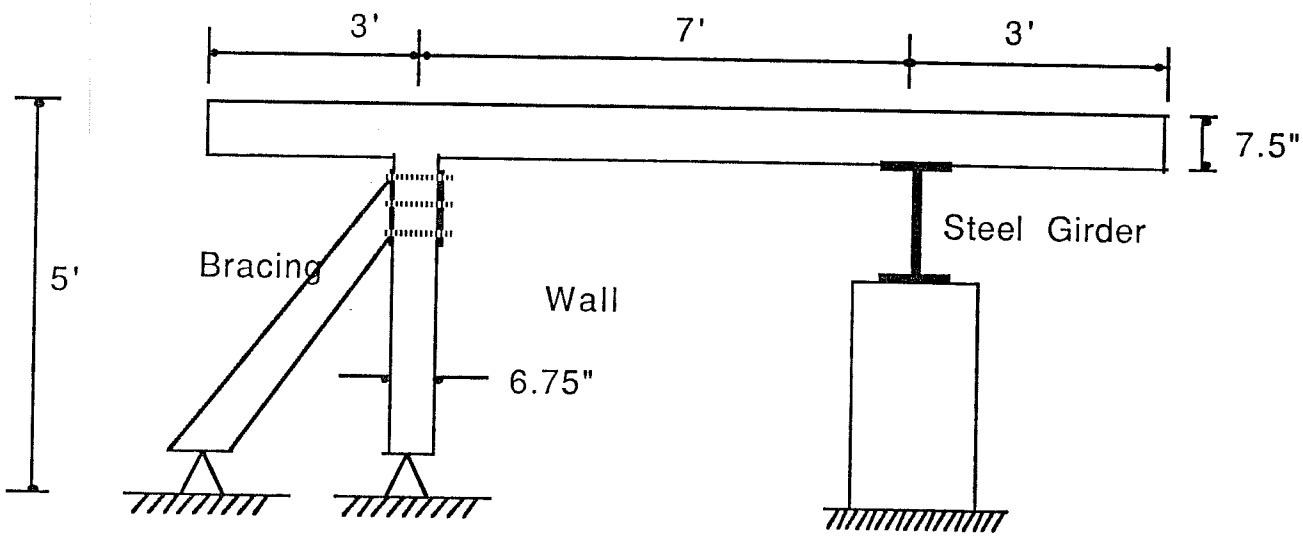

Fig. 4.15 Elevation view of skew bridge model showing wall and lateral bracing

$$\frac{3\ E\ I_w}{H} = \frac{3\ E\ I_d}{L}$$

where, H = height of wall,
L = transverse span of deck slab,
I_w = uncracked moment of inertia of wall, and
I_d = uncracked moment of inertia of deck slab.

This relationship resulted in a required wall thickness of 6.75 in., and a wall height of 5 ft for trial skew bridge specimen No. 2.

To duplicate the in-plane stiffness normally provided by the adjoining bridge deck, the deck slab was extended by 3 ft from the center of the wall (Fig. 4.15). This overhanging portion of the deck provides some in-plane stiffness, but still not enough to develop as much membrane action as in the full bridge. Since the calculated performance of the trial skew bridge specimen was not affected much even by doubling the thickness of the overhang, the additional in-plane stiffness was provided by external braces (Fig. 4.15). Several trial analyses were conducted to find the proper combination of overhang thickness and the brace stiffness, and the results are shown in Fig. 4.16. As the braces become stiffer and the overhang becomes thicker, membrane forces correspond more closely to those of the full skew bridge. The final configuration consisting of 7 braces each using two 8x4x1/2-in. angles at 2-ft spacing, was selected along with a 7.5-in. overhang, the same as the deck slab thickness.

Because this was planned as the last test specimen of Project 350, some geometric changes were made so that different variables could be studied in one test specimen:

1) The span length was increased to 9 ft, which is more frequently used in Texas.

2) The transverse beam at one side of the skew edge was eliminated because it is seldom used in practical applications. Instead, the edges were stiffened by increasing the thickness of the deck by 2 in., in accordance with details proposed by the Texas SDHPT.

3) Different skew angles were used at each edge of the deck.

4) The wall height was changed to 5 ft 6 in. with a corresponding thickness of 8 in., to accommodate the test setup.

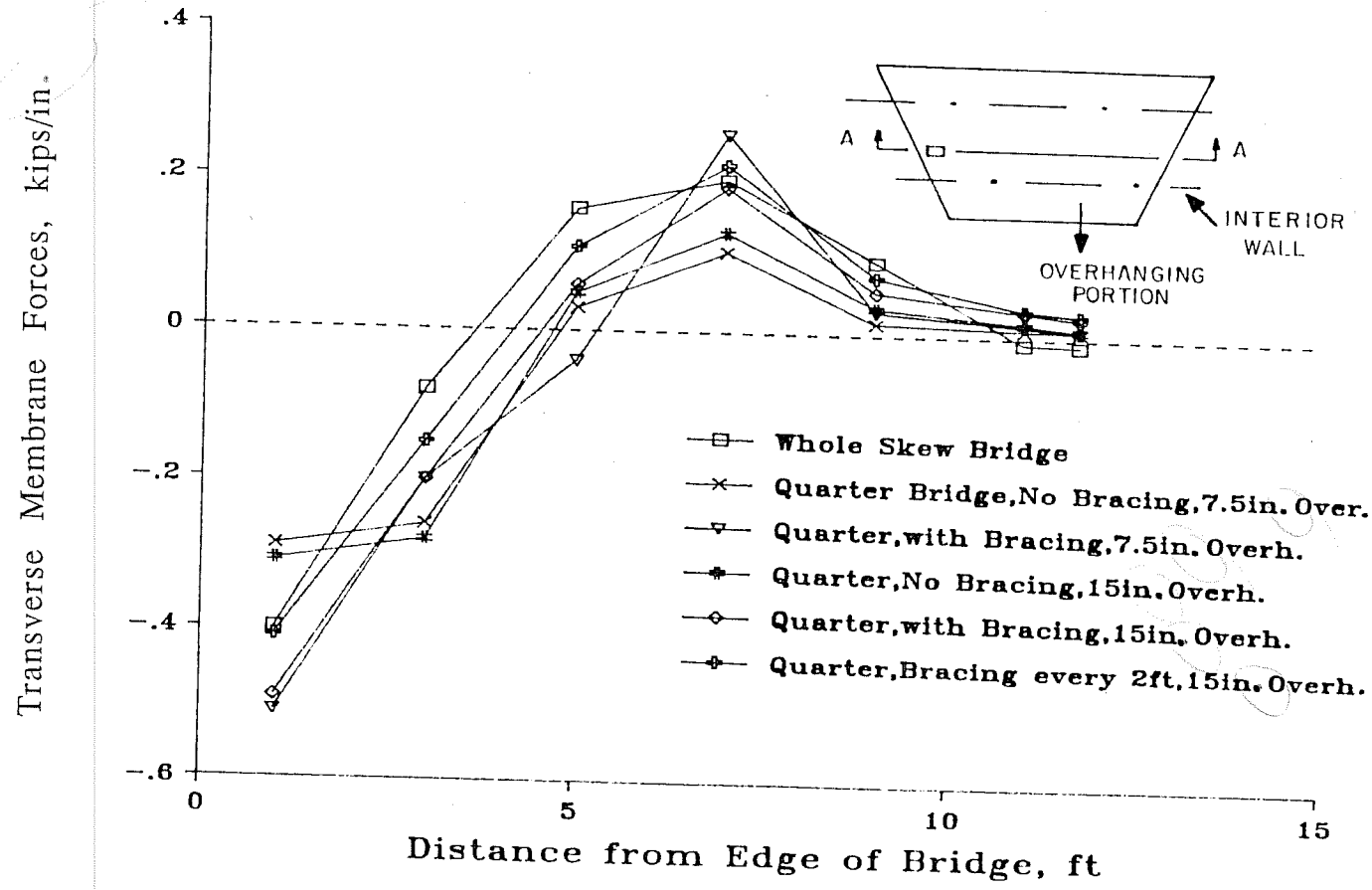

Fig. 4.16 Calculated transverse membrane forces assuming different lateral bracing conditions and overhanging thicknesses (at the interior girder)

It was also decided to post-tension the wall vertically to avoid any loss of wall rotational stiffness associated with flexural cracking. The required intensity of post-tensioning was that necessary to make the cracking moment of the wall exceed that of the deck.

Details of the final trial test specimen are shown in Figs. 4.17, 4.18, 4.19, and 4.20. The test specimen was then modeled and analyzed to compare its performance with that of the full bridge. The finite element mesh used for the test specimen is shown in Fig. 4.21. Transverse moments are compared in Fig. 4.22; longitudinal moments, in Fig. 4.23; and transverse membrane forces, in Fig. 4.24. As shown in those figures, the final skew bridge test specimen could be expected to perform almost identically to the complete skew bridge with respect to transverse moments, longitudinal moments, and transverse membrane forces.

4.4 Summary of Development of Test Specimen

It was decided to use a test specimen which would represent one-quarter of a skew bridge. Several analytical trials were conducted to find a model that would behave like the full skew bridge model.

A quarter rectangular bridge model was studied first to obtain appropriate boundary conditions. Elastic supports were necessary at the interior girder supports of this model, to simulate the vertical restraint of the interior girder in the full bridge model. Also, lateral movement was prevented in the quarter bridge model to obtain better agreements of membrane forces.

Using the same boundary conditions, a skew bridge model was then studied. When the loading point was far from the edge of the slab, the skew did not significantly affect the behavior of the slab. Results from the rectangular bridge and the skew bridge were very similar.

When the loading point was near the skew edge of the slab, rotational restraint equivalent to that of the adjacent deck was required at the interior girder of the test specimen to obtain good agreement between its performance and that of the full bridge. This equivalent stiffness was provided by placing a wall at the interior girder location of the quarter bridge. In addition, external braces were provided at the slab overhang to simulate the in-plane stiffness of the adjoining deck in the full bridge.

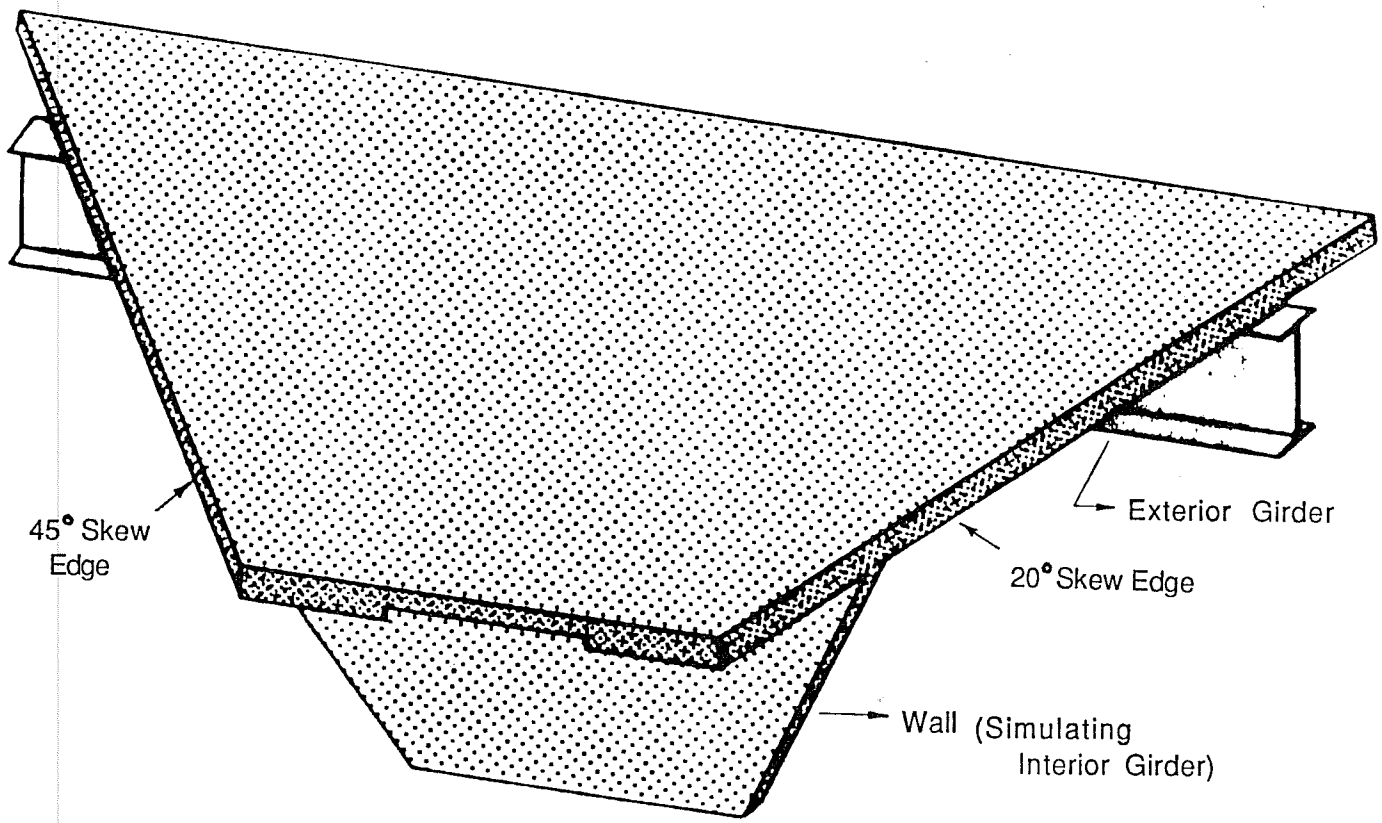

Fig. 4.17 Three dimensional view of skew bridge test specimen

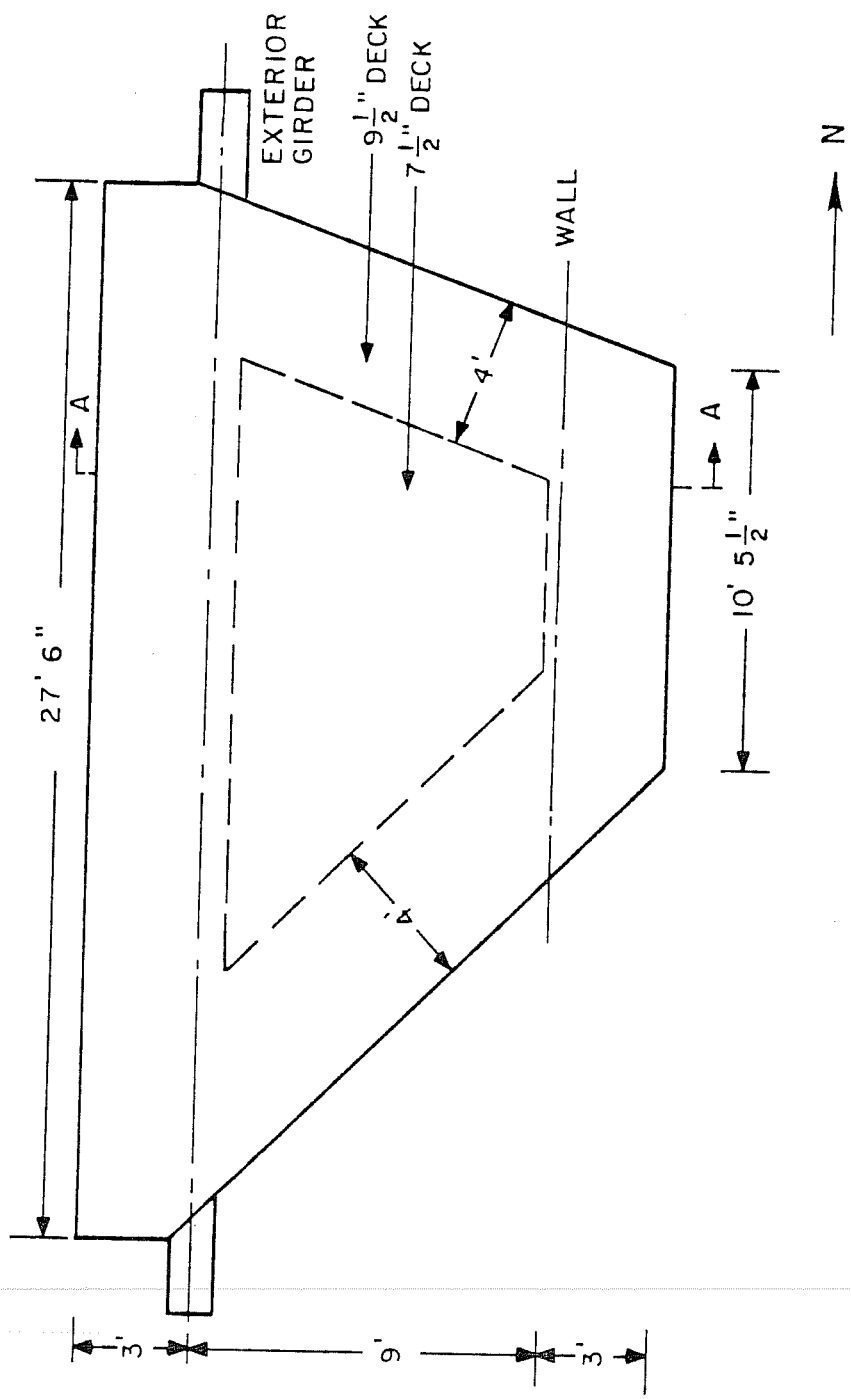

Fig. 4.18 Plan view of skew bridge test specimen

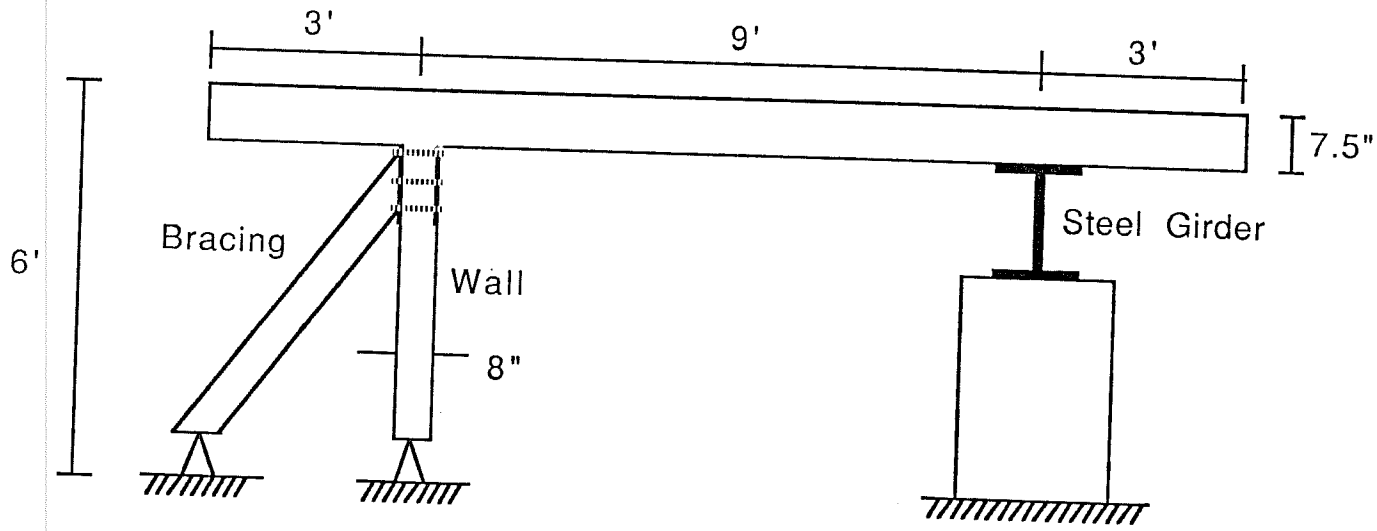

Fig. 4.19 End elevation of skew bridge test specimen showing wall and lateral bracing

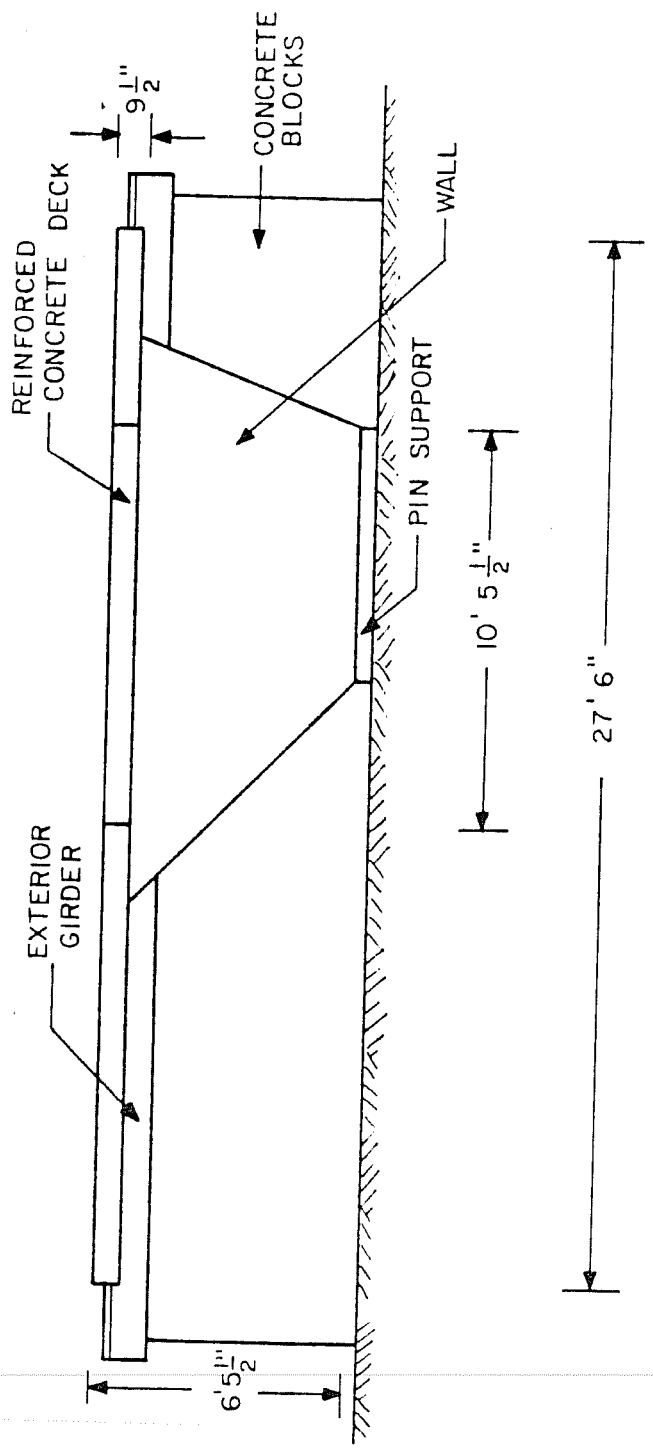

Fig. 4.20 Side elevation of skew bridge test specimen

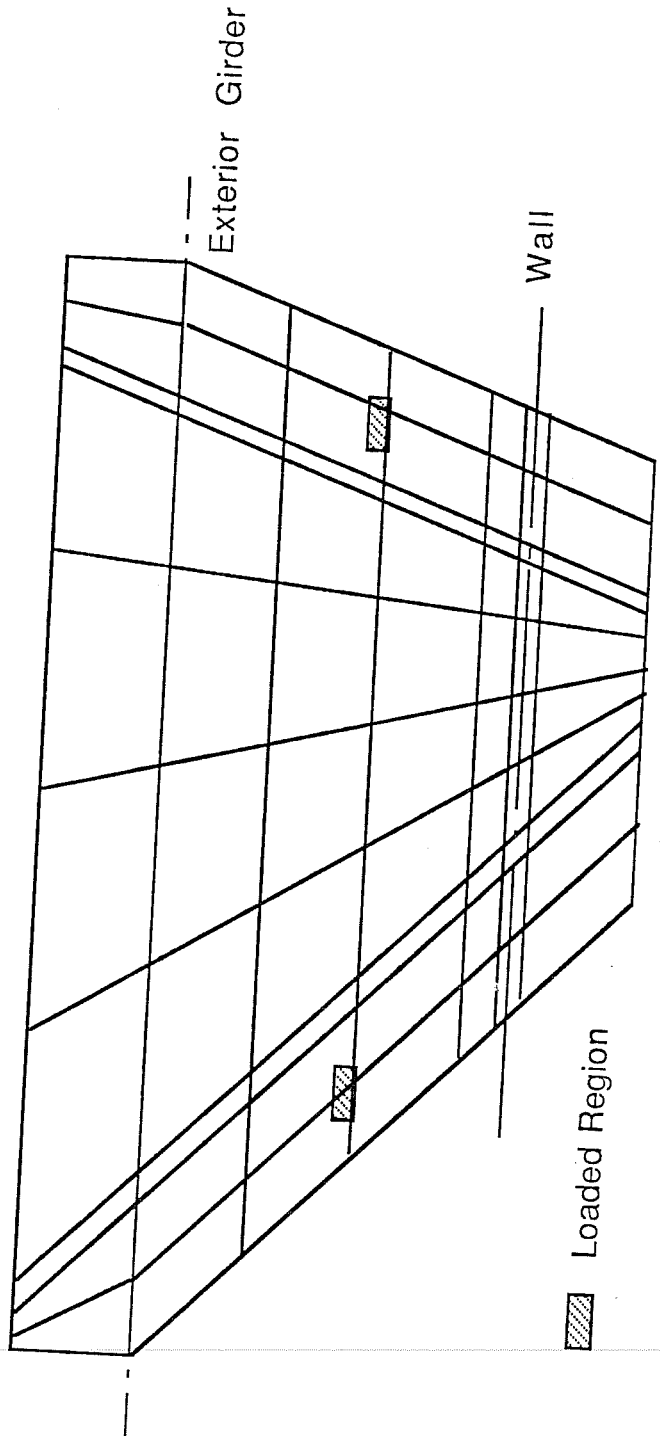

Fig. 4.21 Finite element mesh for skew bridge test specimen

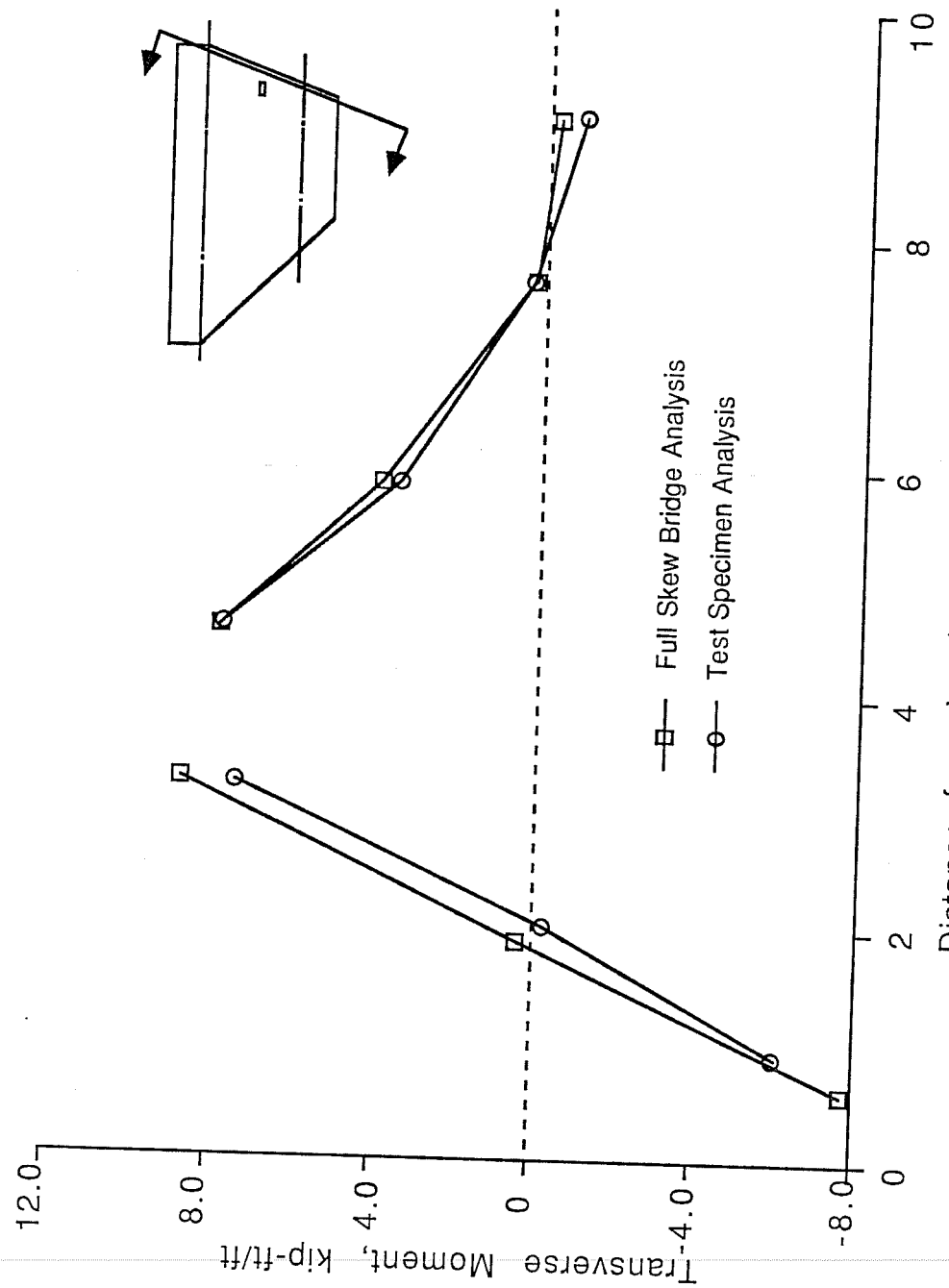

Fig. 4.22 Calculated transverse moments at 20-degree skew edge for full skew bridge and skew bridge test specimen (after cracking, P = 40 kips)

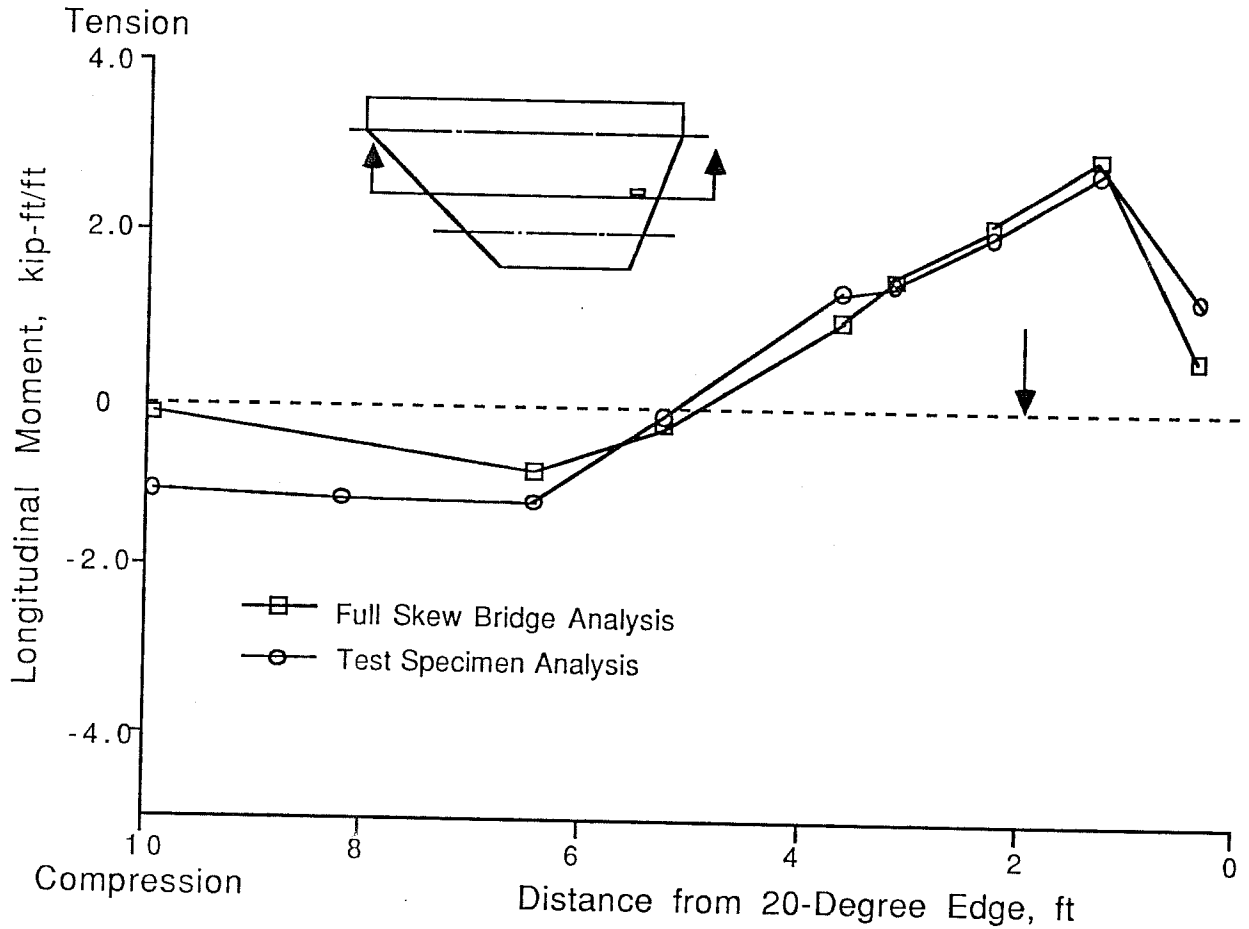

Fig. 4.23 Calculated longitudinal moments along line through loading point for full skew bridge and skew bridge test specimen (loaded at 20-degree skew edge, after cracking, P = 40 kips)

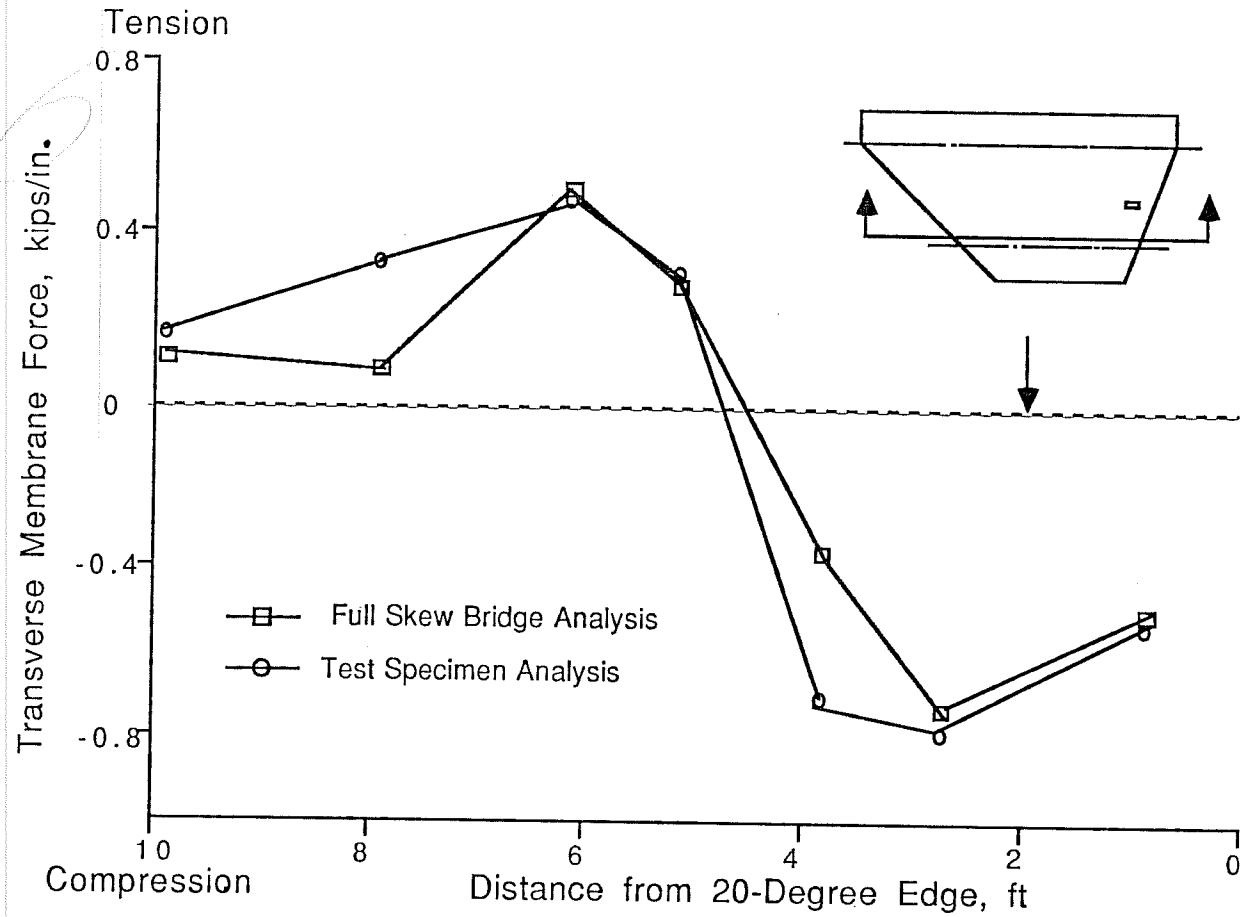

Fig. 4.24 Calculated transverse membrane forces along interior girder for full skew bridge and skew bridge test specimen (loaded at 20-degree skew edge, after cracking, P = 40 kips)

CHAPTER 5

DETAILS OF TEST SPECIMEN AND CONSTRUCTION

5.1 Details of Test Specimen

The test specimen had details similar to those required by the Ontario Highway Bridge Design Code. Those details were modified as recommended by the Texas SDHPT: at both edges of the specimen, the deck thickness was increased from 7.5 in. to 9.5 in. up to 4 ft from the skew edge, measured perpendicular to the skew edge. Deck reinforcement was modified as discussed later in this section. A three-dimensional view of the test specimen is shown in Fig. 4.17. Plan and elevation views are shown in Figs. 4.18, 4.19, and 4.20.

The wall had two curtains of conventional reinforcement, each consisting of horizontal #5 bars spaced at 12 in. and vertical #5 bars spaced at 5.5 in. (Fig. 5.1). The post-tensioning bars ran in steel ducts placed between the two layers of conventional wall reinforcement, and were placed at varying angles. The bars were anchored using 5x2x1-in. plates placed at the top and the bottom of the wall.

Deck reinforcement was designed using Ontario-type details, modified by the Texas SDHPT [34]. As shown in Fig. 5.2 and Fig. 5.3, the edges of the bridge deck were reinforced differently from the center part. All deck reinforcement consisted of #5 bars. The transverse edge reinforcement was placed parallel to the skew edge also require nominal reinforcement of about 0.5 % in both directions [35], more than the 0.3 % required by the Ontario Highway Bridge Design Code. In the Texas details, twice the nominal amount of transverse reinforcement is also required in the bridge deck near each thickened edge. As a result, the actual amount of interior transverse steel near each thickened edge was 0.98 %.

Nominal longitudinal reinforcement is provided in the deck near each thickened edge. Since the length of the test specimen is so small, no nominal transverse reinforcement of the typical interior deck away from the skew edges was shown (Figs. 5.2 and 5.3).

Shear studs 3/4 in. in diameter were fillet-welded to the top flange of the exterior steel girder, and were used to ensure composite action between the deck and the steel girder.

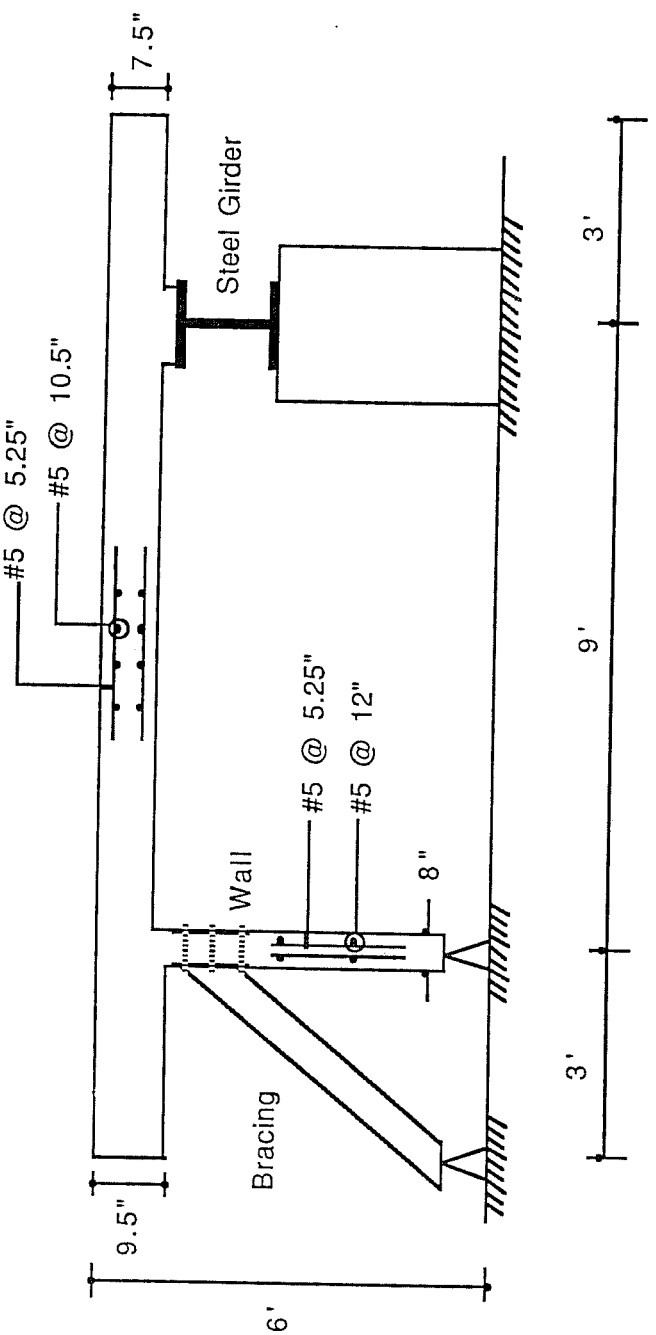

Fig. 5.1 Cross section of test specimen

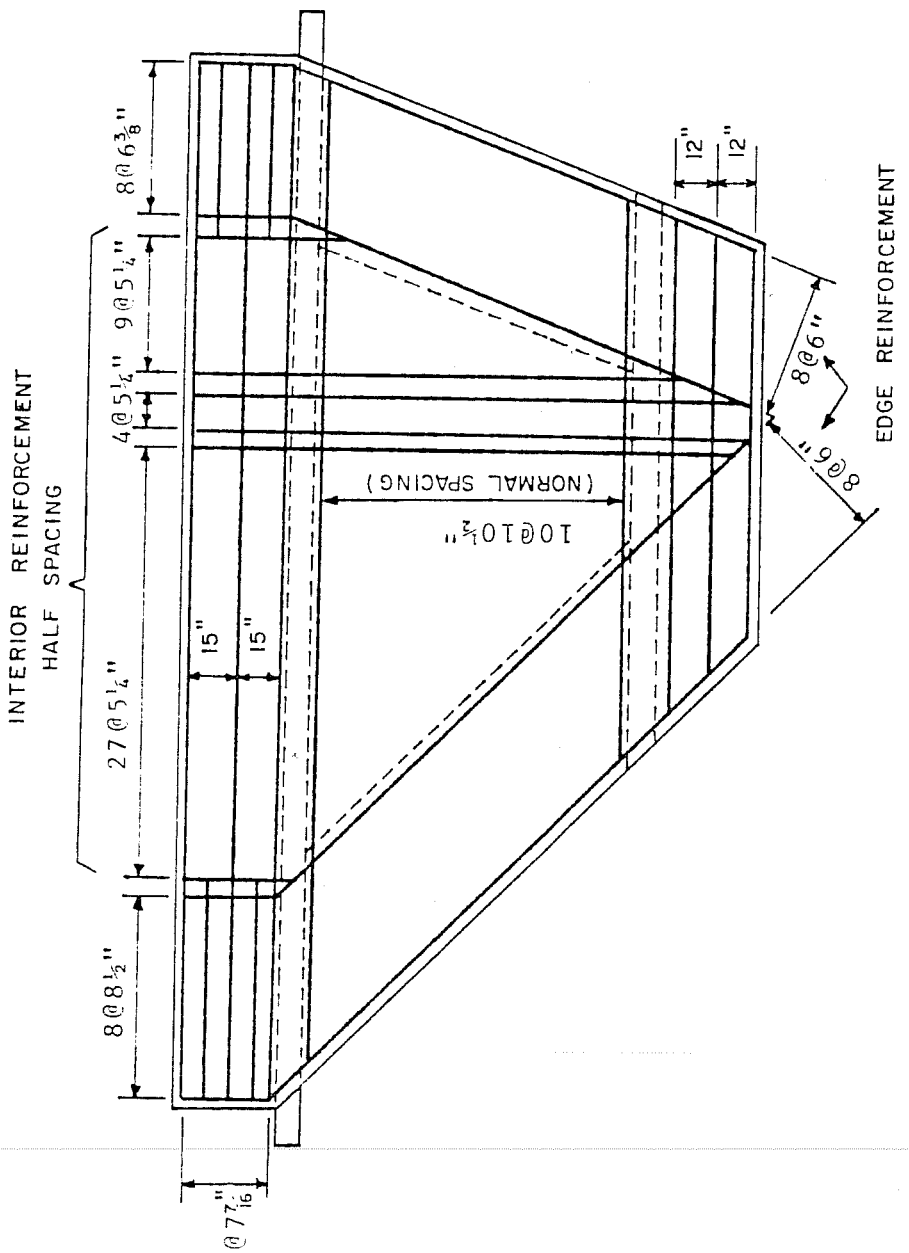

Fig. 5.2 Top deck reinforcement

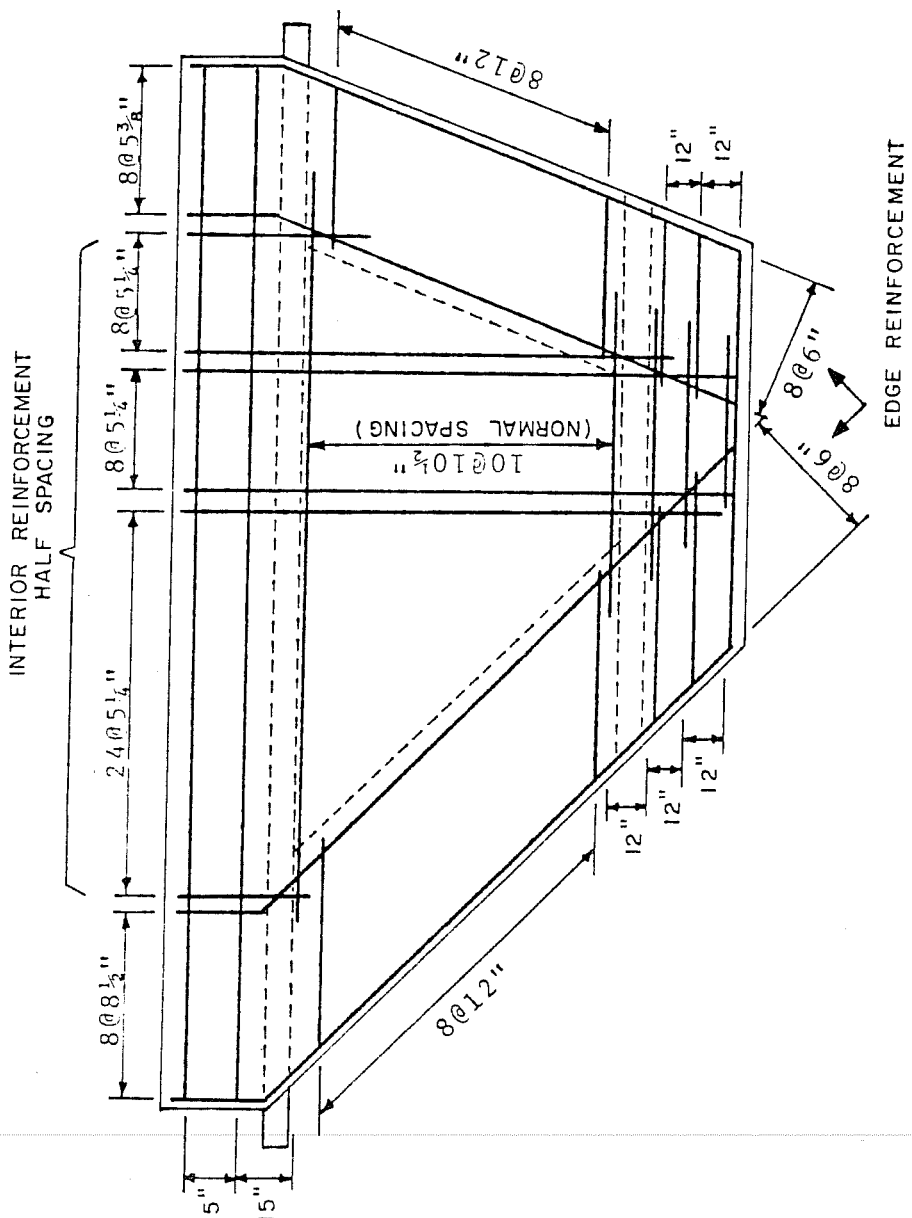

Fig. 5.3 Bottom deck reinforcement

In the analytical study of the specimen, the wall was modeled with a pin support along its bottom edge. In the test specimen, two details were used to provide the pin support. One involved steel plates; the other, wooden blocks. Both types of support were placed on top of a 3/8-in. steel plate, bolted to the floor.

The first type of support is shown in Fig. 5.4(a). A 2- in. diameter steel bar was fillet-welded to the top steel plate supporting the concrete wall. The top plate was restrained laterally on each side of the plate by 5x5x1/2-in. angles welded to the bottom plate. These steel pin supports were located at each end of the wall.

The second type of support is shown in Fig. 5.4(b). The wood support was simply a permanent formwork for the wall. Because of its small rigidity compared to that of the steel support, little load would be transferred through this type of support.

The exterior steel girder consisted of a W12x58 steel beam supported by concrete blocks (Fig. 5.1). These concrete blocks were used to provide continuous vertical support to the exterior girder, which did not have enough stiffness to span the length of the specimen.

Seven 8x4x1/2-in. structural angles were used as external braces, connected from the corner of the wall and the deck slab to the floor reaction beam.

5.2 Material Properties

5.2.1 Concrete. The concrete was supplied by a local readymix plant and met the Specification of the Texas SDHPT for Class C concrete [34]. The mix had a 28-day design compressive strength of 3600 psi. Two readymix concrete trucks were required to cast the specimen. Concrete from each truck differed slightly in material properties. Seventeen cylinders and nine beams were made at the time of casting, and were tested at various times during the testing period to evaluate strength at each stage. Material test results are presented in Appendix A.

5.2.2 Reinforcing Steel. All conventional steel reinforcement met the requirements of ASTM A-615 Grade 60, and came from a single heat. The average tested yield strength was 73 ksi. Dywidag high strength bars were used for wall post- tensioning. The specified ultimate tensile strength of these bars was 157 ksi.

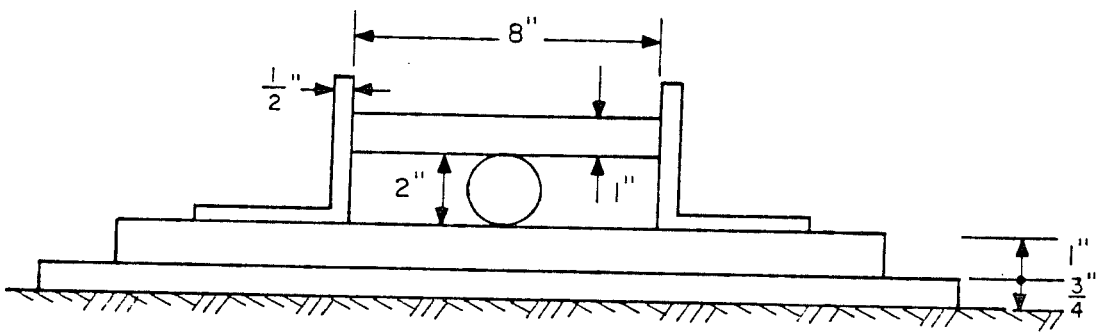

a. Steel detail

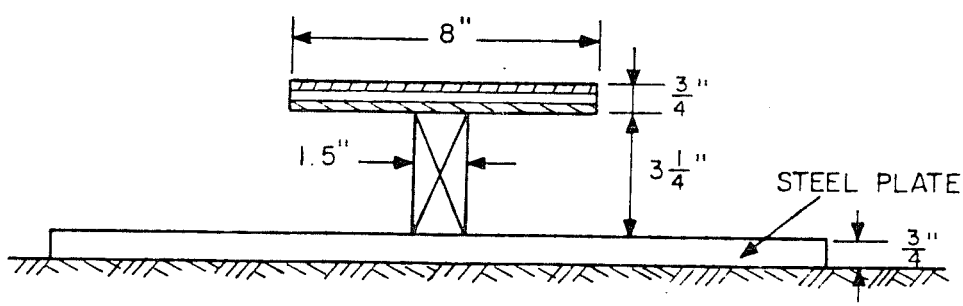

b. Wood detail

Fig. 5.4 Detail of support at bottom of wall

5.2.3 Structural Steel. All structural steel conformed to ASTM A36, with a specified yield strength of 36 ksi and a minimum specified tensile strength of 58 ksi.

5.3 Construction of Test Specimen

The skew bridge specimen was constructed at the Ferguson Structural Engineering Laboratory at the University of Texas at Austin. The first step in the construction was to place the concrete blocks (previously used as test specimens for another project) which would support the exterior girder. Two different levels of blocks were used to raise the specimen to the desired height. The lower blocks were leveled on the floor with hydrostone. The upper blocks were then grouted on top of these bottom blocks using portland cement mortar. The exterior steel girder was then placed on top of the upper concrete blocks. The gap between the upper blocks and the girders was first filled with wooden blocks, and later grouted with portland cement mortar.

Eight- x 4-ft panels were used to form the deck slab between the exterior girder and the wall. The panel forms were donated from a local construction site, and were in good condition. For the cantilever portion of the deck, formwork panels from the previous bridge construction of Project 350 were used. The forms were supported by 2-x 4-in. beams and 4-x 4-in. shores.

Wall formwork consisted of a series of 3/4-in. plywood panels stiffened with vertical 2-x 4-in. studs spaced at 12 in., and three pairs of horizontal 2-x 4-in. wales tightened with form ties at 2-ft intervals. Pin supports for the wall were constructed before placing the formwork and reinforcement. Vertical wall reinforcement was placed on the top of the pin supports. Each post-tensioning duct was positioned at the proper angle and then tied to the wall reinforcement.

Deck reinforcement was supported by slab bolsters to provide the required clear cover, and was secured with wire ties. Strain gages were mounted on the reinforcing bars at the planned locations, and were waterproofed. Wires from the strain gages were marked to identify the corresponding gages, and were routed outside of the specimen through holes in the side forms of the deck.

At the planned load points, 6-in. diameter cans were embedded and tied to the reinforcing bars to act as blockouts for the holes. A third hole was later cored to allow an additional load point in the middle part of the deck.

Concrete was placed using a concrete bucket carried by a overhead crane. The top surface was leveled using a vibrating screed, and then covered with plastic sheets to ensure proper curing.

Wall formwork was removed three days after casting, and the deck formwork was removed after seven days. Surface strain gages were placed at the planned positions, and other instrumentation was mounted before testing (See sections on instrumentation in the next chapter).

CHAPTER 6

TEST PROCEDURE

6.1 Test Sequence

Three series of tests were conducted: 45-degree skew edge tests; 20-degree skew edge tests; and center tests. The load location used for each test series is shown in Fig. 6.1. The center test series was not planned during the development of the specimen, but was added later at the suggestion of the Texas SDHPT contact. The specimen was statically loaded to failure at each loading point. The following sequence of tests was conducted:

1) The 45-degree skew edge was first loaded until visible cracks occurred. It was unloaded, and then re-loaded to 51 kips. This load level caused deck cracks to propagate halfway between the 45-degree skew edge loading point and the central loading point. This load level is also 2.5 times the service live load of 20.8 kips (current AASHTO HS20 truck load, including impact factor).

2) The 20-degree skew edge and then the center were tested as above. The maximum applied load was 60 kips for each test, about 3 times the service live load.

3) The 45-degree skew edge was tested to failure. Crack propagation and test results were carefully examined to ensure that behavior was not significantly affected by previous tests on other parts of the deck.

4) The 20-degree skew edge was loaded to failure.

5) The center was tested to failure.

In each test, test data were scanned at 5- or 10-kip intervals of applied load.

6.2 Loading System

Because previous tests of Project 350 had demonstrated that fatigue loading within these load levels did not significantly affect deck behavior, only static load tests were conducted (Subsection 2.4.3).

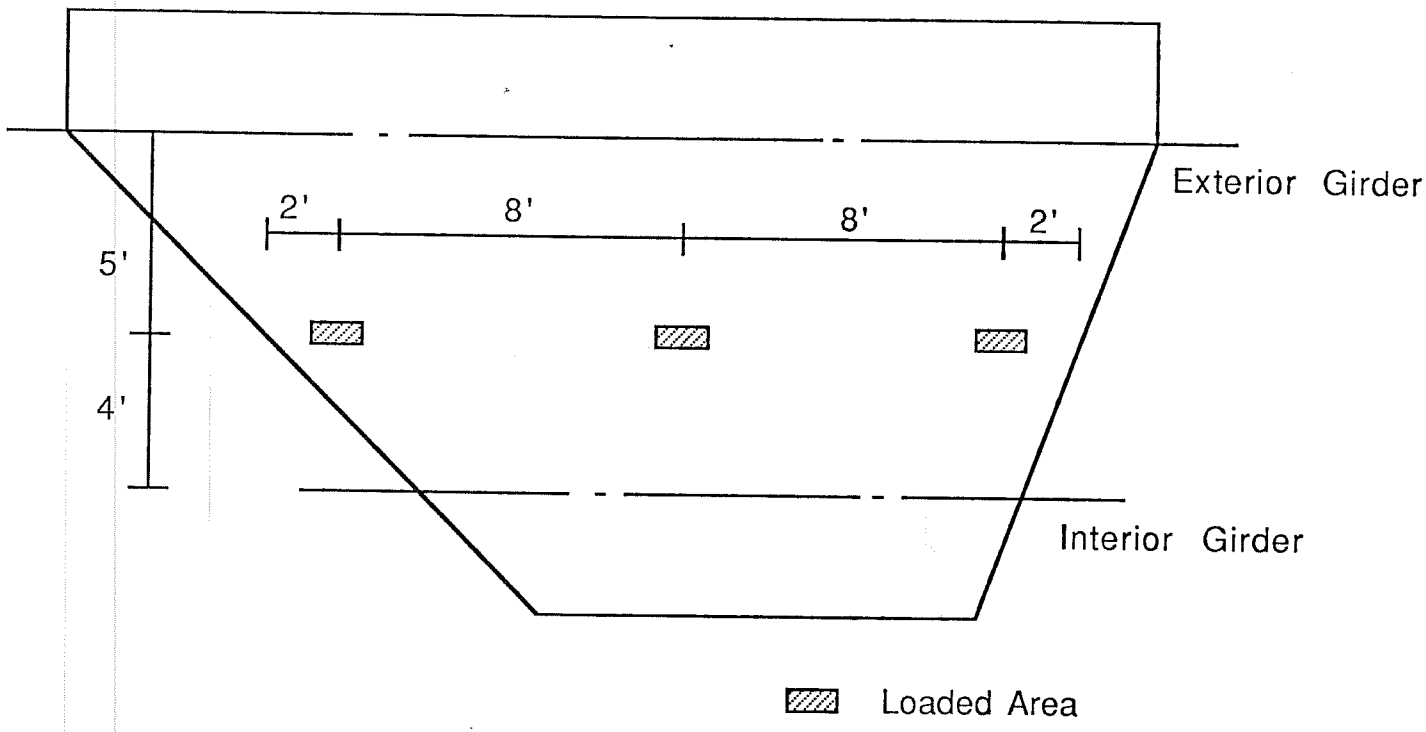

Fig. 6.1 Placement of load

The cross section of the test setup is shown in Fig. 6.2. Test load was applied to the bridge from below by a hydraulic ram. The hydraulic ram was attached at the bottom end to the reaction beam secured to the testing floor, and at the top end, to a connecting rod passing through the hole in the bridge deck and connected to a loading plate on top of the deck. The 8- x 20-in. loading plate simulated the wheel footprint of an AASHTO HS20 truck. Between the ram and the connecting rod, a 300-kip load cell was installed. To reduce ram installation time, supporting frames were built so that the ram and the reaction beam could be moved as a unit from one loading point to the other.

The loading system is shown schematically in Fig. 6.3.

Hydraulic fluid was supplied using a 10,000-psi capacity hand pump.

6.3 Instrumentation

The behavior of the specimen was monitored during the test through instruments located at various points on the test specimen. The desired data were: applied loads; deflections of the deck and horizontal displacements of the specimen; strain of concrete and steel; strain in the bracing; and crack pattern and crack width.

6.3.1 Loads. The applied load was measured three ways: by a 300-kip load cell mounted between the hydraulic ram and the connecting rod; by a 5000-psi pressure transducer mounted between the pump and the ram; and by a 3000-psi pressure gage. Before the first test, the load cell was calibrated using a 600- kip loading machine in the Laboratory. The pressure transducer and pressure gage were calibrated using a dead-weight pressure gage tester. Tests showed that the effects of friction in the ram were negligible compared with the test loads, and the load readings from each instrument agreed very closely.

6.3.2 Displacements. Displacement gages were located as shown in Fig. 6.4. Vertical deflection of the deck at the loading point was measured with a 2-in. linear potentiometer and a 0.001-in. dial gage. Several dial gages were used to measure the vertical displacements of the deck at interior and exterior girders, and also the horizontal displacements there. The linear potentiometer and the dial gages were removed after one edge was tested, and were installed at the other edge for the next test.

6.3.3 Strains. Strains in the deck reinforcement were measured using 6-mm electrical resistance strain gages. Concrete surface strains were measured using 60-mm surface-mounted gages.

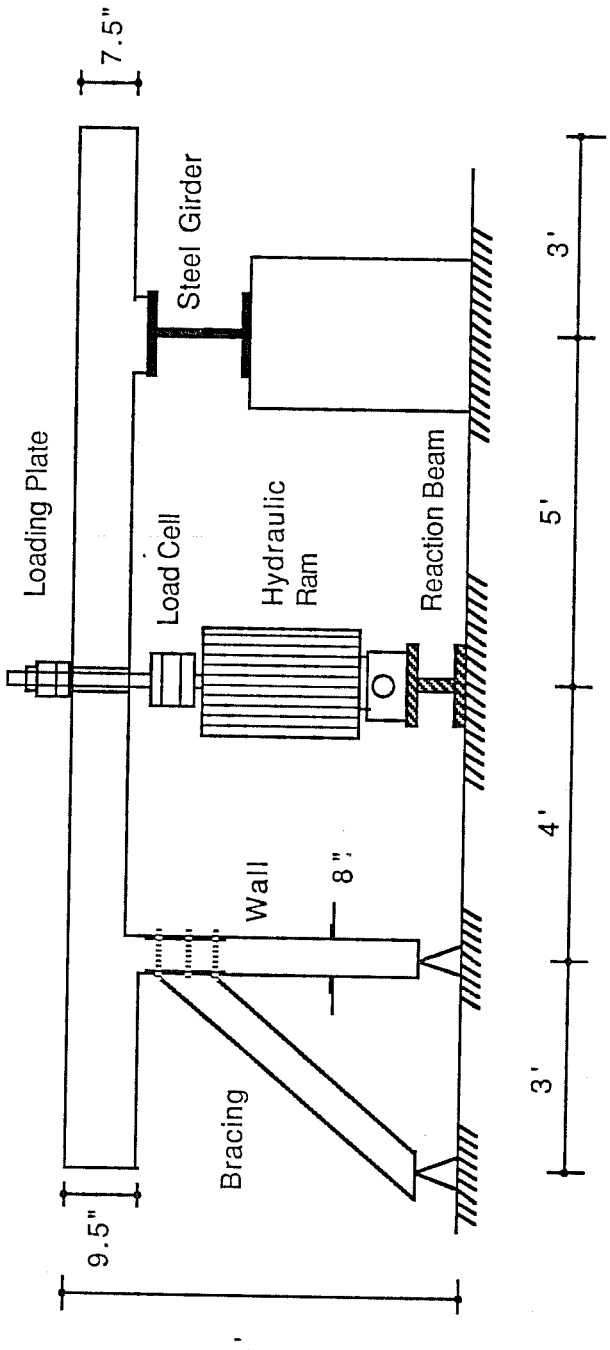

Fig. 6.2 Cross section of test setup

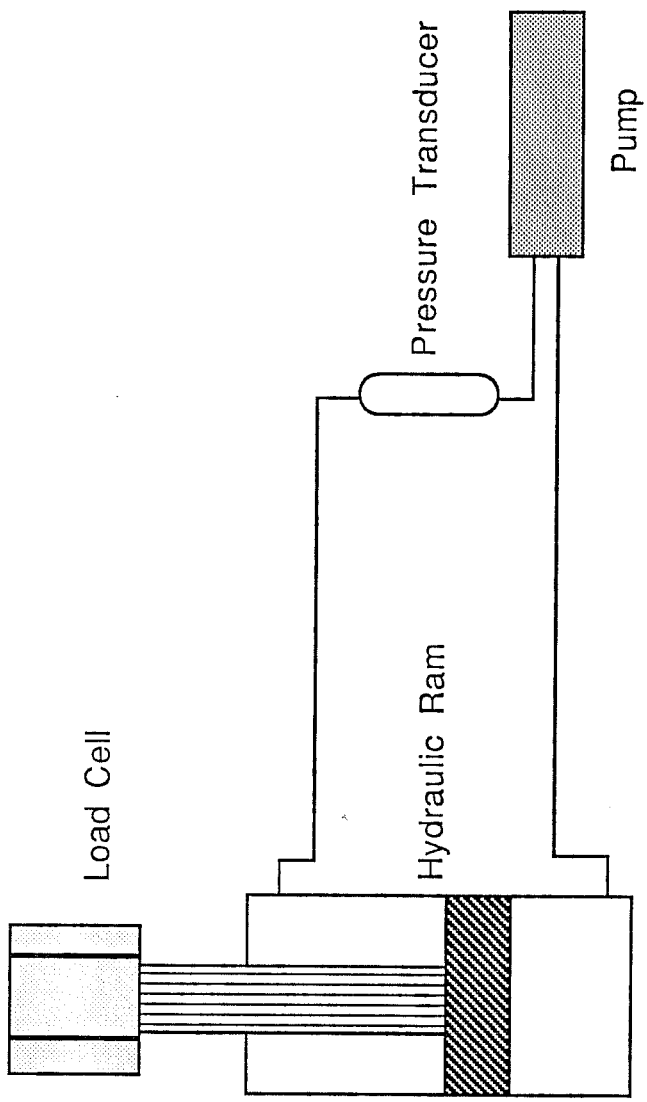

Fig. 6.3 Schematic view of loading system

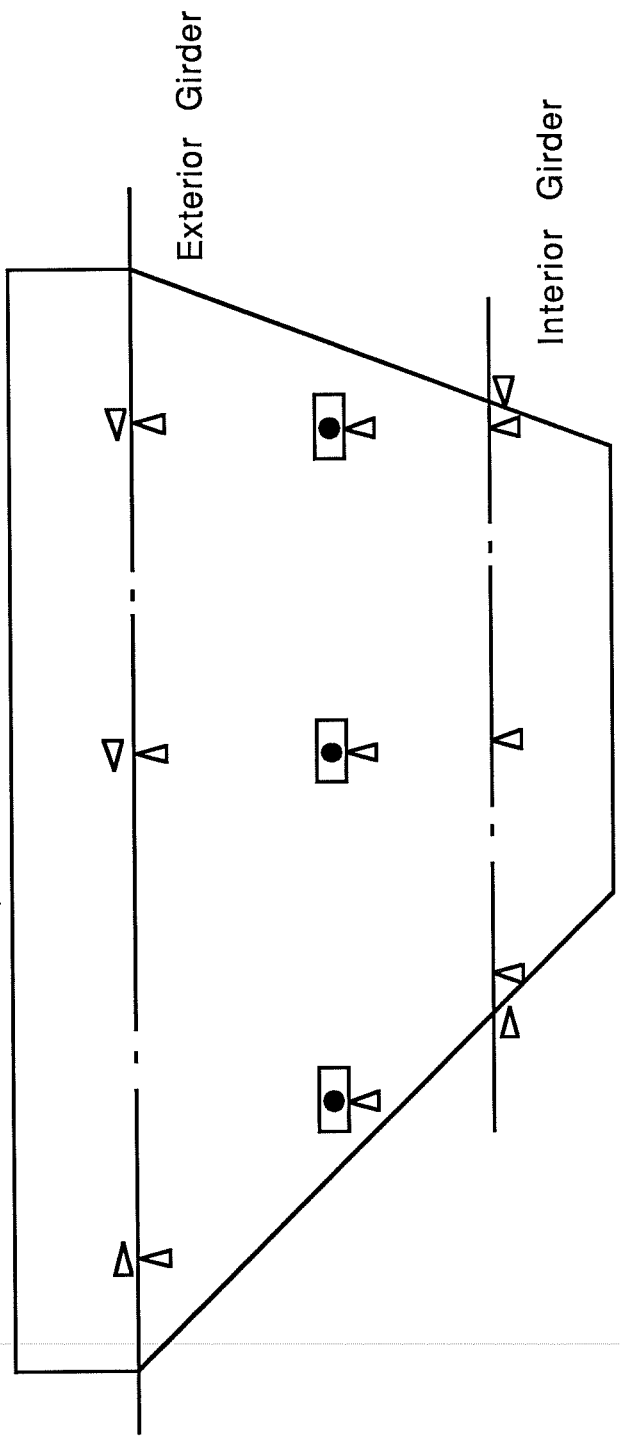

Fig. 6.4 Instrumented locations for deflection measurement

Strain gage locations are shown in Fig. 6.5. To measure the strain gradient, three strain gages were installed at each point: two on the top and bottom reinforcement, and one at the concrete surface on the side of the compression fiber. To record the force in the braces, a 6-mm strain gage was mounted on each bracing member. To provide temperature compensation, three-wire hookups were used for all strain gages.

6.3.4 Cracking of Deck. Careful examination before testing revealed no significant shrinkage cracks on either the top or the bottom faces of the deck. During the tests, crack propagation was recorded at each load level. Crack widths were measured using a crack-width template whose smallest scale is 0.002 in. To show the cracking patterns, photographs were taken during and after testing.

6.4 Data Acquisition

A total of 102 channels of instrumentation were used. Data from the instruments were read and recorded electronically by a digital voltmeter connected to scanners and controlled by a Hewlett-Packard microcomputer. Test data from all 102 channels were read and recorded onto the microcomputer diskette in about 7 seconds, fast enough to avoid any creep-induced variations during scanning. Data were converted to engineering units, printed for immediate review during the test, and also processed later using a microcomputer-based spread sheet program.

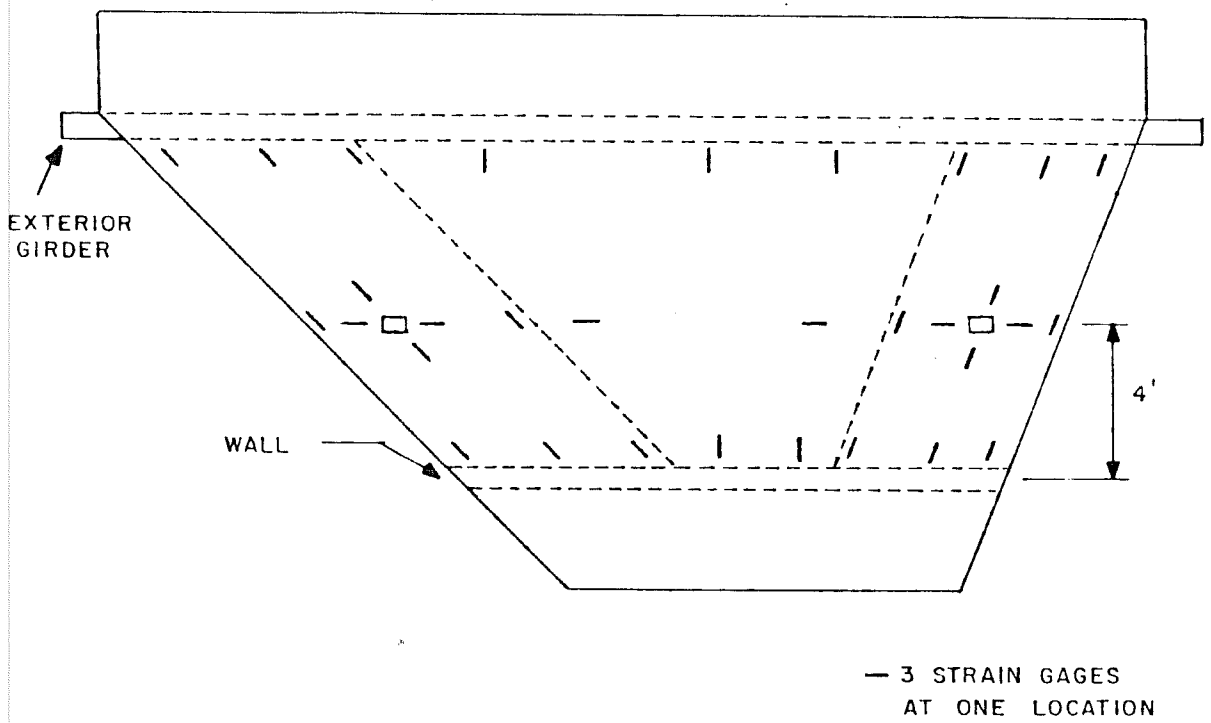

Fig. 6.5 Location of strain gages

CHAPTER 7

TEST RESULTS

7.1 Introduction

As described in Section 6.1, the following sequence of tests was performed on the skew bridge specimen:

1) Overload test on 45-degree skew edge

2) Overload test on 20-degree skew edge

3) Overload test on center

4) Test to failure, 45-degree skew edge

5) Test to failure, 20-degree skew edge

6) Test to failure, center

Results of each test are described below in terms of cracking patterns and load-deflection behavior. Stress-strain results and response quantities derived from these results are discussed in Chapter 8.

7.2 Overload Test on 45-Degree Skew Edge

7.2.1 Cracking Patterns. The final cracking pattern after all overload tests is shown in Fig. 7.1. During the overload test on the 45-degree skew edge, the first deck crack was observed at the bottom surface near the loaded point, and was oriented almost perpendicular to the skew edge of the deck. The cracking load was about 24 kips. The specimen was then unloaded to zero. Upon re-loading to 20.8 kips (AASHTO service-level live load), this crack was about 0.003 in. wide, well below the implied maximum allowable crack widths of Ref. 26 (0.014 in. for interior exposure and 0.01 in. for exterior exposure). As the load increased, the crack propagated to the center part of the bridge, and other cracks developed at the bottom surface. Most bottom cracks propagated perpendicular to the skew edge.

The first crack on the top of the deck occurred at the corner of the deck and the wall, at a load of about 35 kips. Like the bottom cracks, this top crack was oriented perpendicular to the skew edge. As the load increased, the top cracks propagated towards the interior

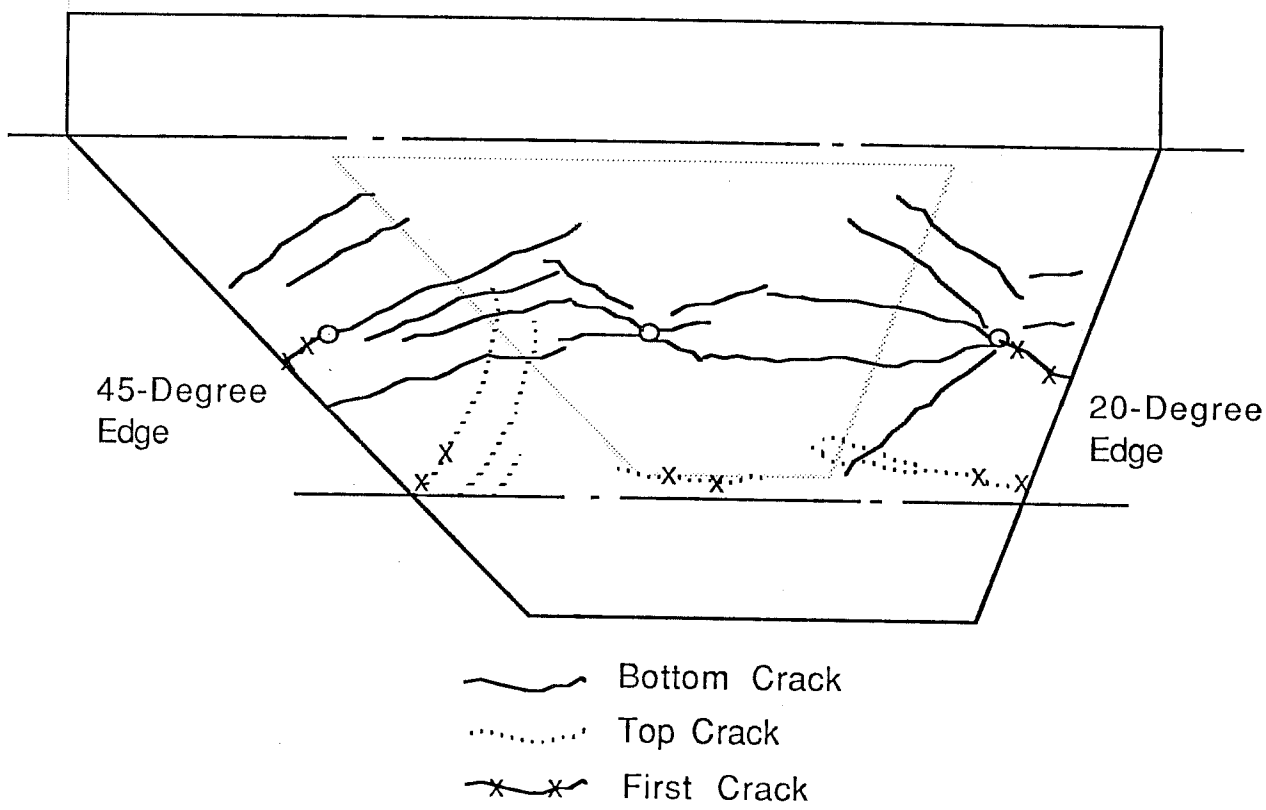

Fig. 7.1 Final cracking patterns in deck after overload tests

support, forming circular arcs around the loaded point. After loading to 51 kips, the specimen was unloaded for the next test at the 20-degree skew edge, since the bottom cracks had extended almost to the center loading point. After unloading, all deck cracks closed almost completely, and the maximum residual crack width did not exceed 0.002 in.

7.2.2 Load-Deflection Behavior. During the test, the relationship between applied load and vertical deflection at the loaded point was monitored using an X-Y plotter. Load-deflection behavior of the specimen was essentially linear up to a load of 30 kips. Beyond this load, slight nonlinear behavior was observed (Fig. 7.2). During the unloading and re-loading procedure, the specimen recovered its deformation well. After the specimen had been subjected to overloads as high as 40 kips, the deflection at the load point was about 0.075 in. under an applied load of 20.8 kips (AASHTO service-level live load). This deflection corresponds to a ratio of deflection to transverse span of 1/2036.

During the test, lateral movement of the specimen was measured by dial gages located at various points. There was no significant lateral movement in either the longitudinal or transverse directions. Movement never exceeded a few thousandths of an inch.

7.3 Overload Test on 20-Degree Skew Edge

7.3.1 Cracking Patterns. The final cracking pattern of this test is shown in Fig. 7.1. Cracking in the deck was first observed at the bottom surface near the loaded point, and occurred at a load level of 25 kips, very close to the cracking load previously observed for the 45-degree skew edge. The crack was oriented almost perpendicular to the skew edge of the deck. As in the 45-degree skew edge test, the specimen was unloaded to zero and then re-loaded. The crack width at a load of 20.8 kips was about 0.003 in., again well below the maximum allowable crack width of 0.01 in. implied by Ref. 26 for exterior exposure. However, the cracks were oriented differently from those of the 45-degree skew edge test. While most of the bottom cracks in the 45-degree skew edge test propagated perpendicular to the skew edge (Fig. 7.1), fan-type bottom cracks developed around the loaded point near the 20-degree skew edge.

For the 20-degree skew edge test, the first top crack was observed at a load of about 35 kips, and was oriented perpendicular to the skew edge, as in the 45-degree skew edge test. However, the top cracks developed less than in the 45- degree skew edge test. The 20-degree skew edge test was stopped at a load level of 60 kips, since

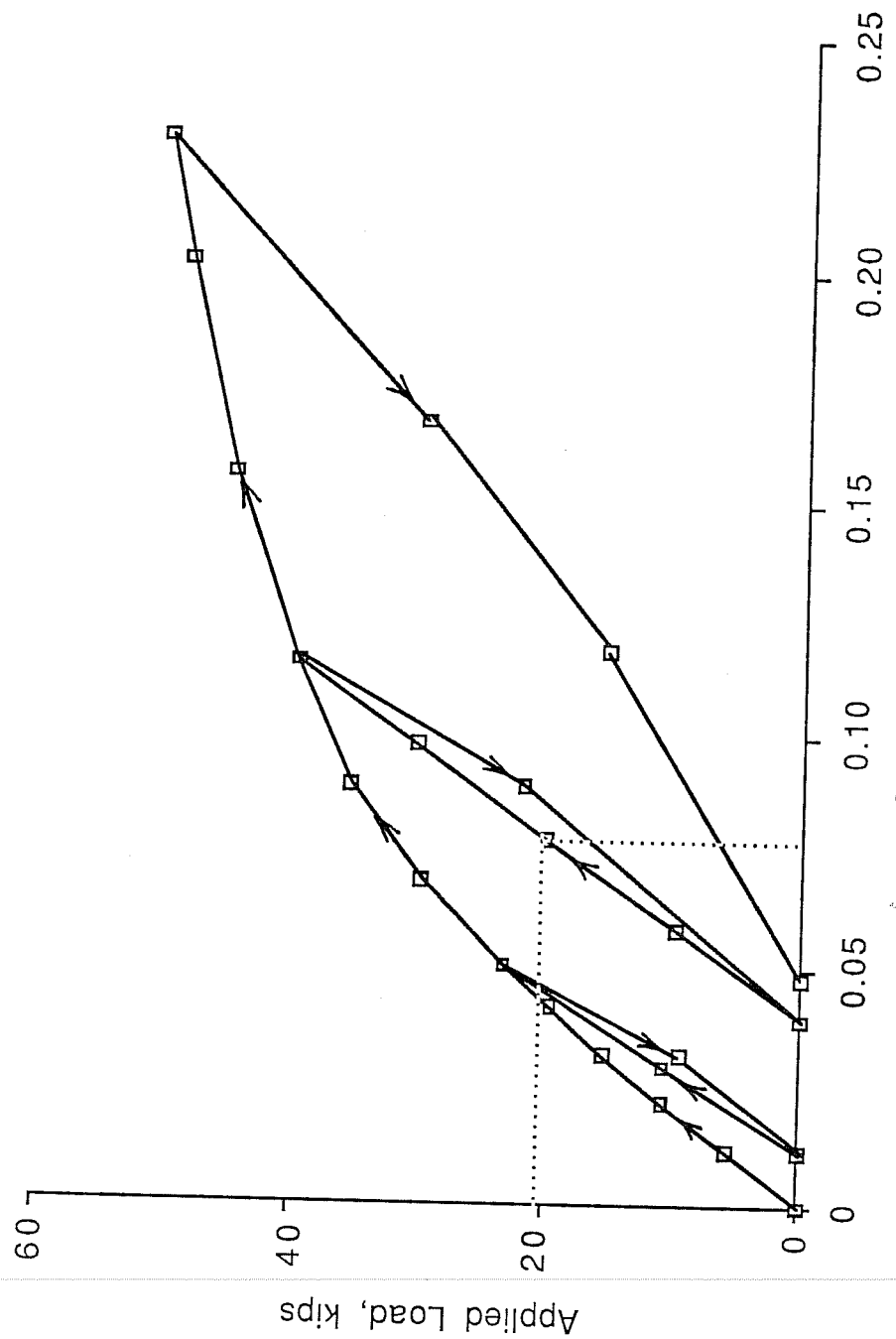

Fig. 7.2 Load-deflection at loaded point, 45-degree edge overload test

some of the bottom cracks had extended almost to the center loading point.

7.3.2 Load-Deflection Behavior. Load-deflection behavior for the 20-degree skew edge test is shown in Fig. 7.3. Behavior of the specimen was essentially linear up to a load level of 35 kips. When re-loaded, the specimen behaved very linearly up to the previous maximum load level, as in the 45- degree skew edge test. After the specimen had been subjected to overloads of 40 kips, the vertical deflection of the loaded point was about 0.045 in. under a subsequent AASHTO service live load of 20.8 kips. This deflection corresponds to a ratio of deflection to transverse span of 1/2565. No significant lateral movement occurred in either the longitudinal or transverse directions.

7.4 Overload Test, Center Portion

7.4.1 Cracking Patterns. The final cracking pattern of this test is shown in Fig. 7.1. It was difficult to measure the first cracking load, since several cracks from the previous tests had already extended very close to the loading point. Under a 25-kip load, a bottom crack occurred and met a nearby crack which had been produced by the 45-degree skew edge test. New cracks from the center test were observed near the loading point at a load of about 40 kips. Thus, first cracking for the center test would probably have occurred at a load level between 25 and 40 kips. As in the previous skew edge tests, the specimen was unloaded to zero and then re-loaded again. At a load of 20.8 kips, the maximum crack width was about 0.002 in., again well below the maximum allowable crack width of 0.01 in. implied by Ref. 7.1 for exterior exposure. The bottom crack orientation was typical of one-way slabs. The first top crack, near the wall and parallel to it, was observed at a load of about 50 kips. Top cracks did not propagate significantly. The test was stopped at a load level of 60 kips, about three times the AASHTO service live load.

7.4.2 Load-Deflection Behavior. Load-deflection behavior for the center test is shown in Fig. 7.4. Behavior of the specimen was fairly linear up to 60 kips. After the specimen was subjected to overloads as high as 40 kips, the deflection at the loaded point was about 0.032 in. under a subsequent AASHTO service live load of 20.8 kips. This deflection corresponds to a ratio of deflection to transverse span of 1/3375. No significant lateral movement occurred in either the longitudinal or transverse directions.

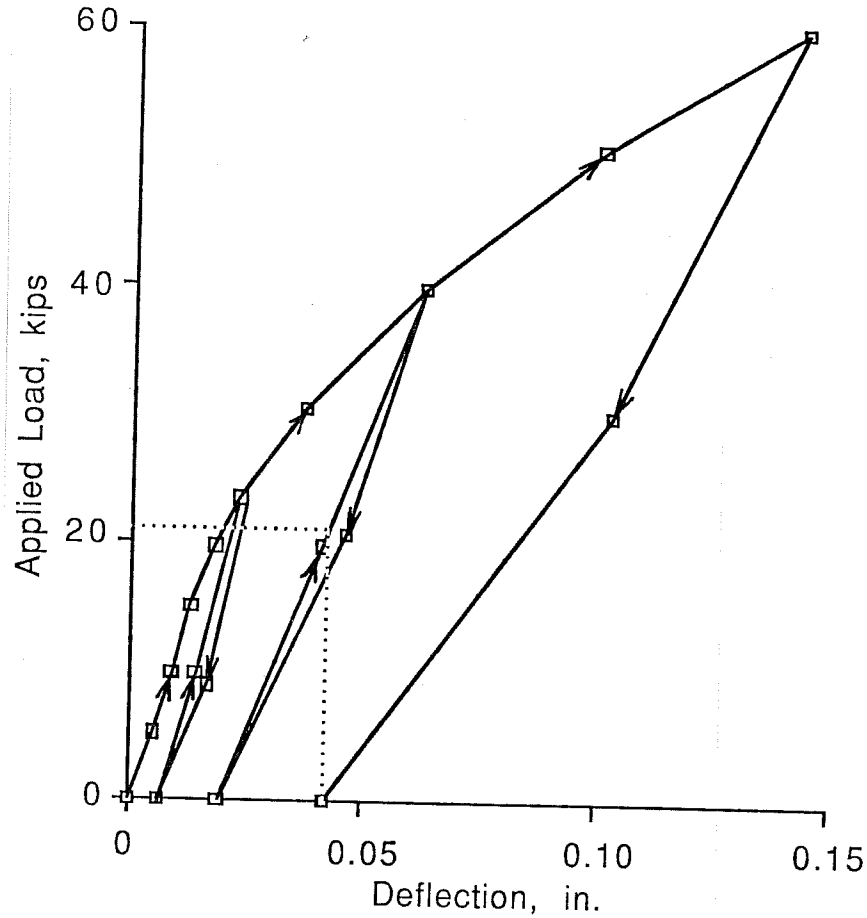

Fig. 7.3 Load-deflection at loaded point, 20-degree edge overload test

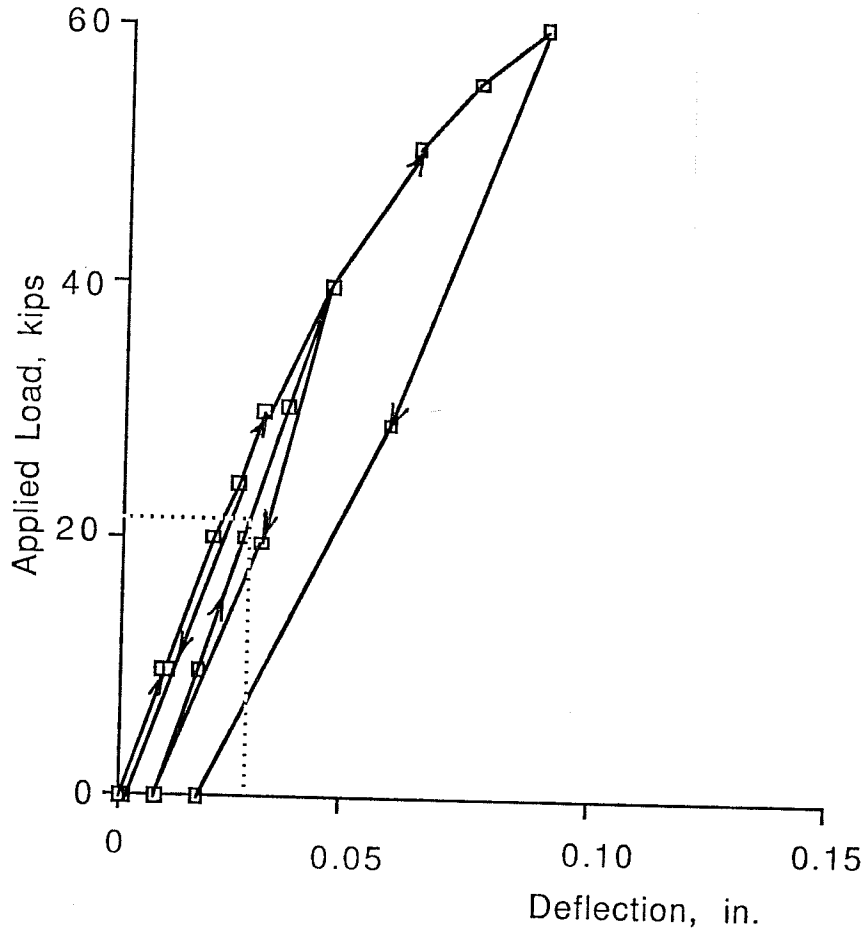

Fig. 7.4 Load-deflection at loaded point, center overload test

7.5 Test to Failure, 45-Degree Skew Edge

The specimen was then tested to failure using monotonically increasing load at the 45-degree skew edge. As the load increased, numerous cracks developed at the bottom of the deck. Most cracks propagated perpendicular to the skew edge. Several bottom cracks propagated as far as the 20- degree skew edge. Top cracks propagated up to the cantilever portion at the interior support, forming circular arcs around the loaded point. As the load increased, top cracks developed from outside to inside: at low load levels, the first top crack developed far from the loaded point; as the load increased, new top cracks developed closer to the loaded point. At a load of 80 kips, diagonal cracks (apparently due to shear) formed at the edge of the deck near the wall. Also, a bottom crack developed in the longitudinal direction at the corner of the wall and the deck. This region was subjected to flexural compression perpendicular to the crack.

Near failure, the diagonal cracks opened to about 1/8 in. wide. The deck failed suddenly by shear near the wall at a load of 97 kips, about 4.7 times the AASHTO service live load. The shear crack was inclined at about 40 degrees from the horizontal, and the failure surface extended to about 4 ft from the edge in the longitudinal direction. The final cracking patterns after all tests are shown in Figs. 7.5 and 7.6.

The deck behaved very linearly up to the previous maximum test load level of 51 kips. Beyond this load level, nonlinear behavior was observed (Fig. 7.7). The specimen exhibited some flexural yielding before failing in shear.

7.6 Test to Failure, 20-Degree Skew Edge

As in the 45-degree skew edge test described above, the specimen was loaded monotonically to failure.

Numerous cracks developed in the bottom of the deck as the load increased. Most cracks propagated to form a fan-type cracking pattern around the loaded point. Many bottom cracks met the cracks which had been formed in the previous 45-degree skew edge test. Top crack propagation was almost identical to that observed for the 45-degree skew edge test. Unlike the 45-degree skew edge test, however, no diagonal shear crack developed before failure. The deck failed very suddenly by shear near the wall at a load of 139 kips, about 6.6 times the AASHTO service live load. The shear crack was inclined at about 30 degrees from the horizontal, and the failure surface extended longitudinally about 40 in. from the 20-degree skew

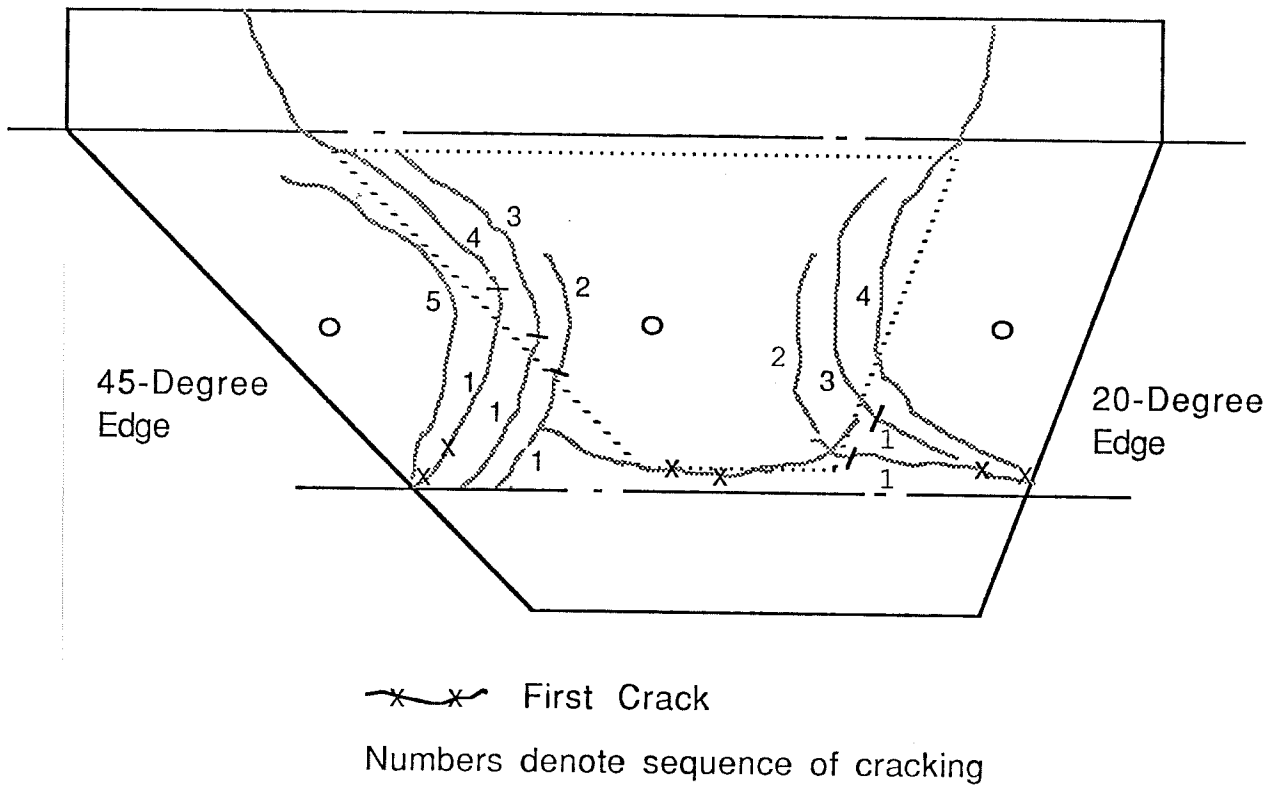

Fig. 7.5 Deck top cracking after failure tests

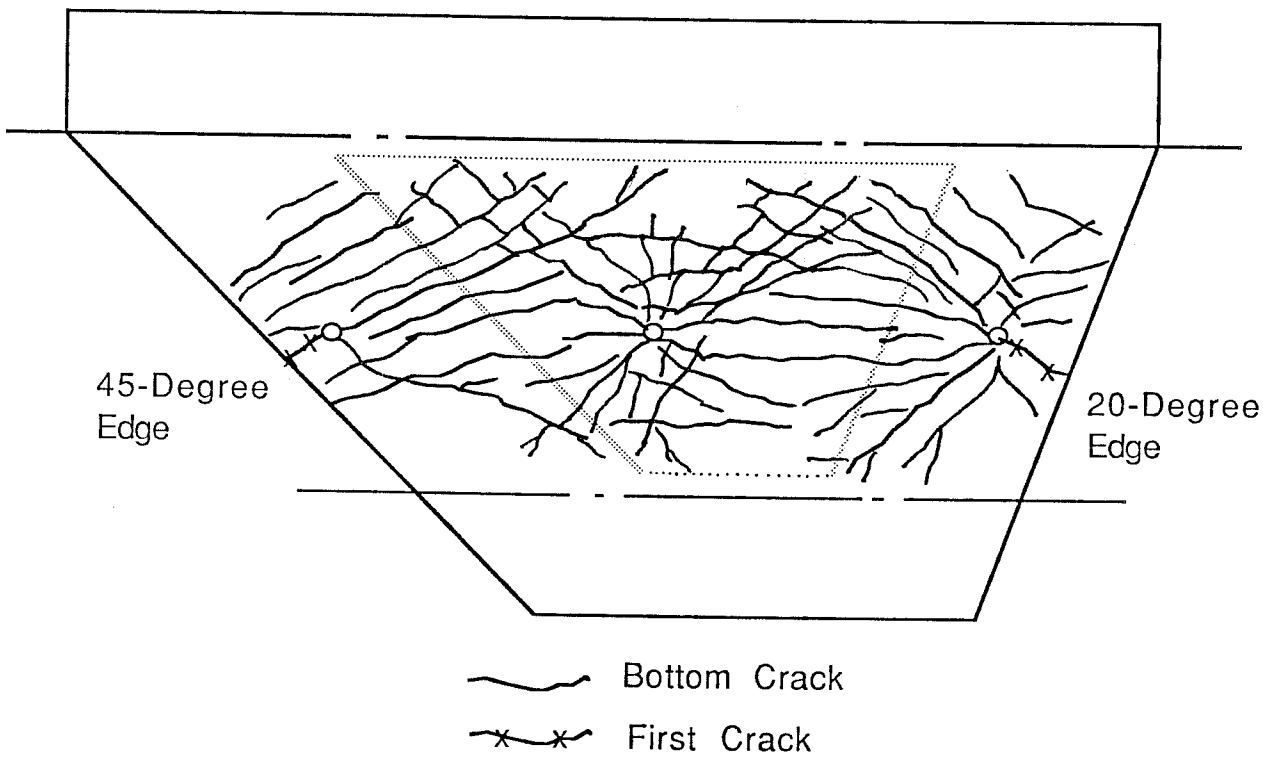

Fig. 7.6 Final cracking pattern on bottom surface after tests to failure

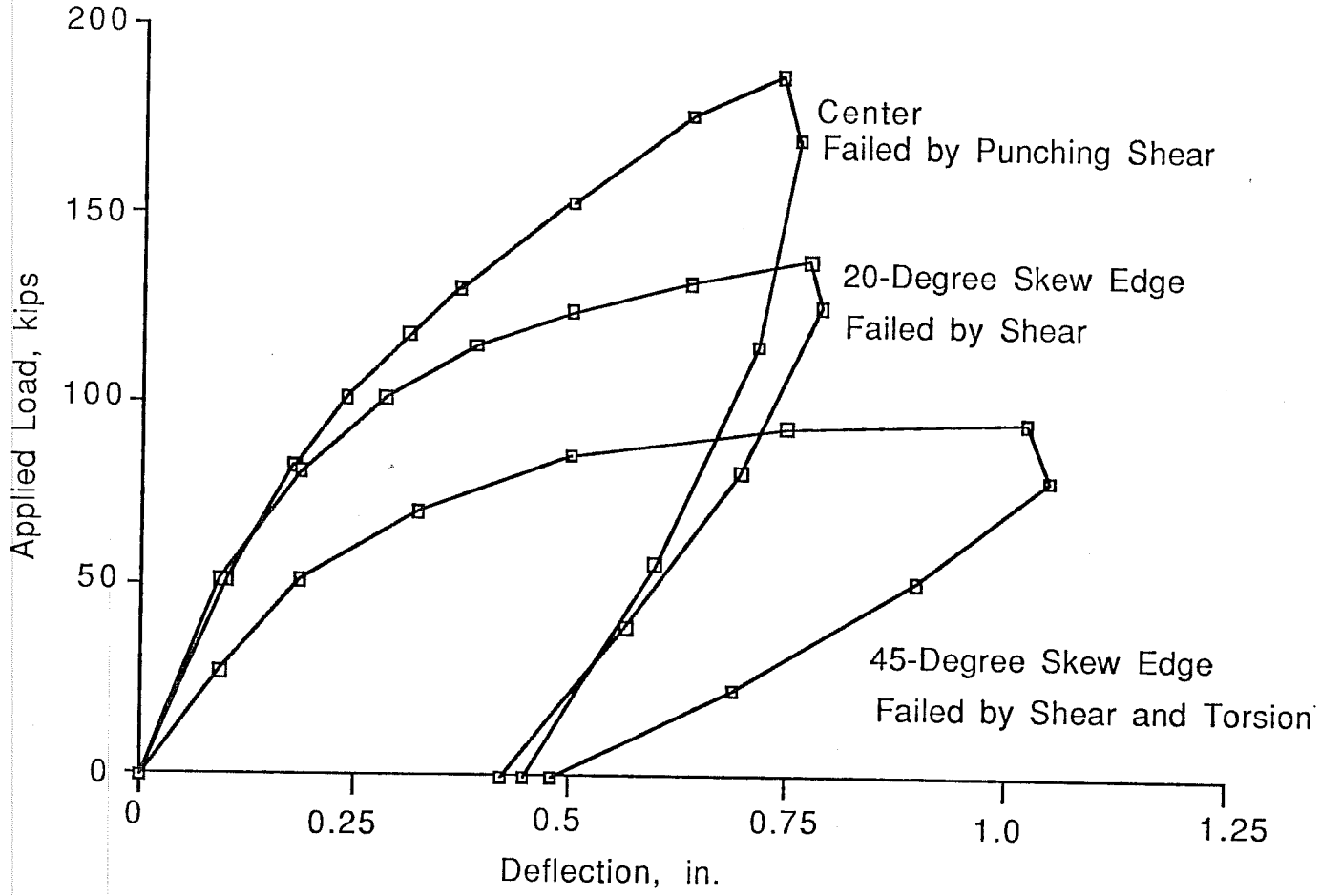

Fig. 7.7 Load-deflection relationships at loaded points, tests to failure

edge. The cracking patterns of the top and bottom surfaces of the deck at failure are shown in Figs. 7.5 and 7.6 respectively.

The deck behaved very linearly up to the maximum previous test load of 60 kips. After that, load-deflection behavior of the deck was nonlinear, but less so than for the 45- degree skew edge test (Fig. 7.7).

7.7 Test to Failure, Center Portion

Finally, the central portion of the bridge was tested monotonically to failure.

Numerous cracks had already developed in the bottom of the deck from the previous tests. As the load increased, many new cracks propagated across the previously formed cracks. Several bottom cracks propagated to the skew edges. Top cracks which had developed in the previous overload test extended as the load increased. However, fewer top cracks were developed than in the skew edge tests. Spalling of the bottom deck surface occurred just before the deck failed. The deck failed very suddenly by punching shear around the loaded point at a load of 179 kips, about 8.6 times the AASHTO service live load. The failure surface was inclined at about 30 degrees from the horizontal. The cracking patterns of the top and bottom surfaces of the deck at failure are shown in Figs. 7.5 and 7.6 respectively.

As shown in Fig. 7.7, little nonlinear behavior was observed during this test. Apparently, the deck's flexural capacity far exceeded its capacity in punching shear (Fig. 7.7).

7.8 Summary of Test Results

In tests conducted at each edge, the first bottom crack occurred at a load of about 25 kips, and the first top crack, at about 35 kips. In the center, first cracking occurred at a load of about 30 kips on the bottom surface of the deck, and about 50 kips for the top. Bottom cracks near the 45-degree skew edge were primarily oriented perpendicular to the edge. Near the 20- degree skew edge and in the center, fan-type bottom cracks developed. Top cracks propagated in circular arcs around each edge loading point, but no significant top cracking occurred from the center test. Crack widths at service load levels were much smaller than the implied maximum allowable crack width of Ref. 26, even after the deck had been severely cracked by prior overload tests.

The specimen behaved very linearly beyond the service live load level. More nonlinear behavior was observed in the skew edge tests than in the center test, especially in the 45- degree skew edge. The 45-degree skew edge was most flexible, while the center was stiffest. The center portion of the deck behaved almost linearly to failure.

The deck failed by shear near the wall at each skew edge, and by punching shear at the center. All failures occurred very suddenly.

CHAPTER 8

DISCUSSION OF TEST RESULTS AND ANALYSIS

8.1 General

In the previous chapter, test results were presented. In this chapter, test results are discussed and compared with analysis results. Strains at the concrete surface and in the reinforcement were used to calculate stresses in concrete and reinforcement at various locations, the strain profile through the deck, and the moments and in-plane membrane forces in the deck. The test specimen was analyzed using the techniques discussed in Chapter 2, and these analytical results were compared with experimental observations.

8.2 Overall Behavior

Load-deflection relationships from overload tests as well as analyses are shown in Fig. 8.1. Analytically predicted deflections agreed very well with measured values. As expected, the 45-degree skew edge was most flexible, while the center was stiffest. In each test, some nonlinear behavior of the deck was observed after first cracking. More nonlinear behavior was observed at the edges than the center of the deck, even though the edges had been stiffened by increasing the slab thickness. Behavior of the center seemed to be affected by the presence of the edges, because in the previous tests of Project 350, the deck had behaved almost linearly up to 3 times the service live load [14].

Under the service-level live load of 20.8 kips, deck deflections were very small: 0.075 in. (1/2036 of transverse span) for the 45-degree skew edge; 0.045 in. (1/2565 of transverse span) for the 20-degree skew edge; and 0.032 in. (1/3375 of transverse span) for the center. These deflections were measured after the specimen had been previously loaded up to about 40 kips, approximately twice the service live load (Figs. 7.2 to 7.4).

Load-deflection relationships for tests to failure are shown in Fig. 8.2. The 45-degree skew edge failed by combined shear and torsion near at the interior support (wall); the 20- degree skew edge failed by shear; and the center location failed by punching shear. The 45-degree skew edge behaved very nonlinearly. Behavior of the center was more nearly linear to failure. Behavior of the 20-degree

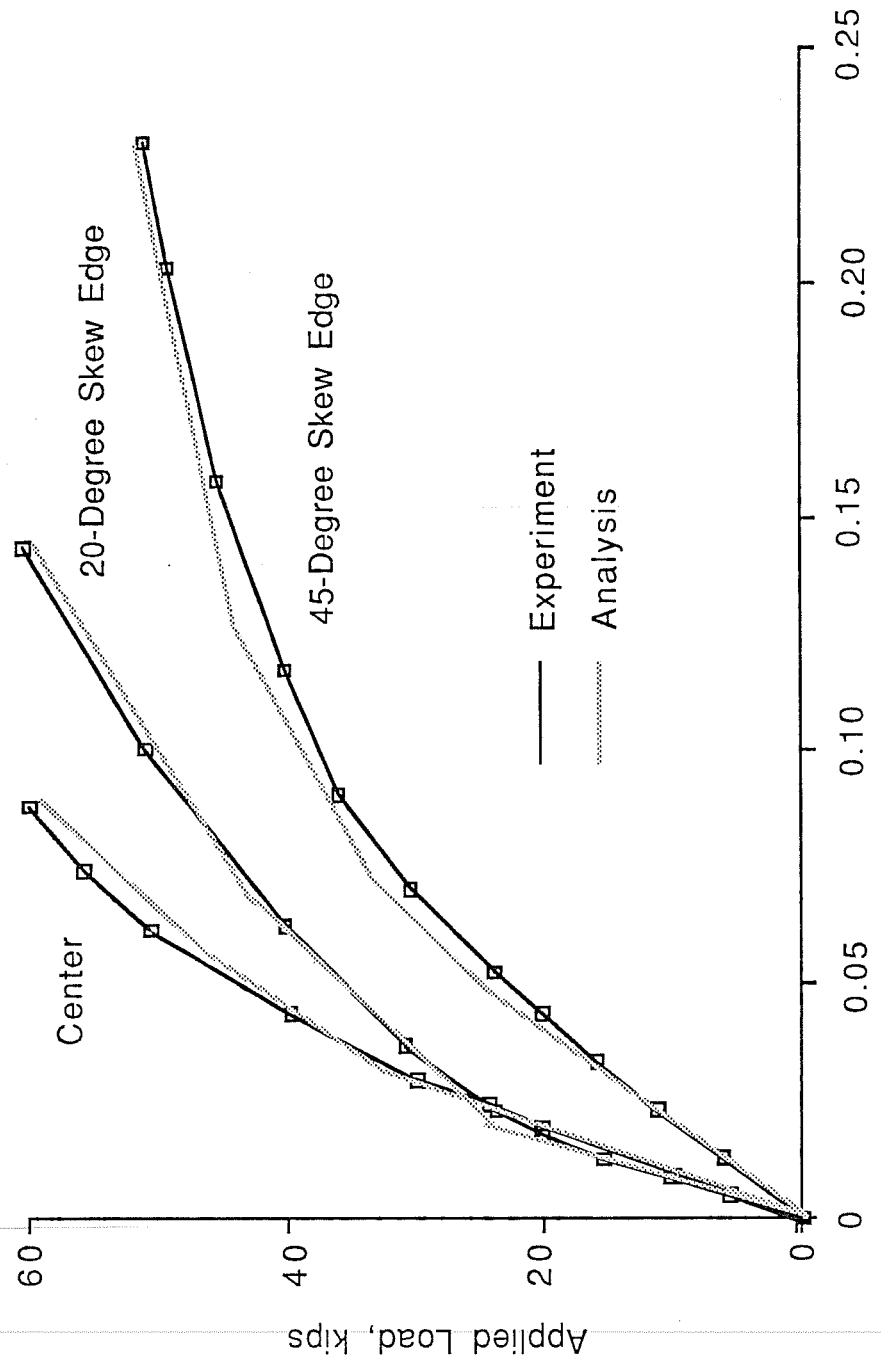

Fig. 8.1 Load-deflection relationships at loaded points, overload tests

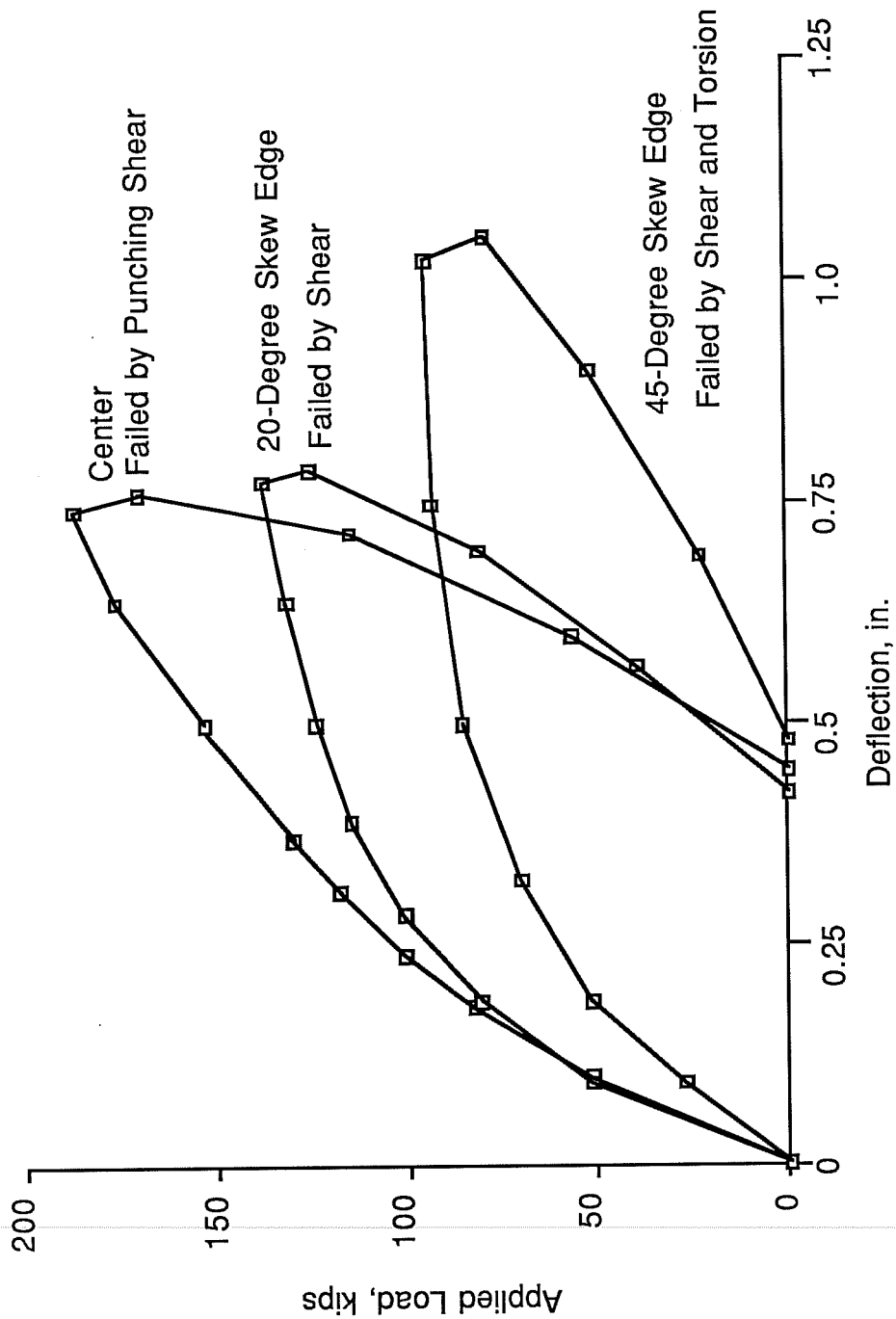

Fig. 8.2 Load-deflection relationships at loaded points, tests to failure

skew edge was between that of the 45- degree skew edge and the center as shown by the load deflection curves in Fig. 8.2.

The cracking patterns are shown in Figs. 8.3 and 8.4. The first bottom crack direction at each edge was almost perpendicular to the edge. This implies that the principal tensile stress is oriented parallel to the skew edge, and that using the skew span length is reasonable in the design of skew bridge decks.

After the overload tests, crack propagation at the 45- degree skew edge was different from that at the 20-degree skew edge. At the 45-degree skew edge, most bottom cracks propagated perpendicular to the edge. However, many fan-type cracks were found at the bottom of the 20-degree skew edge. This implies that beam-type behavior was dominant at the 45-degree skew edge, while there was combination of beam action and slab action at the 20-degree skew edge. Crack propagation at the center was typical of a slab with a concentrated load. At each edge, top cracking consisted of a series of arcs around each loaded point.

8.3 Transverse and Longitudinal Moments in Deck

8.3.1 Computation of Moments from Experimental Data. As noted in Chapter 6, three strain gages were installed at many key locations to measure strain gradients. Some of the strain gradients obtained from test results were not linear, and best- fit lines were used to obtain the linear strain gradients. When one of the three gage readings was found to be erratic, a linear strain gradient was assumed between the two remaining gages.

Based on these linear strain gradients, the corresponding moments were calculated. Concrete was assumed to be cracked, and to carry zero stress, if its tensile strain exceeded the cracking strain of $7.5\sqrt{f'_c}/E_c$. The elastic modulus of concrete E_c was calculated using the secant formula of the ACI Code [2]. Once the stresses in concrete and reinforcement had been calculated, the axial force and bending moment were obtained by equilibrium of the cross section, using the middle surface of the deck as a reference.

8.3.2 Computation of Moments from Analytical Results. As discussed in Subsection 2.4.2, the bridge deck was modeled using two layers of thick shell elements. In each analysis, stresses were requested at the middle of the top and bottom faces of each element. Because the stress output for such points is obtained by extrapolating from stresses inside the element, it is possible to get slightly

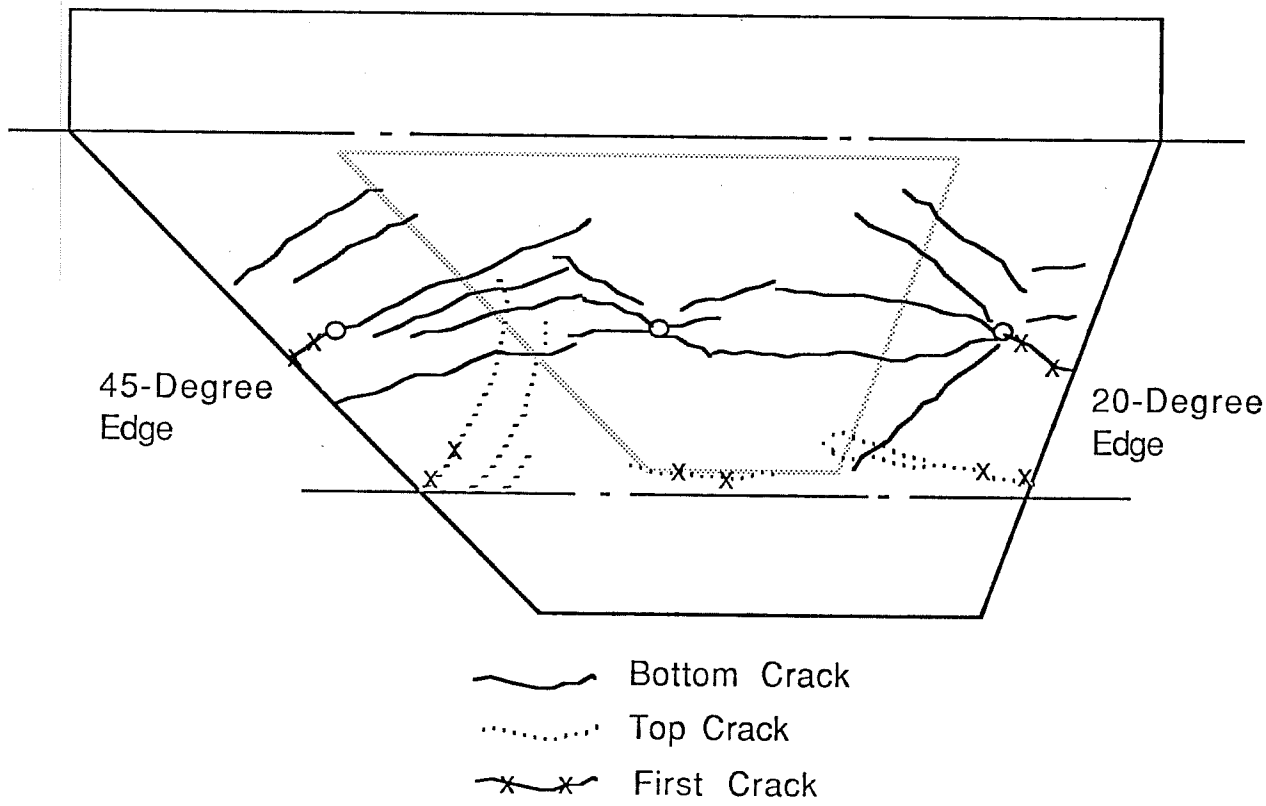

Fig. 8.3 Cracking patterns in deck after overload tests

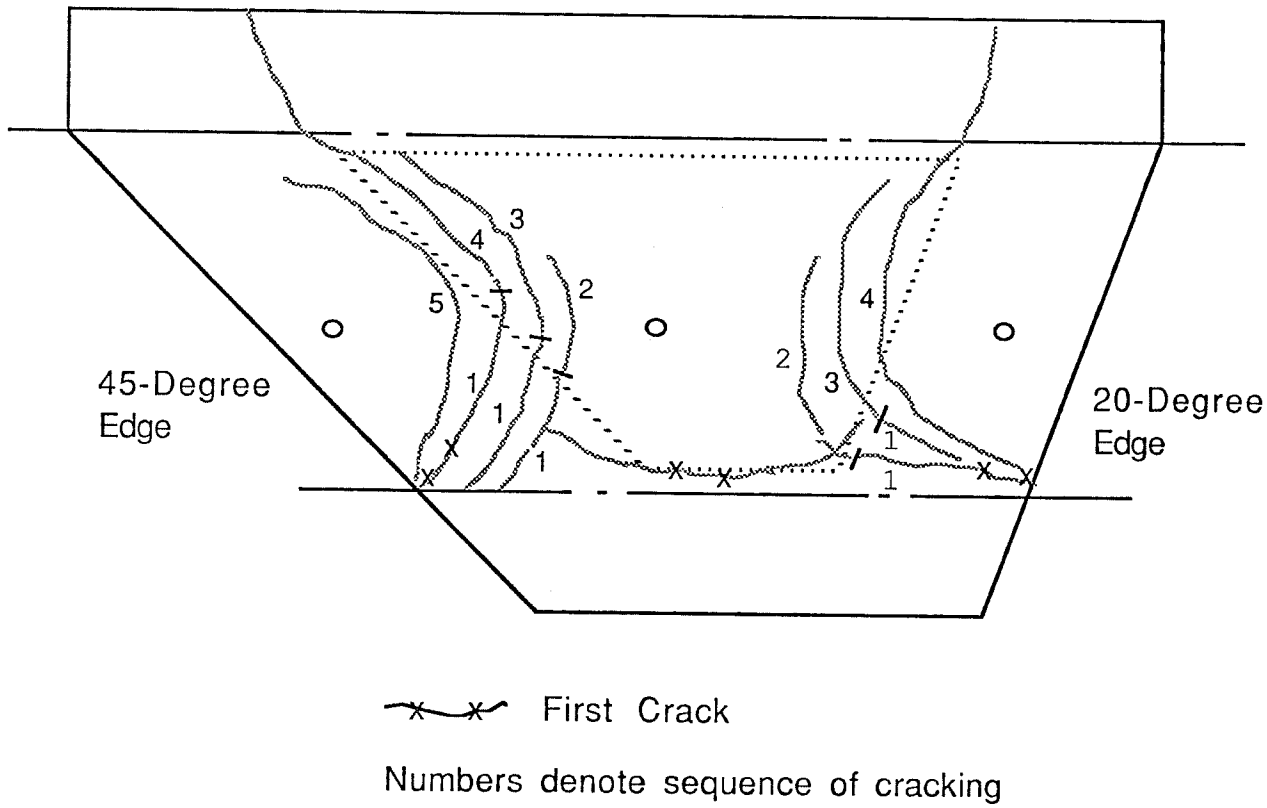

Fig. 8.4 Deck top cracking after failure tests

different calculated stresses at the same point on the interface between the two layers. As shown in Fig. 8.5, in this situation the strain gradient was computed assuming a linear variation between the values on the top and bottom surface of the deck. The interface strains computed using this procedure were always very close to the average of the strain values at the interface. Once the strain values had been computed, the axial force and moment were computed by equilibrium, again using the middle surface of the deck as a reference.

8.3.3 Distribution of Transverse and Longitudinal Moment. In Figs. 8.6 through 8.9, transverse moments calculated from test results are compared with analytical results. In those figures, two calculated values are presented: one from the full skew bridge model; and the other from the test specimen. The experimental and both calculated values agree closely. The negative transverse moment at the interior support was small compared with the positive transverse moment at the midspan of the deck before cracking, and it increased after cracking.

Longitudinal moments calculated from test results were compared with analytical results, as shown in Figs. 8.10 through 8.13. The experimental and calculated values again agree closely. The longitudinal moment decreased very quickly away from the load. At a distance of about 5 ft from the loaded point, longitudinal moments were negligible.

8.4 Compressive Membrane Force

In-plane transverse forces were calculated along with the moments. Using these computed forces, the distribution of transverse membrane force per unit width along the interior girder was plotted, as shown in Figs. 8.14 and 8.15. Analytical and experimental results agree reasonably well. A non-skew bridge with the same span and deck thickness as the skew bridge was analyzed with edge loading, and the transverse membrane forces are shown in Fig. 8.16. Comparing the results of non-skew and the skew bridges, the maximum intensities of the compressive membrane forces are approximately equal. This implies that there is little difference in the presence of arching action between skew and non-skew bridges.

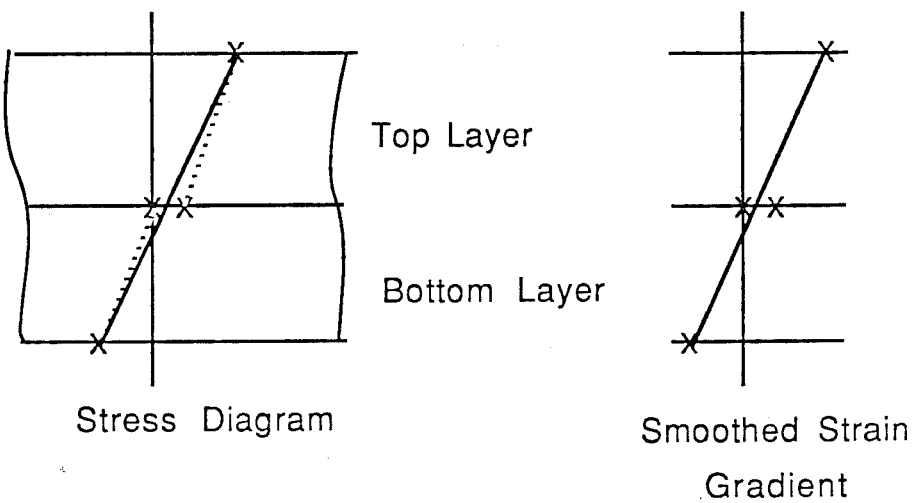

Fig. 8.5 Procedure used to obtain strain gradient from analytical model

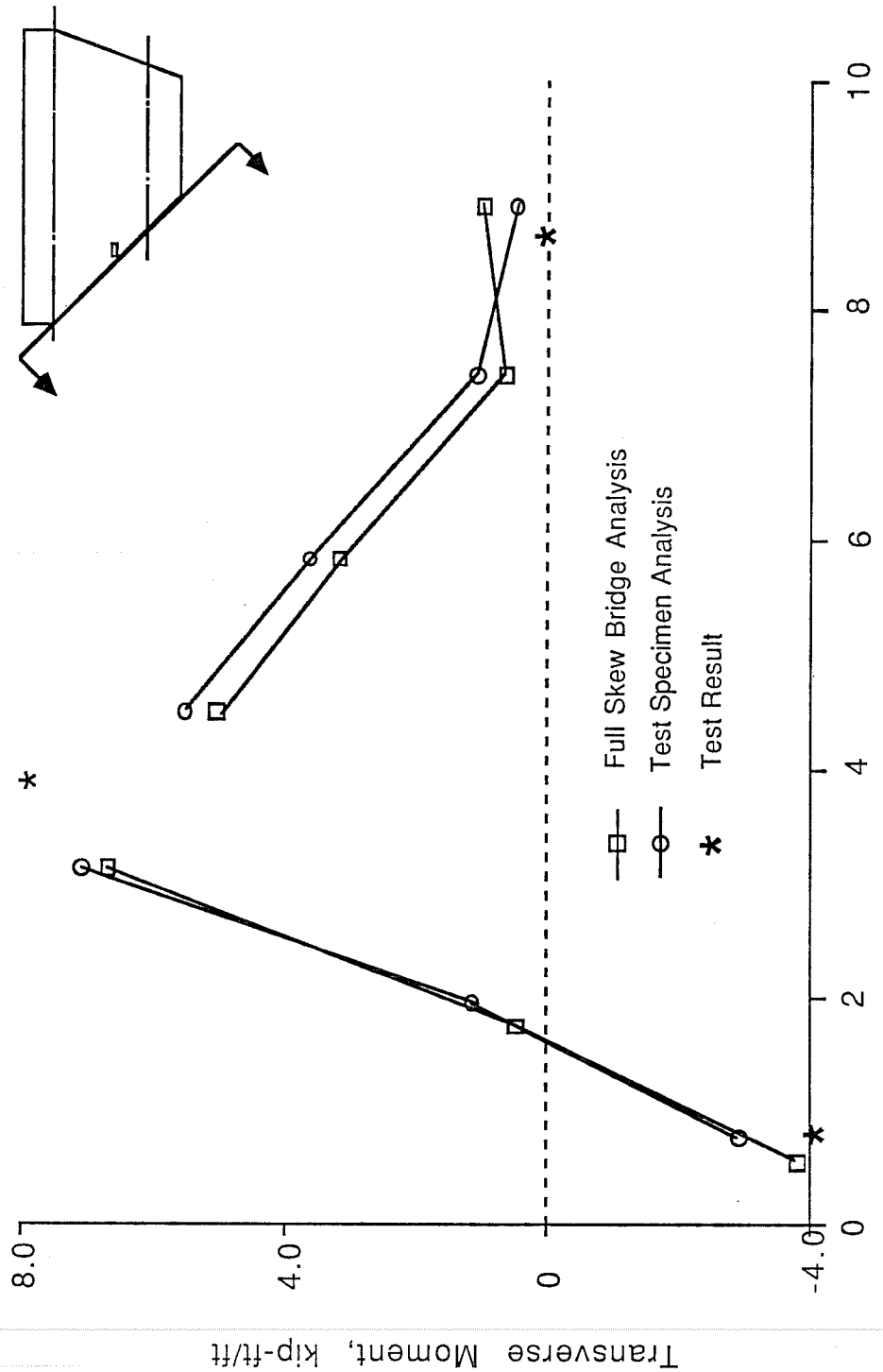

Fig. 8.6 Transverse moments along 45-degree skew edge (before cracking, P = 20 kips)

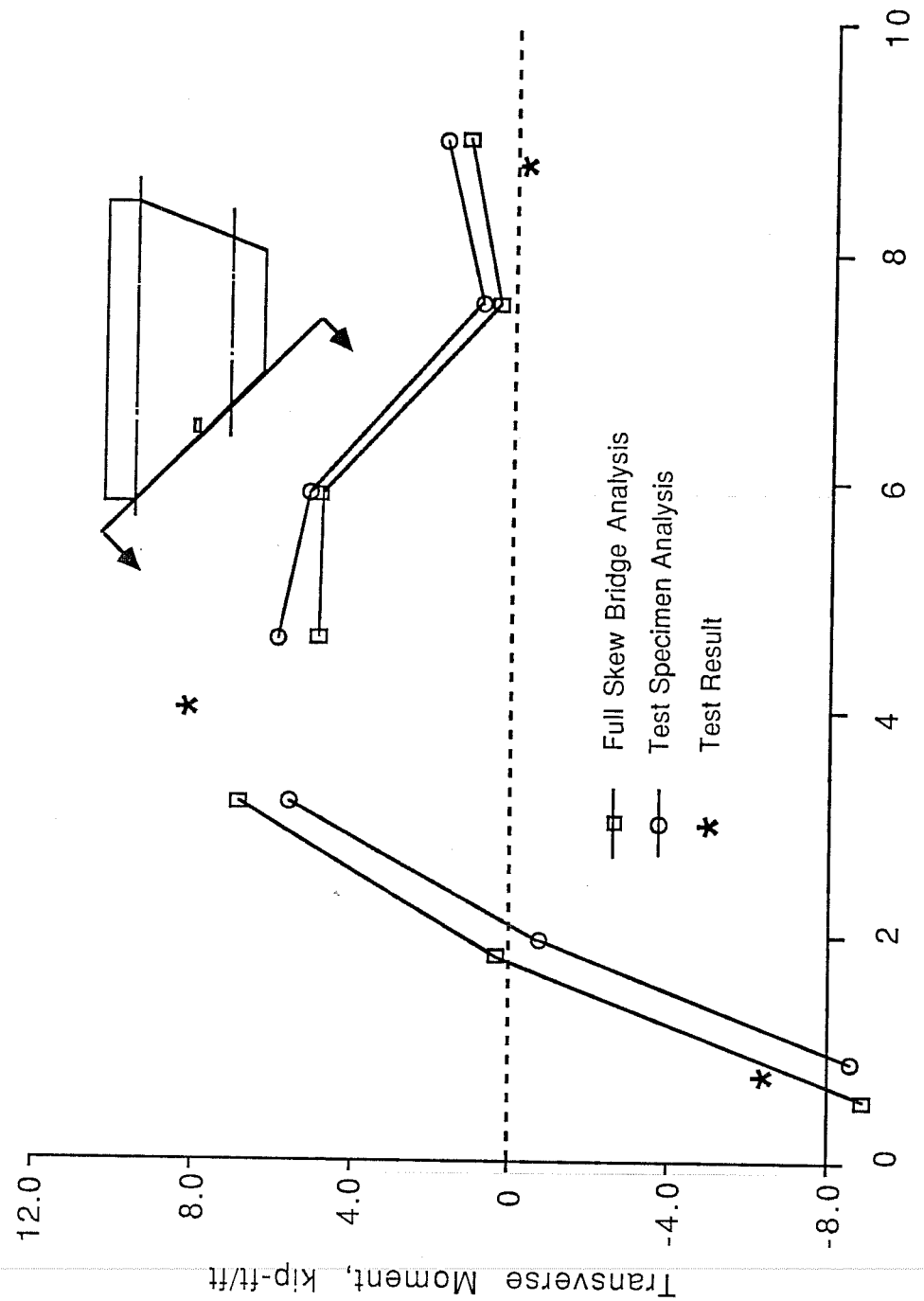

Fig. 8.7 Transverse moments along 45-degree skew edge (after cracking, P = 40 kips)

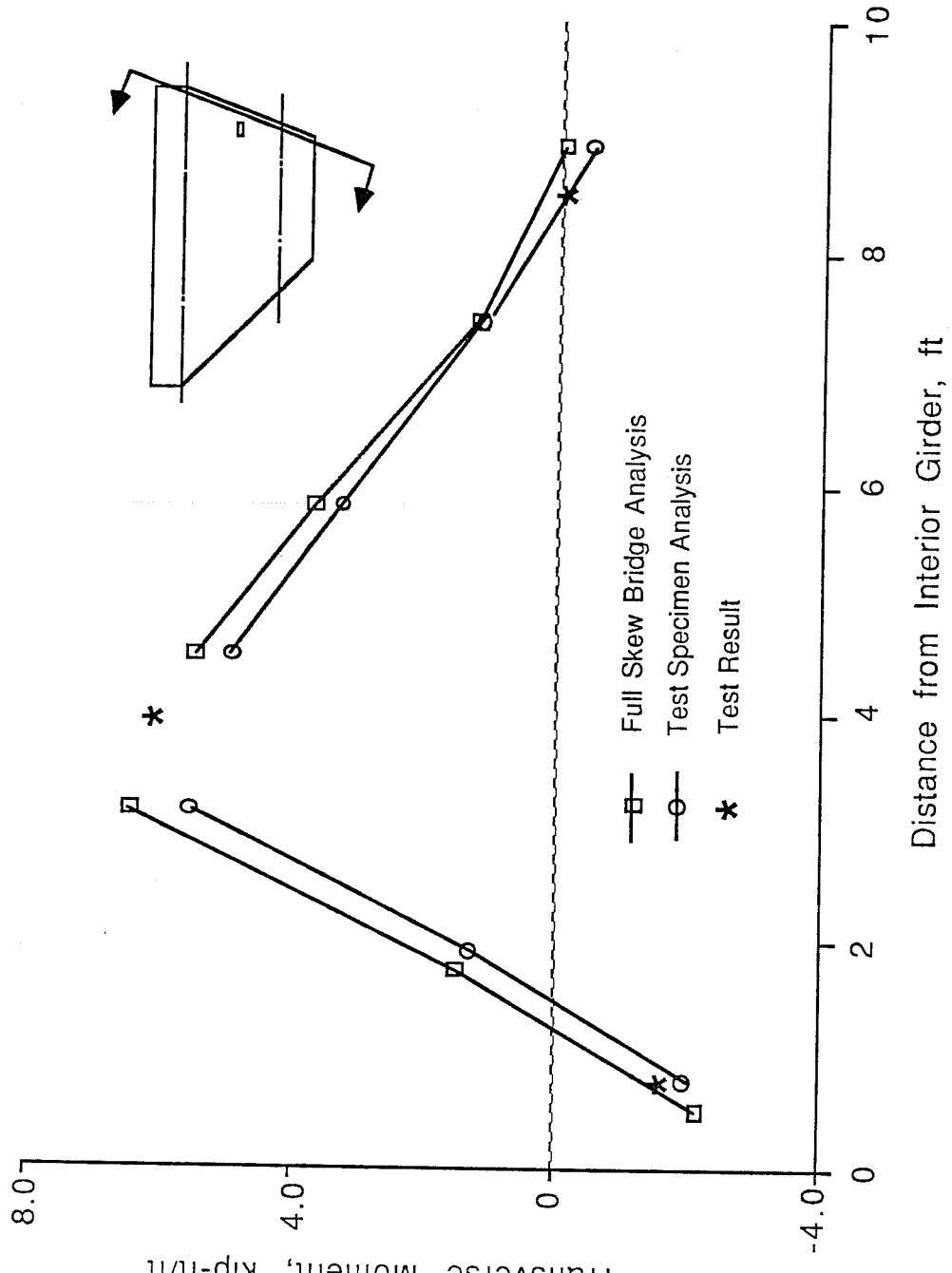

Fig. 8.8 Transverse moments along 20-degree skew edge (before cracking, P = 20 kips)

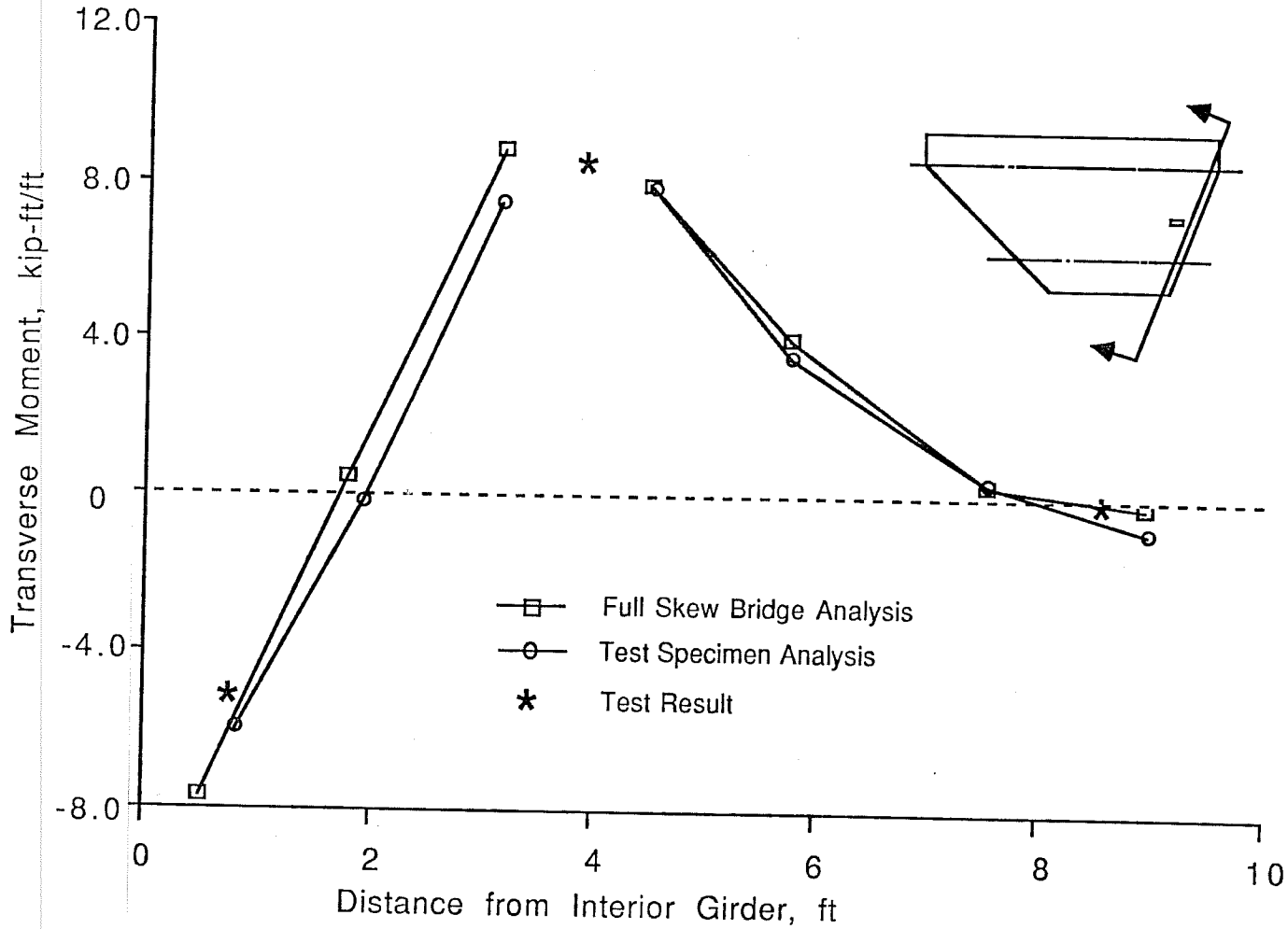

Fig. 8.9 Transverse moments along 20-degree skew edge (after cracking, P = 40 kips)

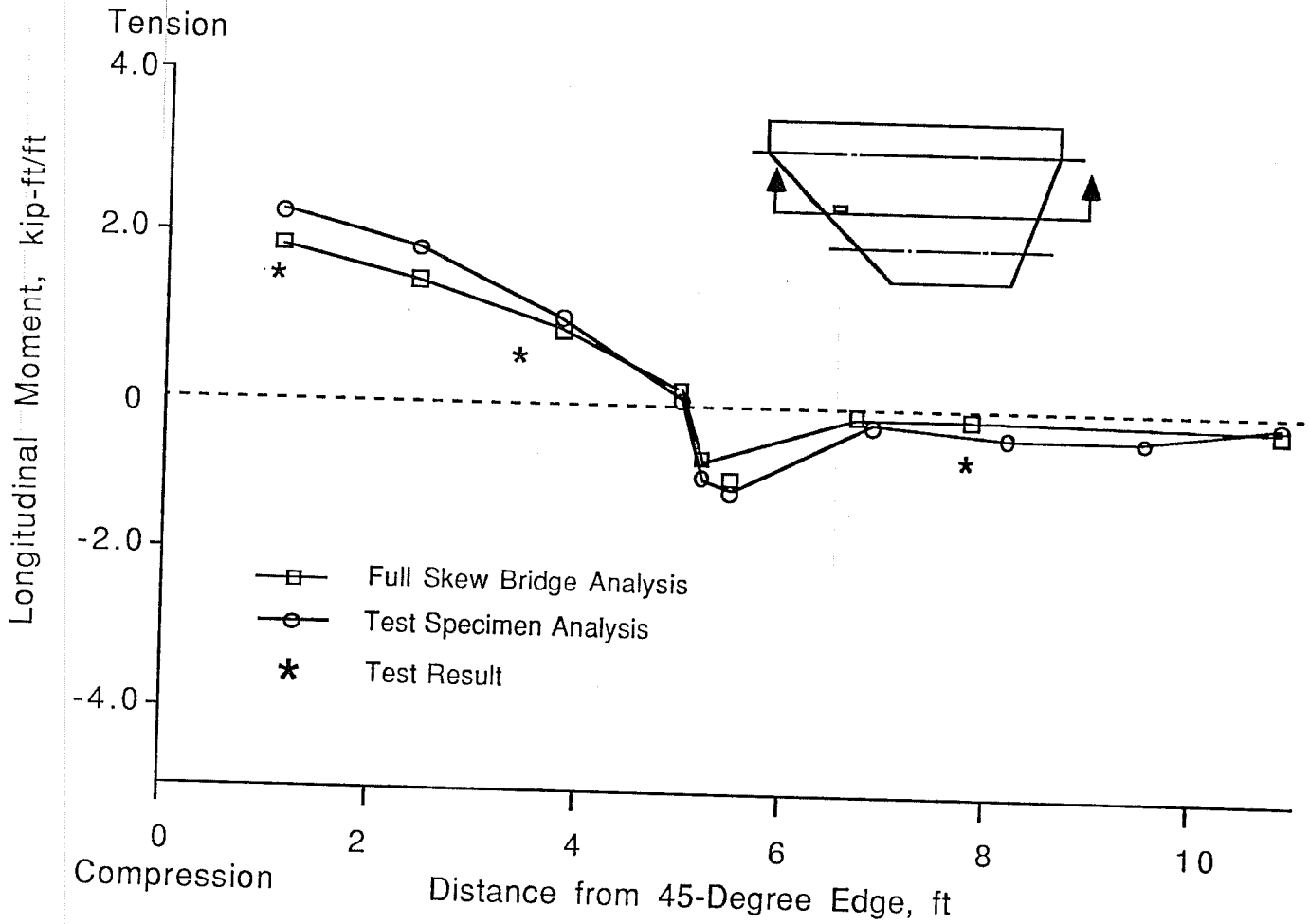

Fig. 8.10 Longitudinal moments along longitudinal line through loading point at 45-degree skew edge (before cracking, P = 20 kips)

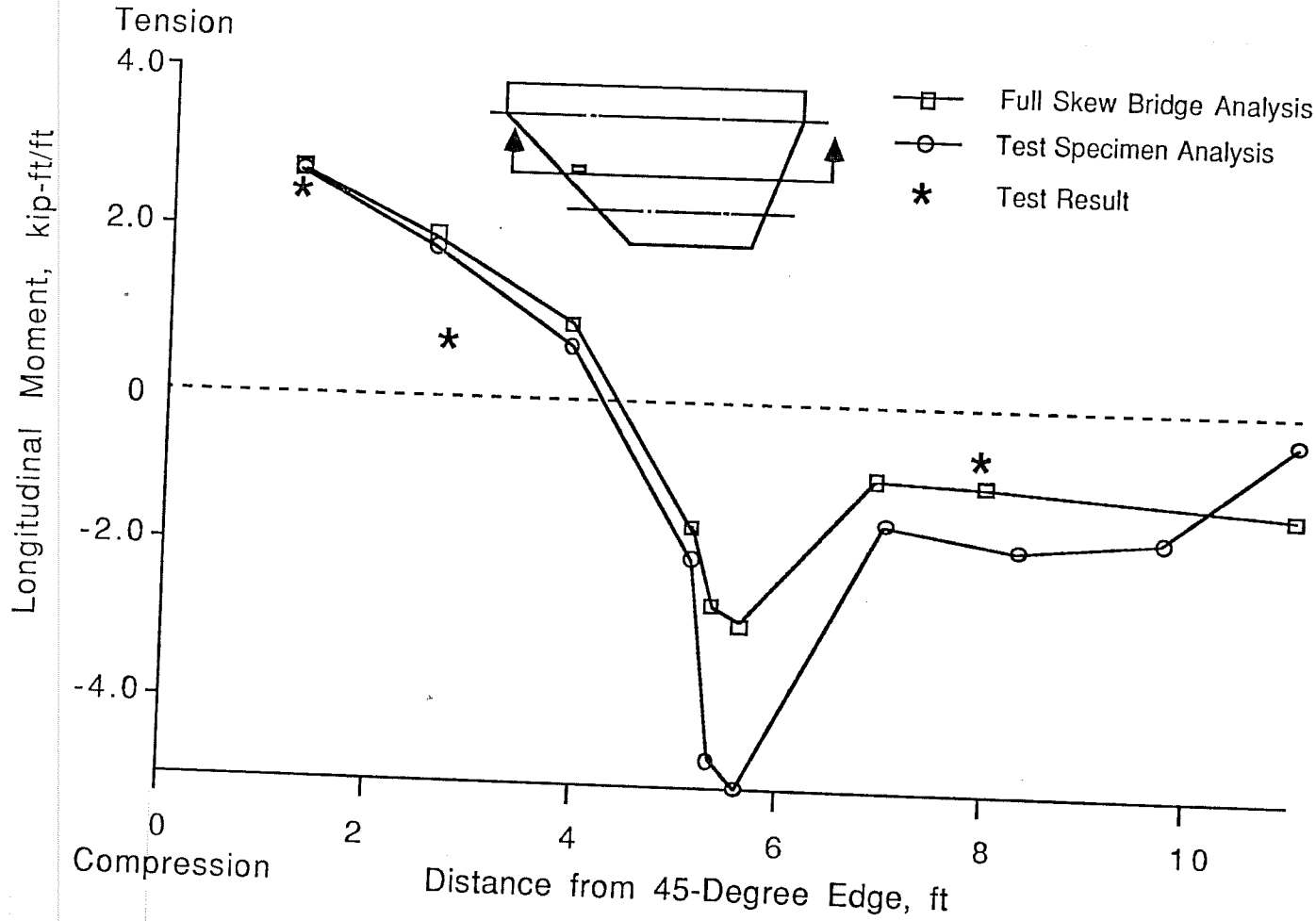

Fig. 8.11 Longitudinal moments along longitudinal line through loading point at 45-degree skew edge (after cracking, P = 40 kips)

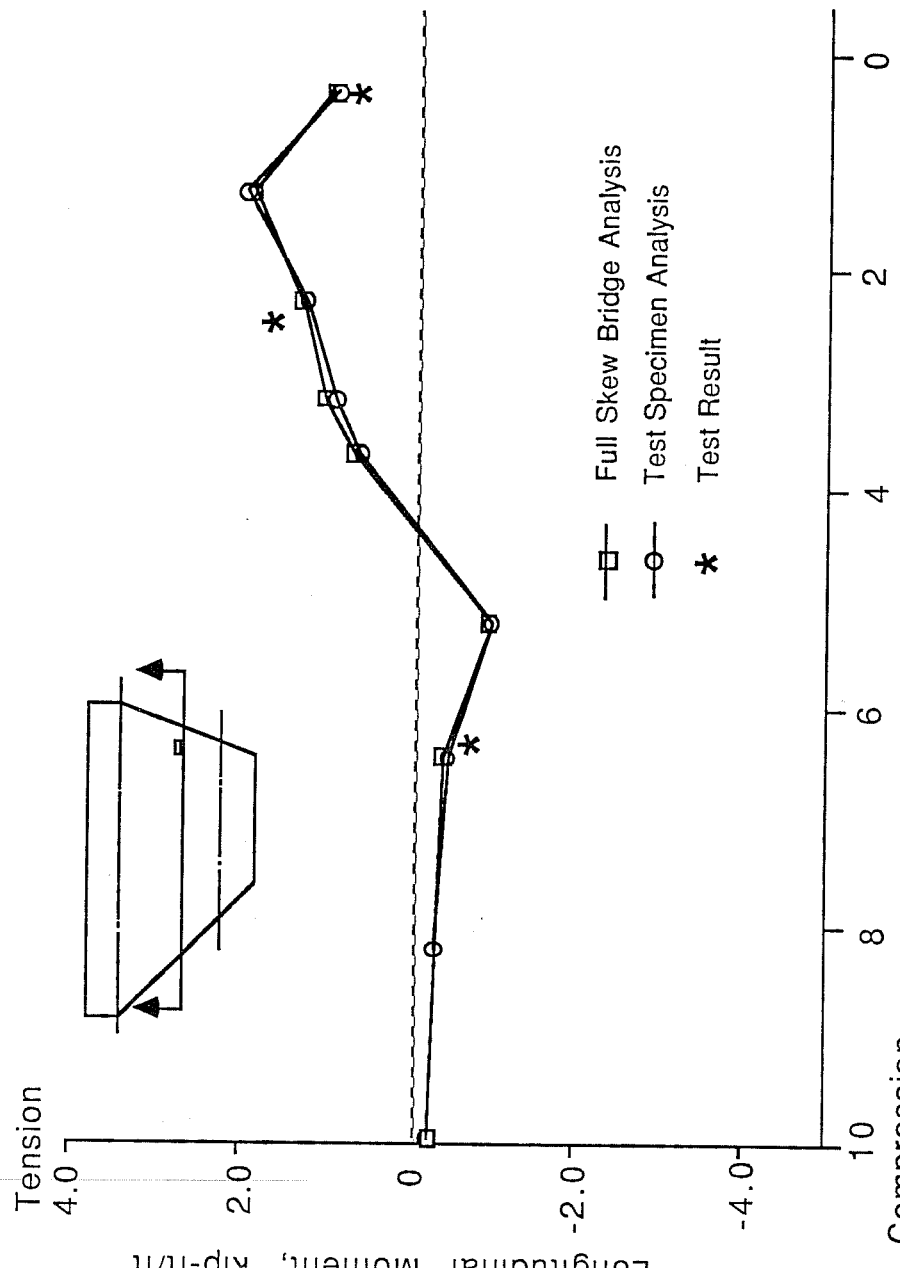

Fig. 8.12 Longitudinal moments along longitudinal line through loading point at 20-degree skew edge (before cracking, P = 20 kips)

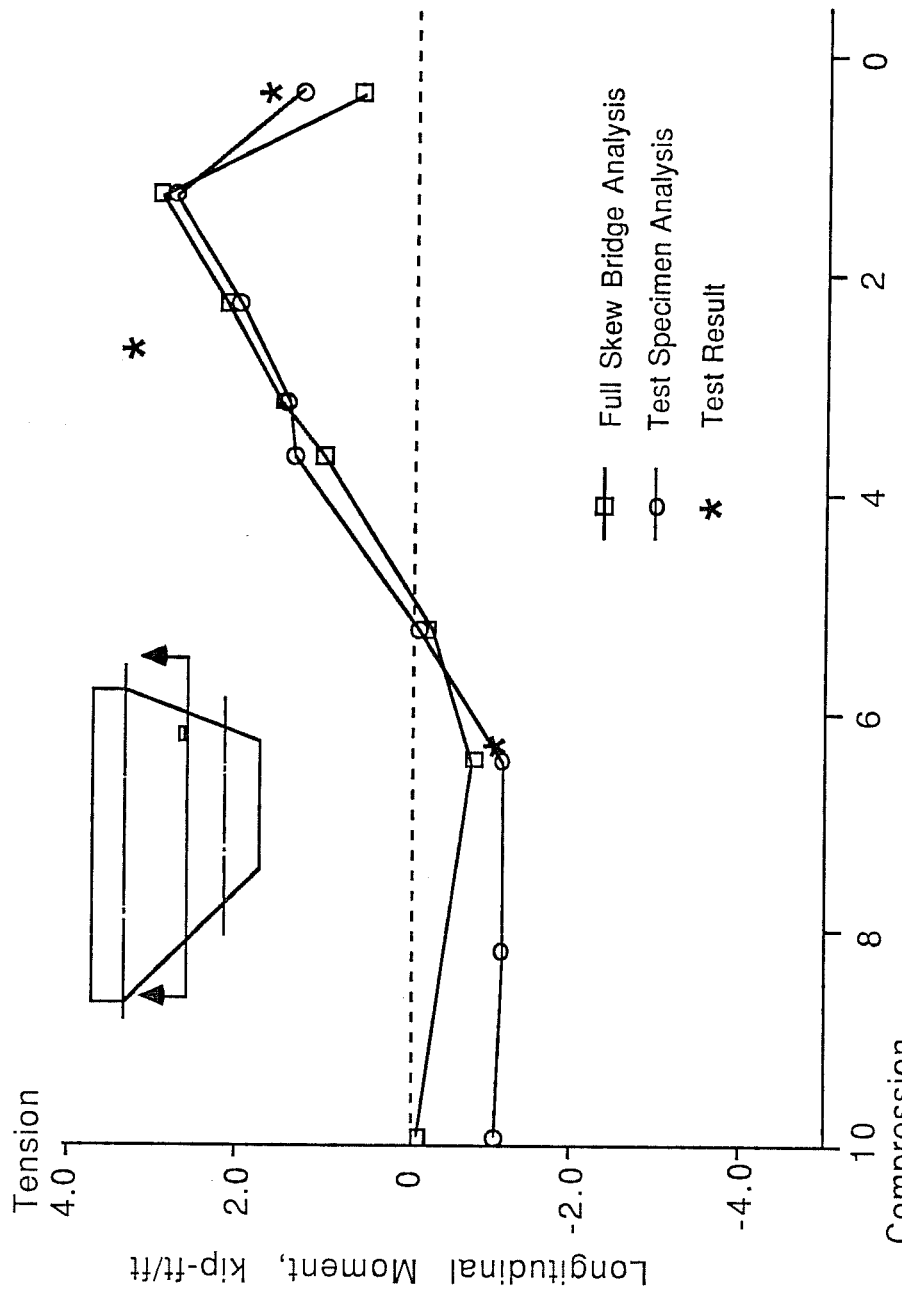

Fig. 8.13 Longitudinal moments along longitudinal line through loading point at 20-degree skew edge (after cracking, P = 40 kips)

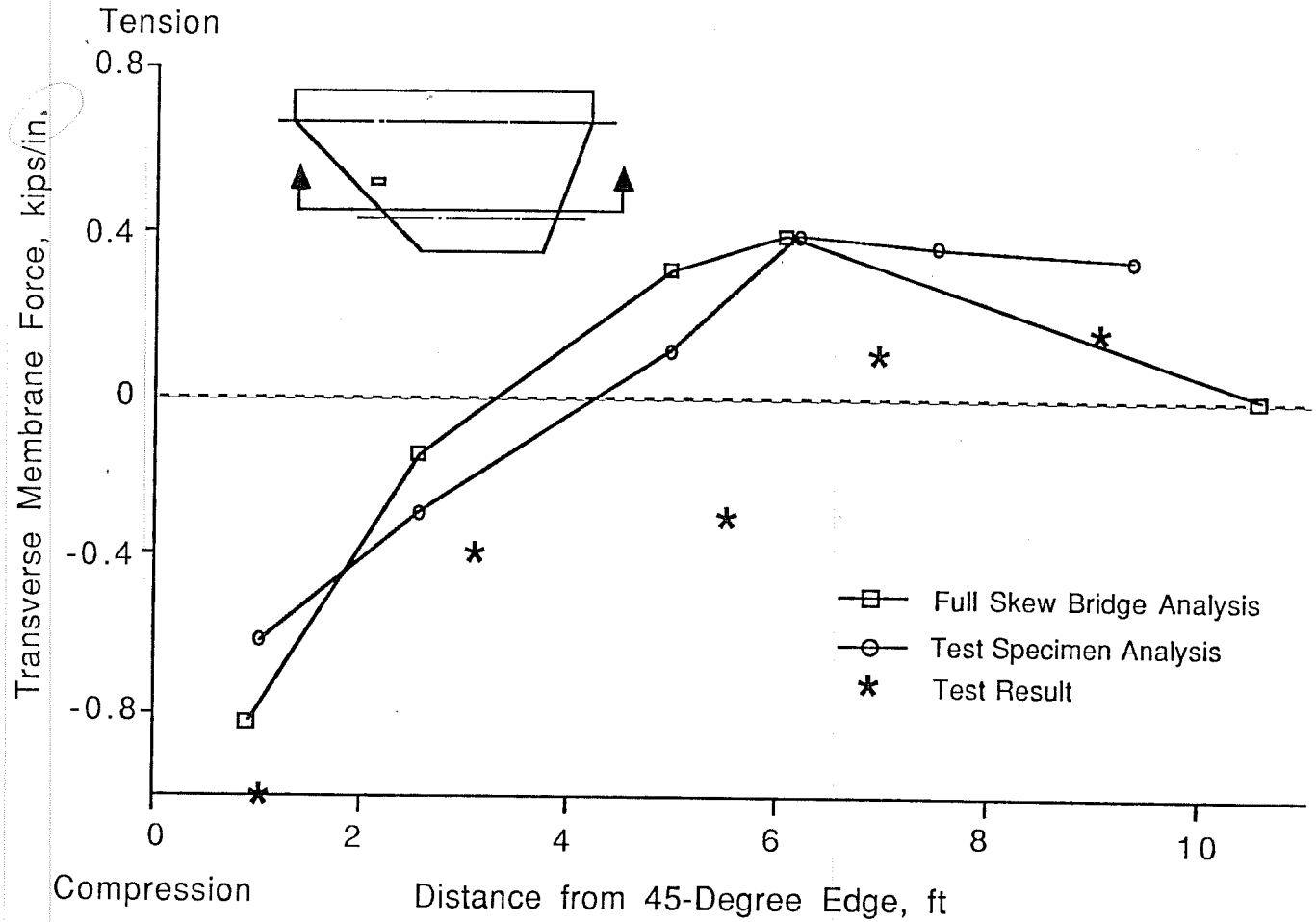

Fig. 8.14 Transverse membrane force at interior girder, 45-degree skew edge test (after cracking, P = 40 kips)

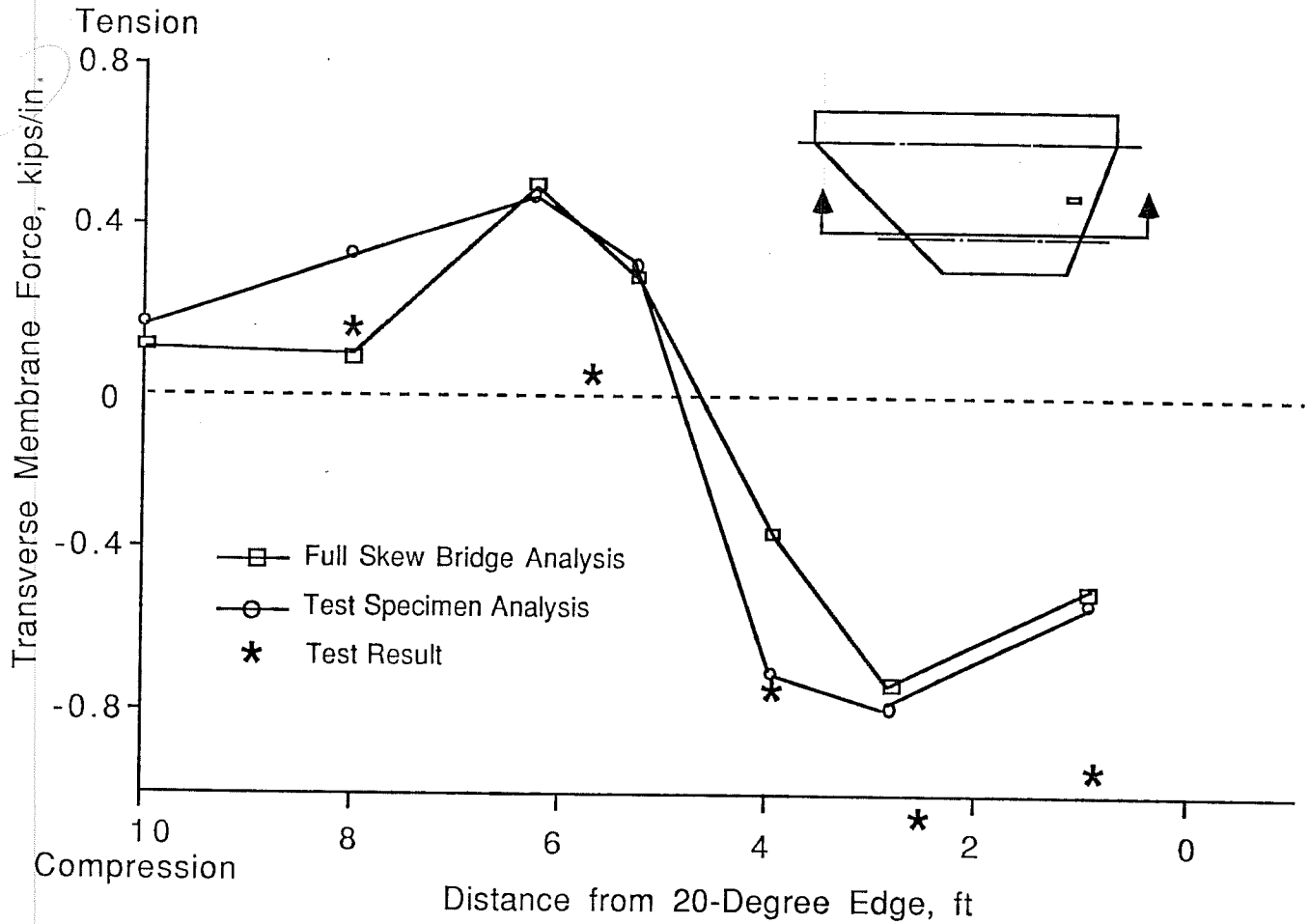

Fig. 8.15 Transverse membrane force at interior girder, 20-degree skew edge test, (after cracking, P = 40 kips)

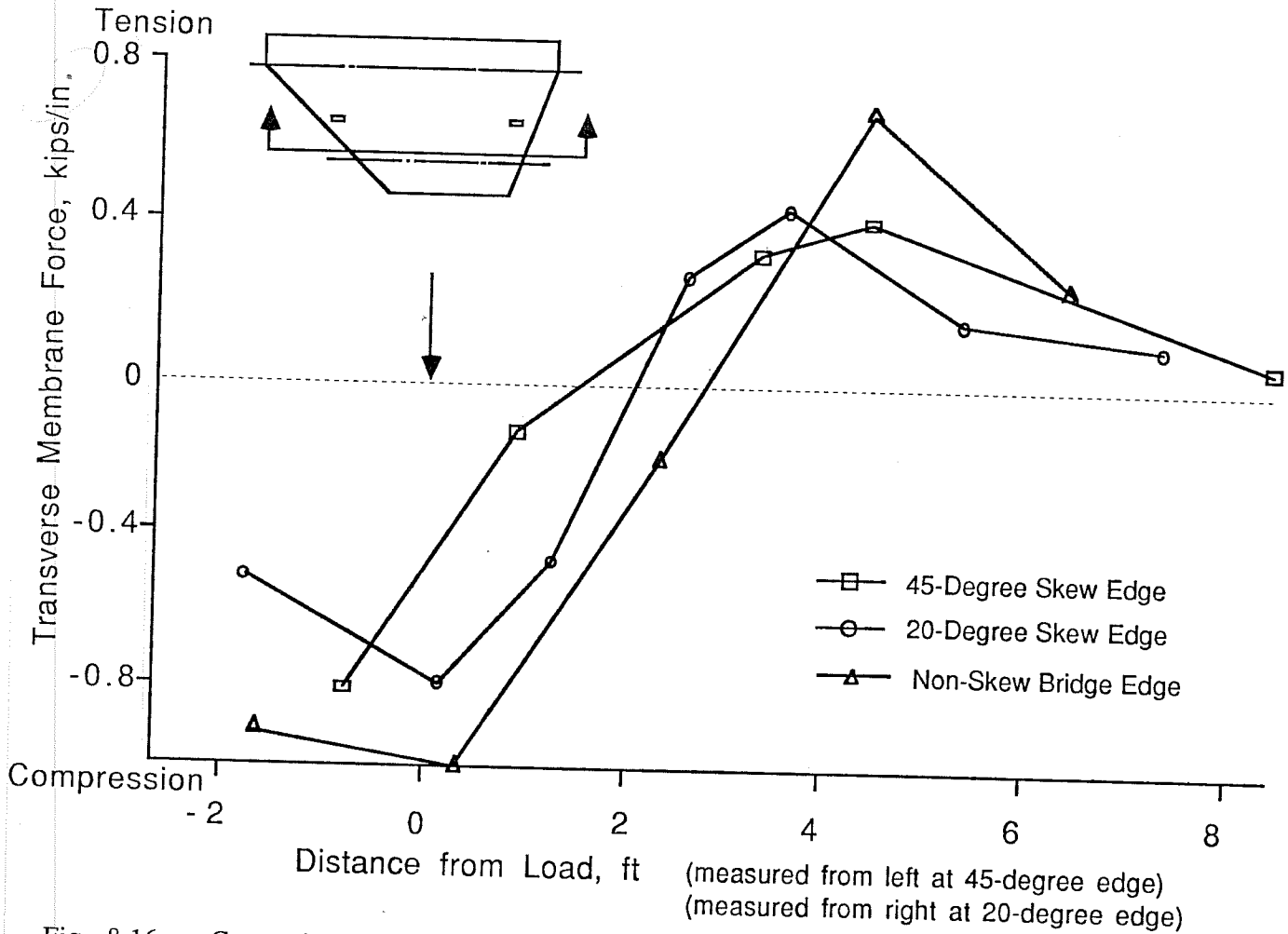

Fig. 8.16 Comparison of transverse membrane force for different skew angles (P = 40 kips)

8.5 Observed versus Calculated Capacities, 45-Degree Skew Edge

8.5.1 Observed Failure Mode. As mentioned before, the 45-degree skew edge failed by combined shear and torsion near the interior support (wall), at a load of approximately 97 kips. The failure surface extended about 48 in. in the longitudinal direction.

8.5.2 Calculated Shear Capacity. The failure load was calculated according to the provisions of ACI 318-83 [2], assuming three different failure modes:

1) Assuming a one-way shear failure over an effective width equal to that of the actual failure surface and neglecting torsion, the calculated failure load was 78 kips;

2) Assuming the entire thickened edge of the deck to be effective in shear, and again neglecting torsion, the calculated failure load was 112 kips;

3) Assuming the entire section of the thickened edge of the deck to be effective, and considering torsion, the calculated failure load was 58 kips.

8.5.3 Calculated Flexural Capacity. Flexural capacity of the deck is increased by in-plane compressive forces. This phenomenon was discussed in a previous report of Project 350 [14], and will be reviewed briefly here. The moment-axial force interaction diagram for the 45-degree skew edge is shown in Fig. 8.17. As shown in Fig. 8.18, transverse compressive membrane force increases with applied load. The curves of Figs. 8.17 and 8.18 are combined in Fig. 8.19. The straight line showing applied actions combines the relationships of load vs. transverse compression and transverse compression vs. transverse moment. Applied moments are related to transverse compressive forces by the ratio of 1 kip-ft/ft (moment) to 2 kips/ft (transverse force). This ratio determines the slope of the line. Transverse compression is related to applied load by the ratio of 16 kips (transverse compression) to 40 kips (applied load). This ratio determines the spacing of the load scale along the line.

Examination of Fig. 8.19 clearly shows that the flexural capacity of the deck is increased from 24.8 to 44.5 kip-ft/ft by the presence of arching action. This method was used in this report to calculate the moment capacity of the deck at various points. The calculated moment capacity was used to evaluate the flexural capacity

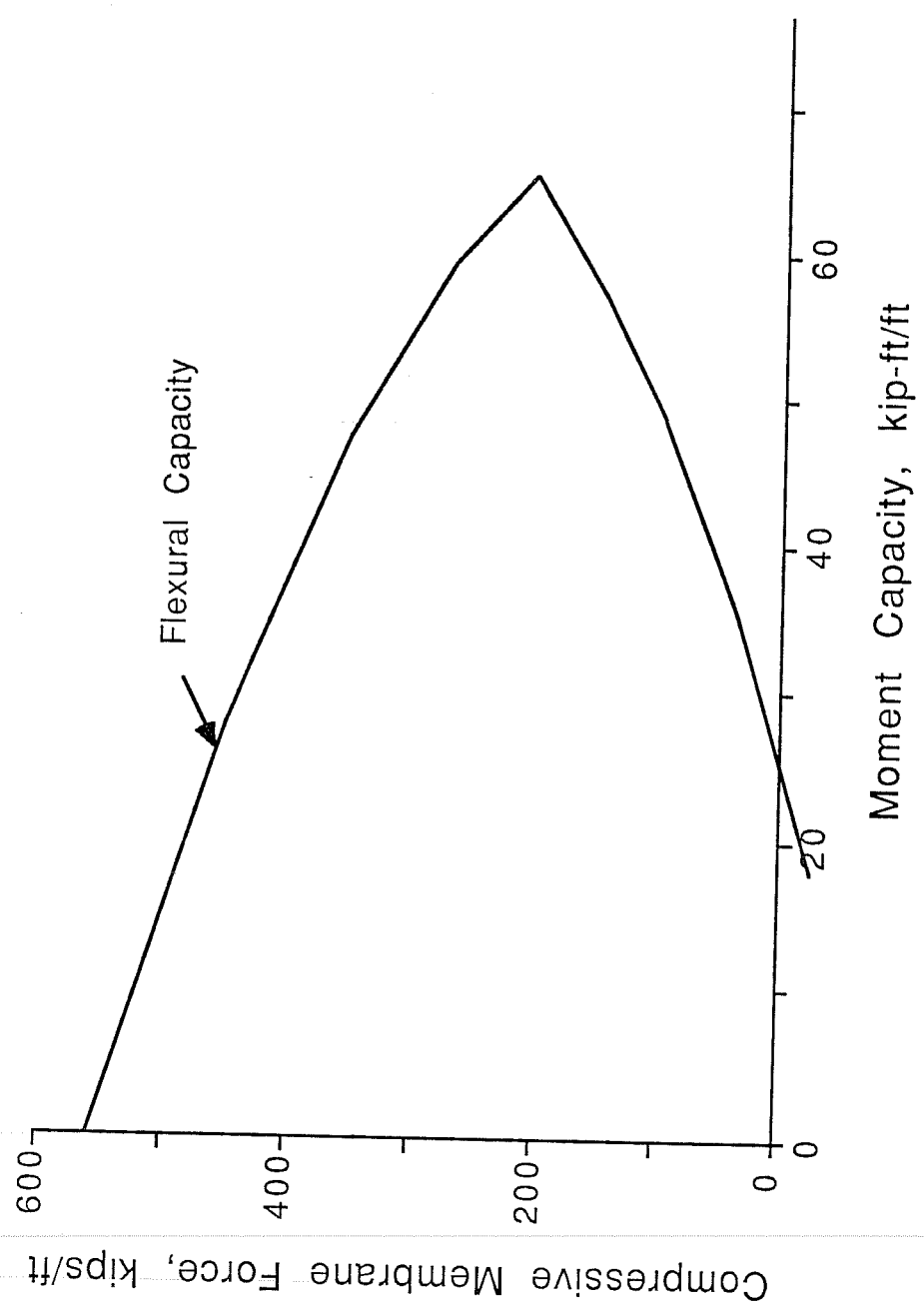

Fig. 8.17 Moment-axial force interaction diagram for 45-degree skew edge

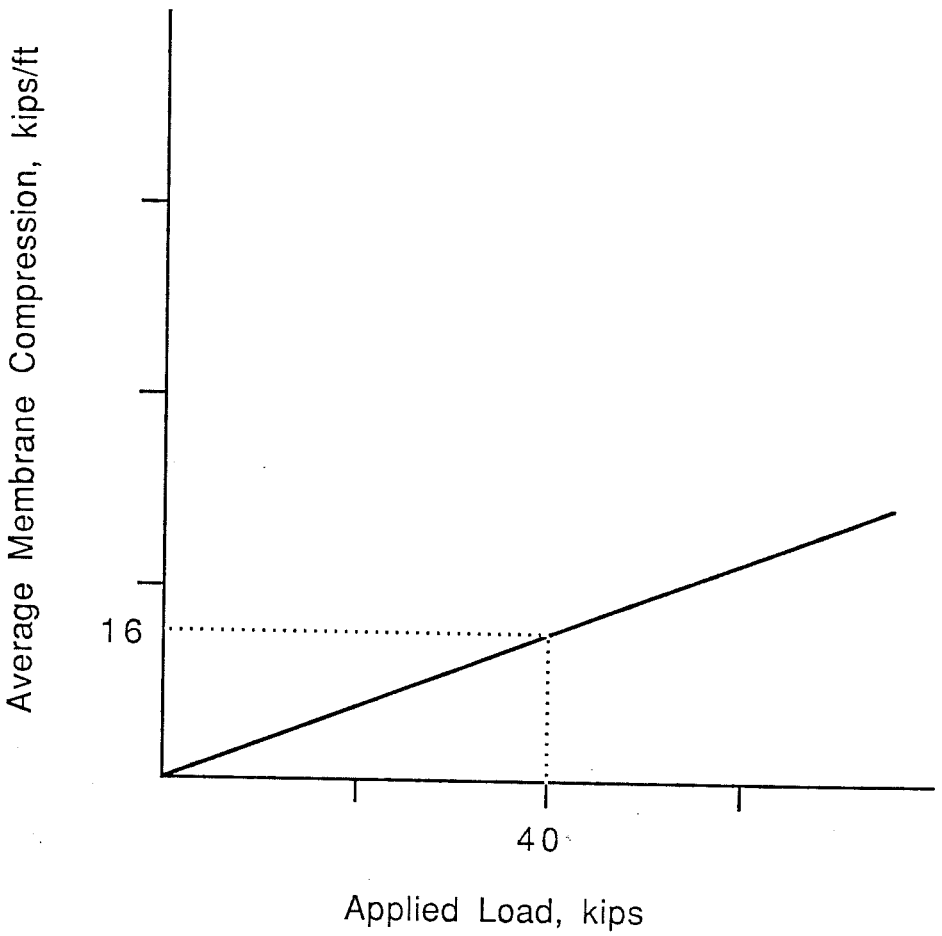

Fig. 8.18 Variation of average analytical value of transverse membrane compression (cracked, 45-degree skew edge)

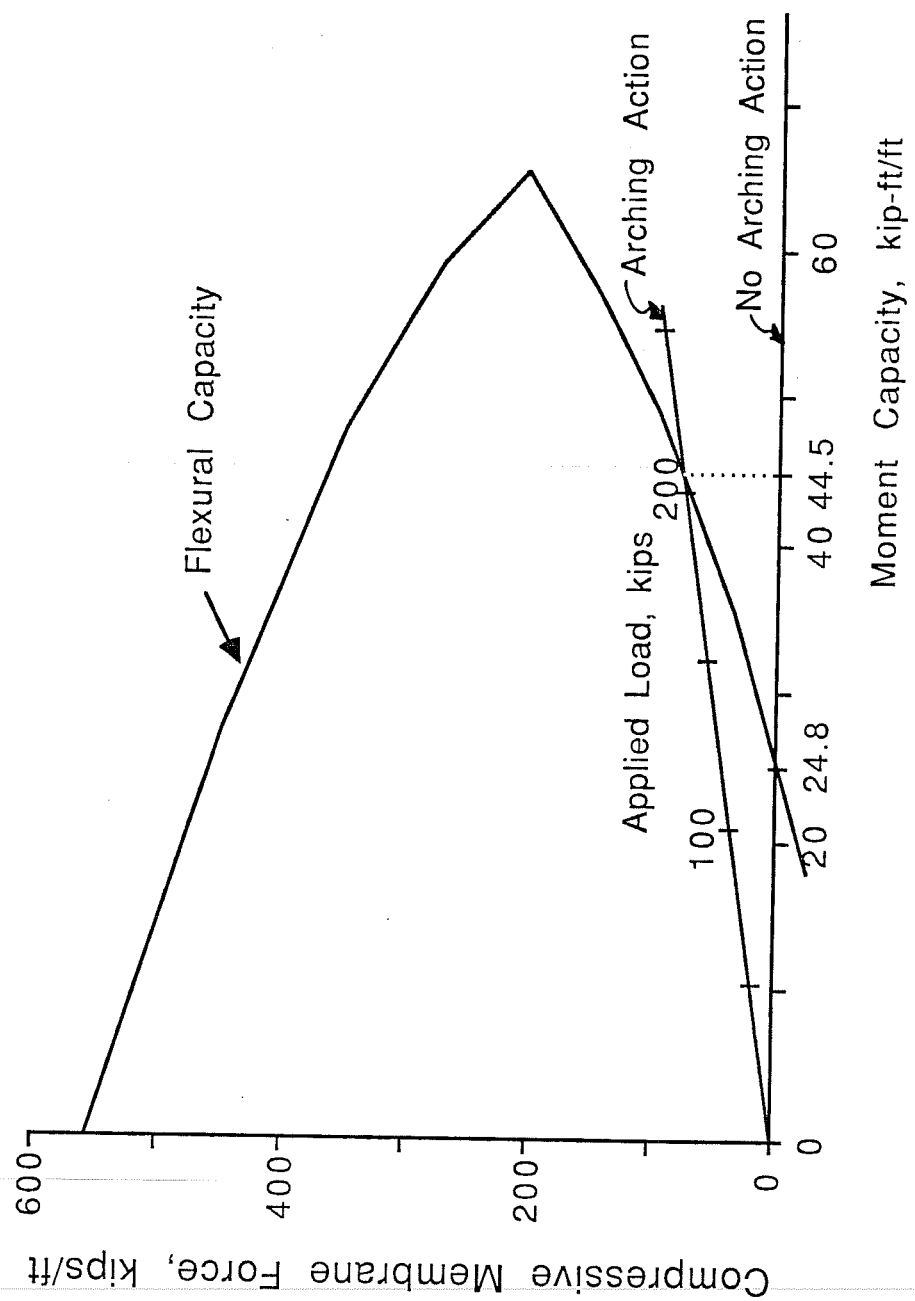

Fig. 8.19 Increase in flexural capacity of 45-degree skew edge due to compressive membrane force

of the deck by yield-line analysis. The moment capacity of the deck increased by 1.7 to 3 times as a result of compressive membrane force, depending on the reinforcement and the magnitude of the compressive force.

The critical yield-line pattern at each edge is shown in Fig. 8.20. The calculated flexural capacity of the deck at the 45-degree skew edge is 103 kips neglecting arching action, but is 212 kips considering it.

8.5.4 Comparison and Discussion of Calculated Capacities. In Fig. 8.21, the predicted capacities assuming different failure modes are compared with the observed failure load.

The actual failure load for the 45-degree skew edge was 97 kips, and the failure mode was shear. This is actual failure load far below the highest predicted capacity of 212 kips, assuming flexural failure and considering arching action. The lowest predicted capacity is 58 kips (shear failure assuming the entire section of the thickened edge of the deck to be effective, and considering torsion). If torsion is neglected, the shear capacity almost doubles to 112 kips.

According to the current AASHTO specification [1] and the Ontario Bridge Design Code [26], edge stiffening acting alone shall be designed to support the full design load. In Texas, the edge is usually stiffened by thickening the deck slab. If this thickened region (diaphragm) is too wide, significant torsion will occur, and must be considered in the design. Considering the combined effect of shear and torsion, the assumption that the stiffened edge acting alone resists the full design load is conservative (predicted capacity of 58 kips, about 60% of the actual failure load of 97 kips).

However, this assumption is probably the best way to compute the edge capacity of the deck, since it provides a conservative and simple estimate of capacity. When the detrimental effects of torsion are neglected, the predicted capacity of 112 kips exceeds the actual failure load of 97 kips. Torsion should be considered in designing the diaphragm, since the width of the diaphragm is usually much larger than the loading length of the wheel.

Neglecting torsion, and assuming an effective width equal to that of the actual failure surface, the predicted capacity is 78 kips, closer to the actual failure load. However, it is not only hard to predict the length of the failure surface, but also unreasonable to neglect the evident torsion.

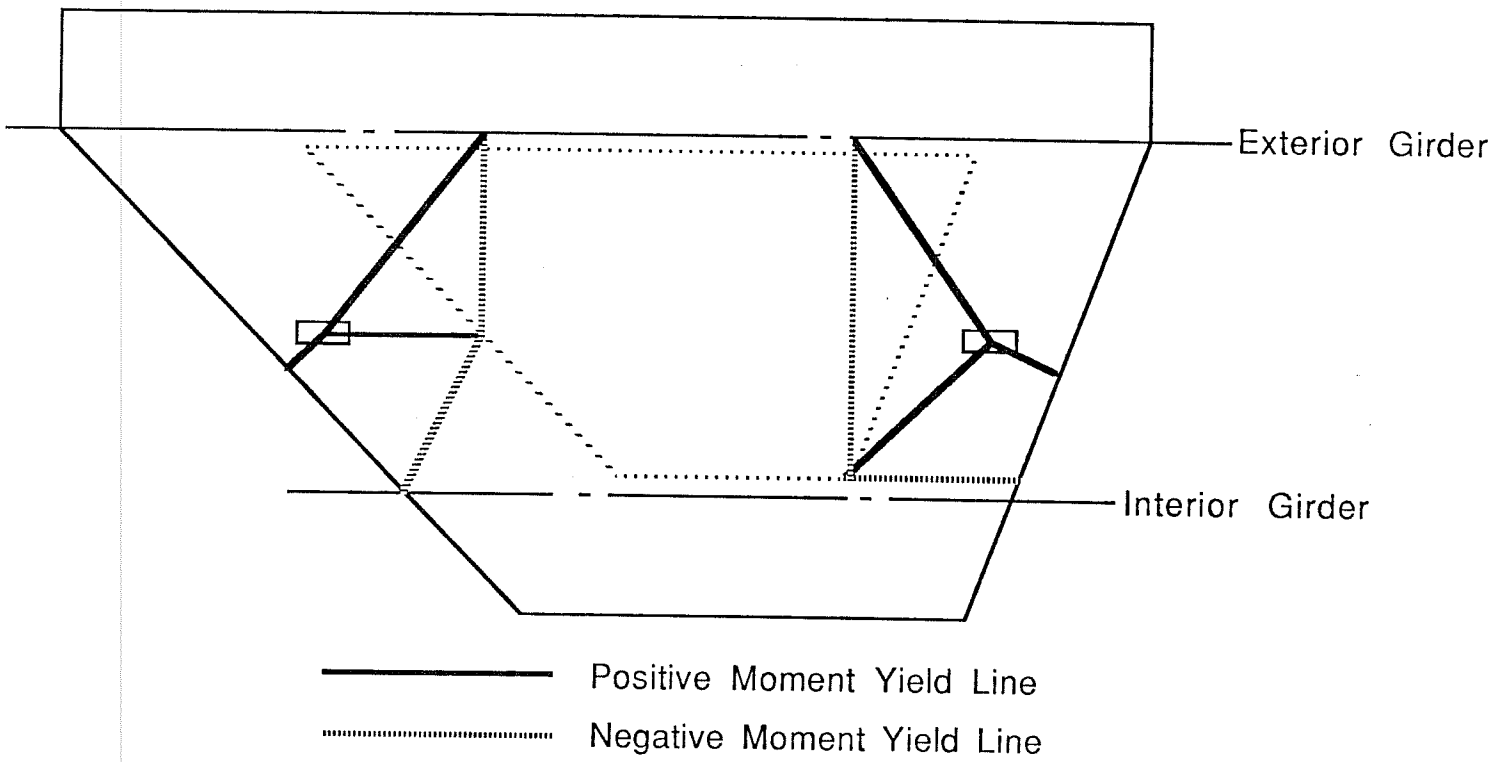

Fig. 8.20 Critical yield-line patterns for skew edges

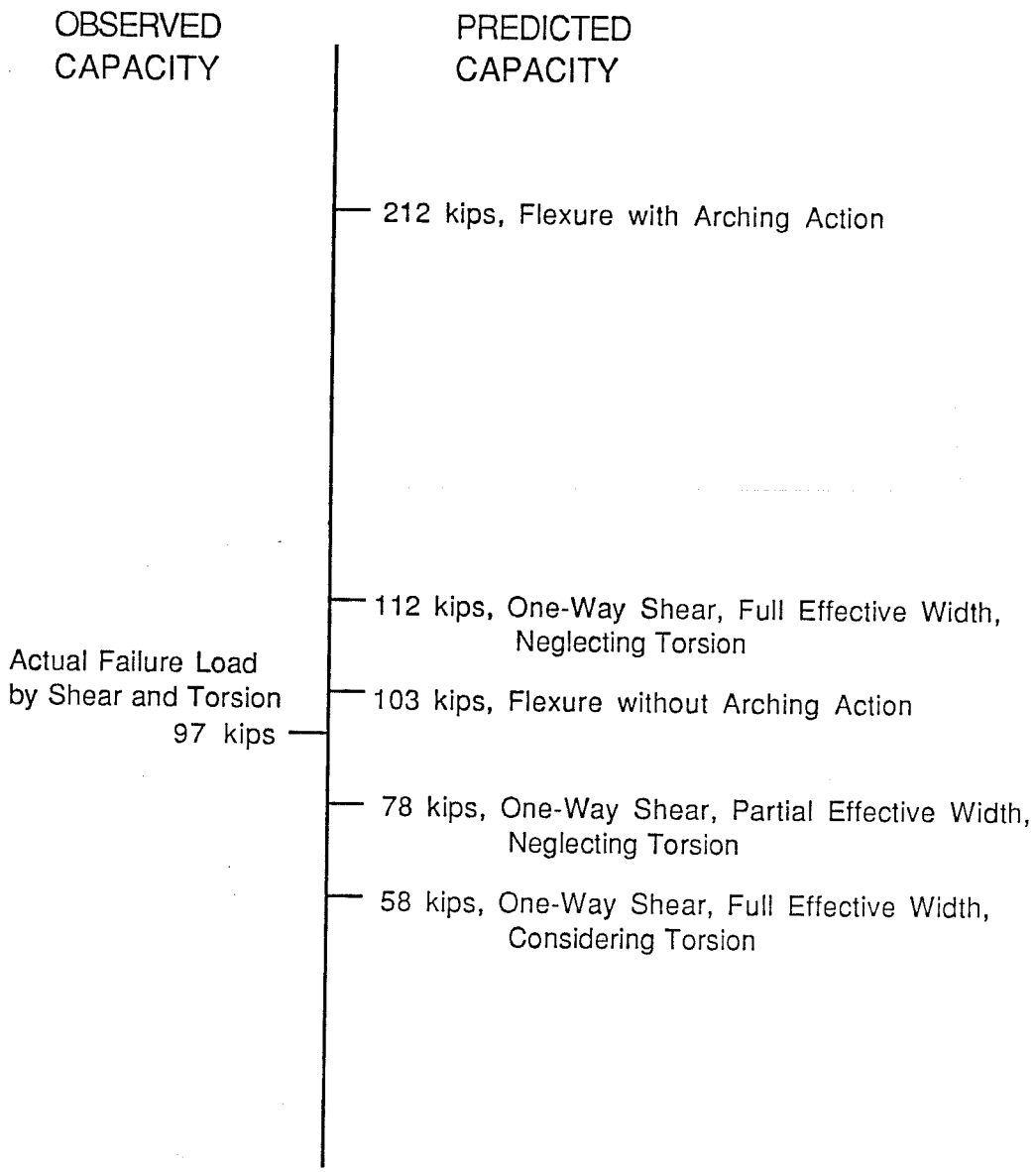

Fig. 8.21 Observed vs. calculated capacities at 45-degree skew edge

Assuming flexural failure without arching action, the predicted capacity is closest to the actual failure load. However, this prediction is not realistic, since the deck failed by shear.

8.6 Observed versus Calculated Capacities, 20-Degree Skew Edge

8.6.1 Observed Shear Failure. The 20-degree skew edge failed by shear near at the interior support (wall), at a load of 139 kips. The failure surface in the longitudinal direction was about 41 in. long. Torsion was negligible, since the load was located almost at the center of the thickened portion of the deck.

8.6.2 Calculated Shear Capacity. The failure load was again calculated according to the provisions of ACI 318-83 assuming two different failure modes:

1) assuming the entire section of the thickened edge to be effective, the calculated failure load was 85 kips; and

2) assuming a one-way shear failure over an effective width equal to that of the actual failure surface, the calculated failure load was 66 kips.

It could be concluded again that a conservative and simple design procedure is to design the stiffened edge to resist the full wheel load alone.

8.6.3 Calculated Flexural Capacity. The critical yield-line pattern at the 20-degree skew edge is shown in Fig. 8.20. Using the same procedures as for the 45-degree skew edge (Subsection 8.5.3), the calculated flexural capacity is 114 kips neglecting arching action, and 235 kips considering arching action.

8.6.4 Comparison and Discussion of Calculated Capacities. In Fig. 8.22, the predicted capacities assuming different failure modes are compared with the observed failure load.

The actual failure load for the 20-degree skew edge was 139 kips, and the failure mode was shear. This is again far below the highest predicted flexural capacity of 235 kips, assuming flexural failure and considering arching action. However, the actual failure load is greater than the predicted flexural capacity neglecting the effects of arching action. This indicates that the flexural capacity

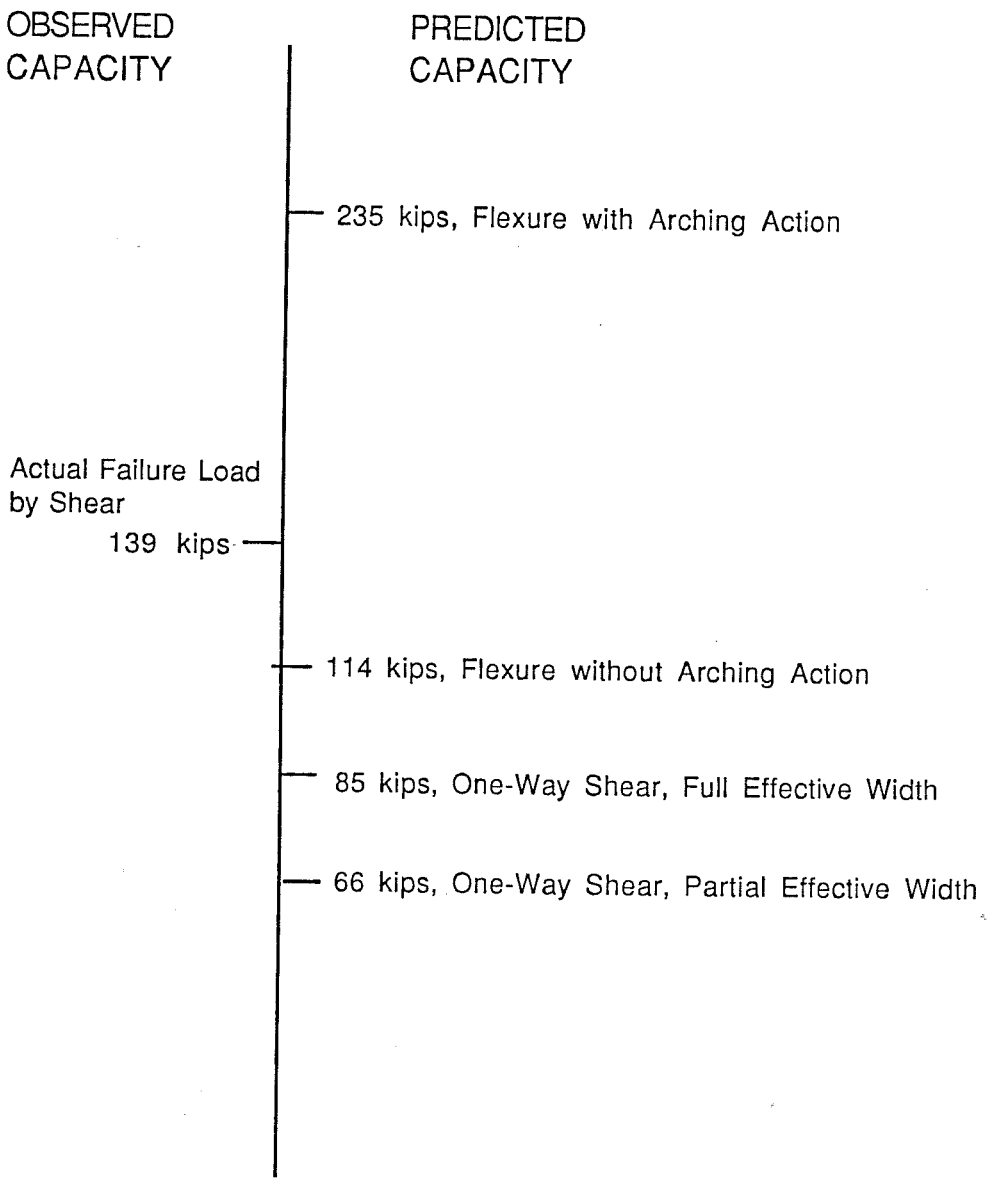

Fig. 8.22 Observed vs. calculated capacities at 20-degree skew edge

of the deck increases with arching action, since the calculated flexural capacity without arching action is less than the actual failure load by shear, even though the calculated capacity by yield-line analysis is the upper-bound value.

The lowest predicted capacity is 66 kips, about 47% of the actual failure load (shear failure assuming an effective width equal to that of the actual failure surface). If the entire section of the thickened edge of the deck is assumed to be effective, the shear capacity increases to 85 kips, about 60% of the actual failure load of 139 kips. This assumption that the stiffened edge acting alone resists the full design load results in a predicted capacity about 60% of the actual failure load, as with the 45-degree skew edge. This assumption is again conservative, but is the best way to compute the capacity of the deck at the edge. The closest predicted capacity is 114 kips by flexural failure without arching action, but is again unrealistic, since the deck failed by shear.

8.7 Observed versus Calculated Capacities, Center

8.7.1 Observed Punching Shear Failure. The center failed by punching shear at a load of 179 kips. The failure surface was inclined at about 30 degrees from the horizontal.

8.7.2 Calculated Shear Capacity. Using the ACI nominal punching shear stress of $4\sqrt{f'_c}$, and the observed capacity of 179 kips, the calculated angle of failure surface is 37.7 degrees, which agrees very well with previous test results (38 degrees) of Project 350 [36]. Using a 45-degree failure surface, the ACI formula predicts a very conservative failure load of 123 kips. As shown in Fig. 8.23, the actual failure surface did not completely encircle the loaded point, and the side nearest the exterior girder did not fail. The angle of the failure surface was about 30 degrees. Shear stress calculated using the actual failure surface was 316 psi or $4.5\sqrt{f'_c}$, fairly close to the ACI value.

8.7.3 Calculated Flexural Capacity. The assumed yield-line pattern at the center is shown in Fig. 8.24. Using the same procedures as for the 45-degree skew edge (Subsection 8.5.3), the calculated flexural capacity is 598 kips considering arching action, and 275 kips neglecting arching action.

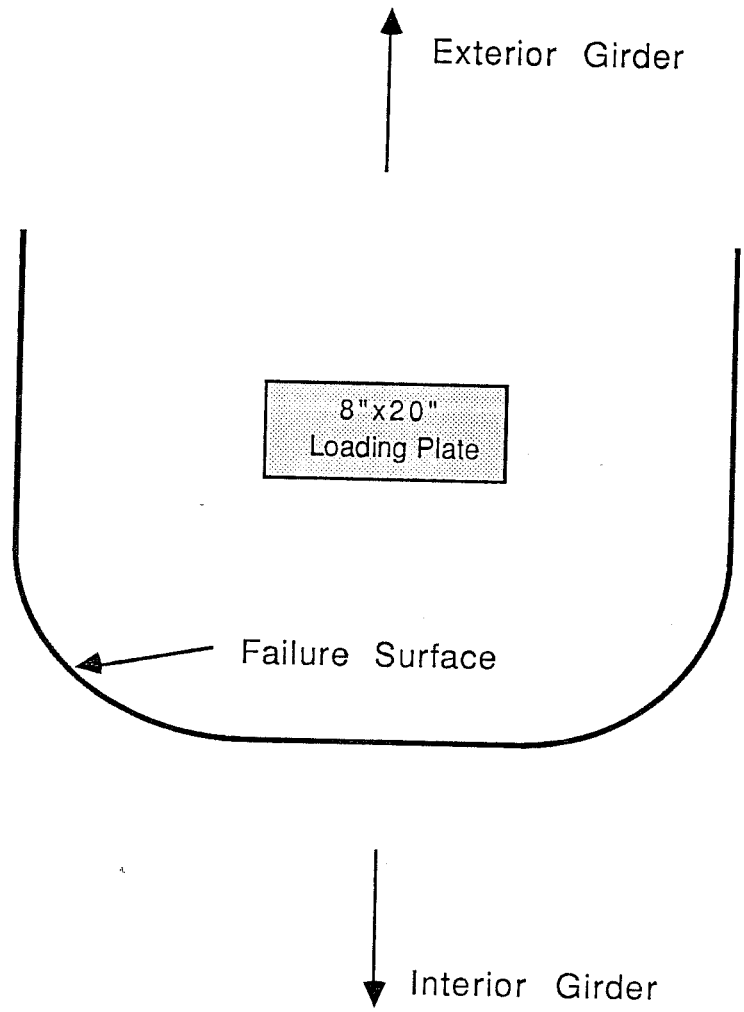

Fig. 8.23 Failure surface on bottom surface of deck at center

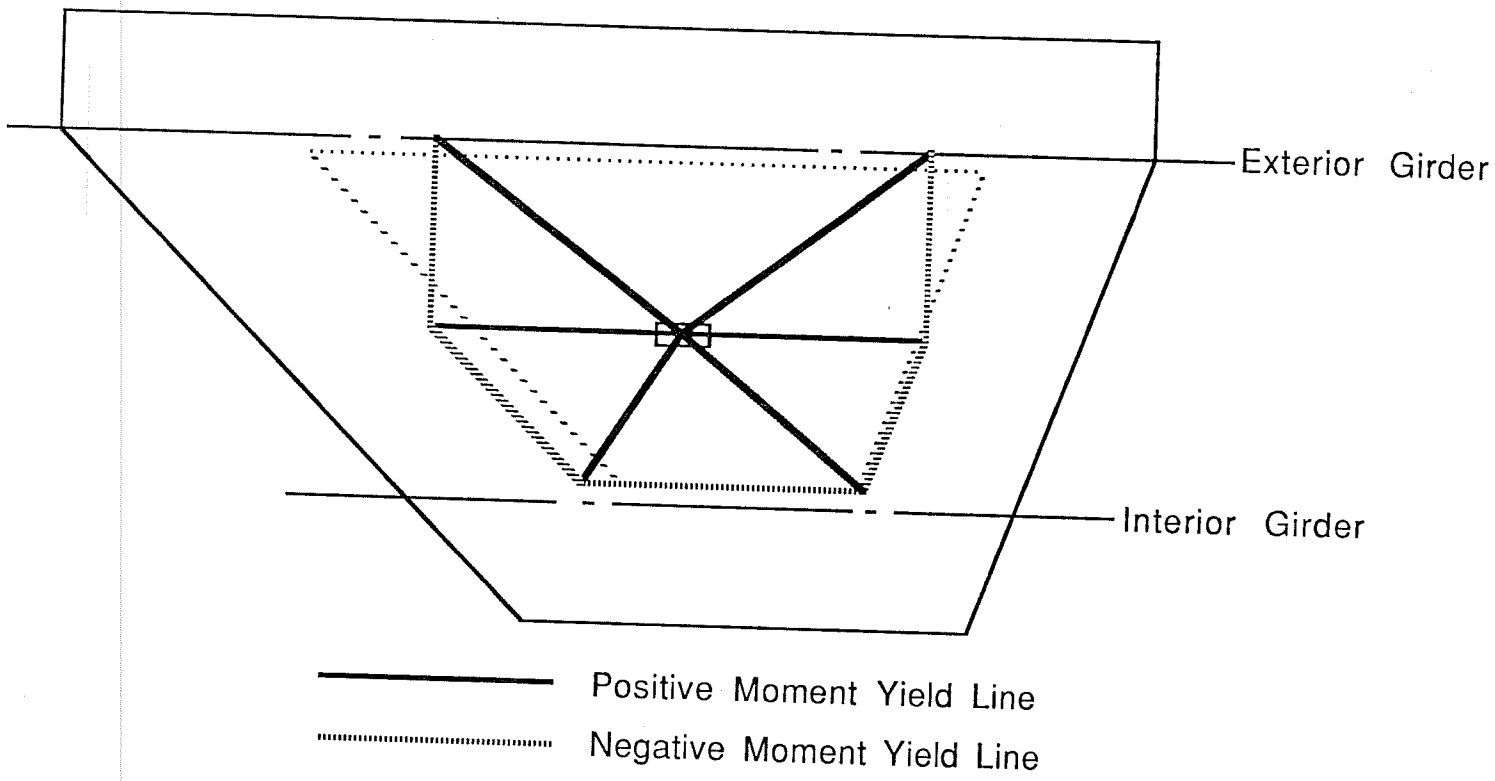

Fig. 8.24 Critical yield-line patterns for center

8.7.4 Comparison and Discussion of Calculated Capacities. In Fig. 8.25, the predicted capacities assuming different failure modes are compared with the observed failure load.

The actual failure load for the center was 179 kips, and the failure mode was punching shear. This is again far below the highest predicted capacity of 598 kips, assuming flexural failure and considering arching action. The actual failure load is even less than the predicted flexural capacity neglecting the effects of arching action. The lowest predicted capacity is 123 kips predicted by the ACI formula (about 70% of the actual failure load). Assuming the actual failure surface to be effective, the calculated shear capacity based on the ACI punching shear stress of $4\sqrt{f'_c}$ is 159 kips (about 90% of the actual failure load). The predicted capacity by the generalized failure model with a failure angle of 38 degrees as in Ref. 36, is 182 kips.

In summary, the flexural capacity of the deck at the center far exceeds the punching shear capacity. The ACI punching shear formula gives a very conservative estimation of the deck's punching shear capacity. Punching shear capacity is predicted very closely by a generalized punching shear model based on a failure surface inclined at an angle shallower than that used in the ACI formula.

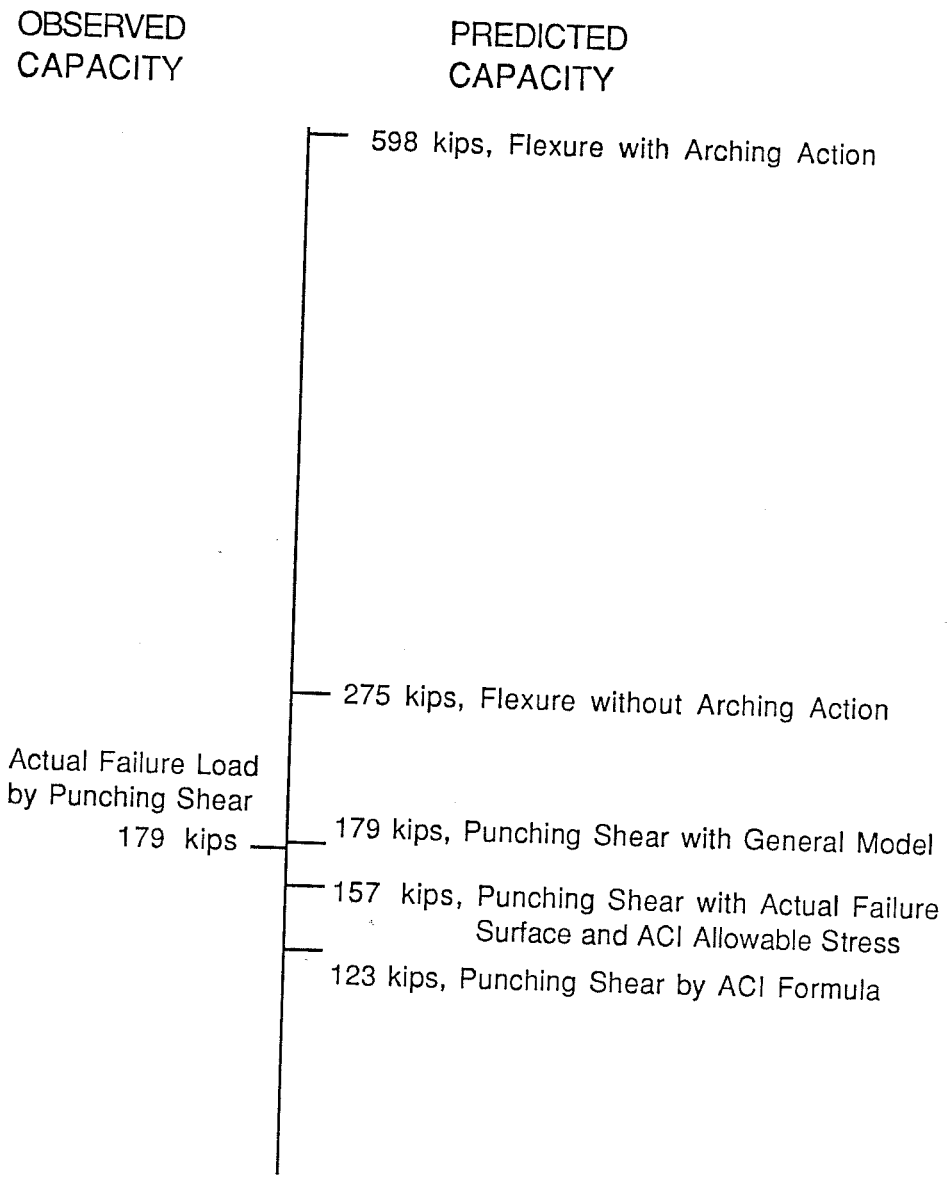

Fig. 8.25 Observed vs. calculated capacities at center

CHAPTER 9

PARAMETRIC STUDIES

9.1 General

As mentioned in Section 1.2, one primary objective of this research was to verify the effects on the bridge performance, of many design variables not studied experimentally:

1) span-to-depth ratio of deck

2) width of cantilever overhang

3) presence of integral barriers

4) longitudinal spacing of live loads

5) longitudinal spacing of diaphragms

As discussed in Section 1.3, these are the major design variables in the empirical design of Ontario-type bridge decks. Parametric studies concerning these design variables would provide better knowledge of the behavior of the Ontario-type decks in a wider variety of applications, and could result in potentially greater economy.

Among the above design variables, the effects of longitudinal spacing of diaphragms had already been studied in the previous phase of Project 350, and is discussed in Ref. 14. According to that reference, the presence of midspan or additional diaphragms does not significantly change the local stiffness, local stresses, moment distributions, nor compressive membrane forces in the deck.

The rectangular bridge studied in the previous phase of Project 350 was used in these parametric studies (Fig. 9.1). Each model in the parametric studies is identical to that of the original rectangular bridge model, except for the design variable to be examined.

9.2 Effect of Span-to-Depth Ratio of Deck

Span length and thickness of the original bridge deck are 7 ft and 7.5 in. respectively, corresponding to a span-to-depth ratio of 11.2. The bridge model was also analyzed with different deck thicknesses of 5.5 in. and 4 in., corresponding to span-to-depth ratios of 15.3 and 21.0 respectively.

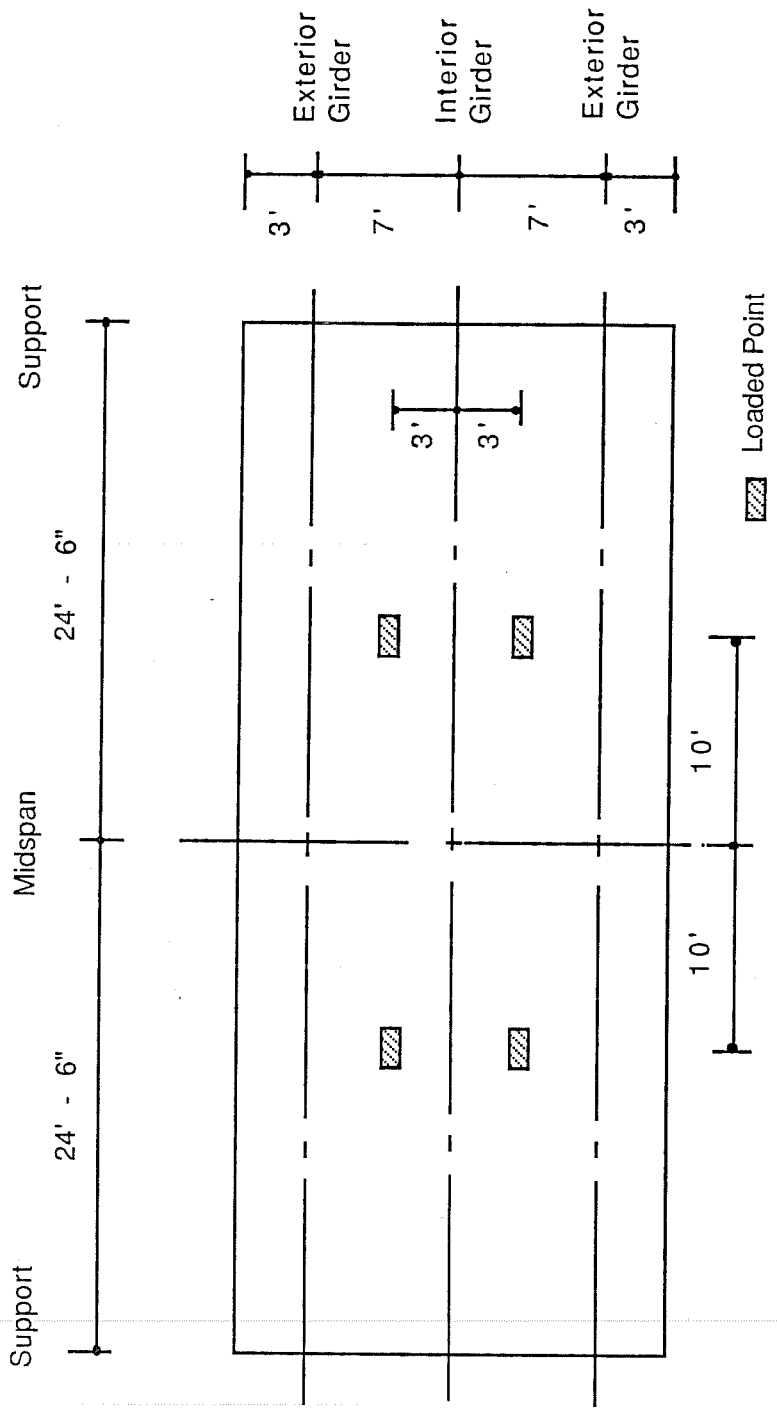

Fig. 9.1 Plan view of previous test bridge specimen

With decreasing deck thickness (increasing span-to-depth ratio), in-plane membrane force increased (Fig. 9.2). This result was unexpected, since more arching action would seem to exist in a thicker member than in a shallower one. However, this phenomenon could be explained by the fact that a shallower arch member develops larger lateral reactions than a deeper member in resisting a load of the same magnitude (Fig. 9.3).

Another series of analyses was performed, increasing the span to 9 ft. Three different deck thicknesses were again used in the analyses: 10 in., 7.5 in., and 5.5 in., corresponding to span-to-depth ratios of 11.4, 15.2, and 20.7, respectively. The results were quite similar to those discussed above: as the deck became shallower, larger membrane forces were developed (Fig. 9.4).

Based on the above analyses, arching action can be developed even in decks with span-to-depth ratios in excess of the limit of 15 specified by the current Ontario Bridge Design Code [26]. However, as reflected in the provisions of that Code, some practical limitation on span-to depth ratio is still necessary. This limitation should be set based on requirements such as deflection control, shear strength, and serviceability. Investigation of these requirements is beyond the scope of this report, and will not be discussed further here.

Negative transverse moments at the interior girder increased with decreasing span-to-depth ratio (Fig. 9.5). However, there was little difference in the basic flexural behavior in the transverse direction.

9.3 Effect of Overhang

The original bridge had a 3-ft overhang beyond each exterior girder. The bridge model was modified to omit this overhang, and was again analyzed. The transverse membrane forces and transverse moments are almost identical in magnitude and distribution to those of the original model (Figs. 9.6 and 9.7).

A minimum 1.0-m (3-ft, 4-in.) overhang at each side of the bridge deck is required by the empirical design provisions of the Ontario Bridge Design Code [26]. Based on this study, however, no overhang is necessary to provide sufficient in-plane stiffness to develop arching action. Transverse membrane forces were zero in intensity at the edge of the deck, and gradually increased closer to the loaded point. In the bridge model studied here, the deck's transverse span of 7 ft (4 ft from the loaded point to the edge) was enough to provide the in-plane stiffness by shear transfer. When the deck's transverse span is very small, an additional overhang portion may be required to provide enough in-plane stiffness. However,

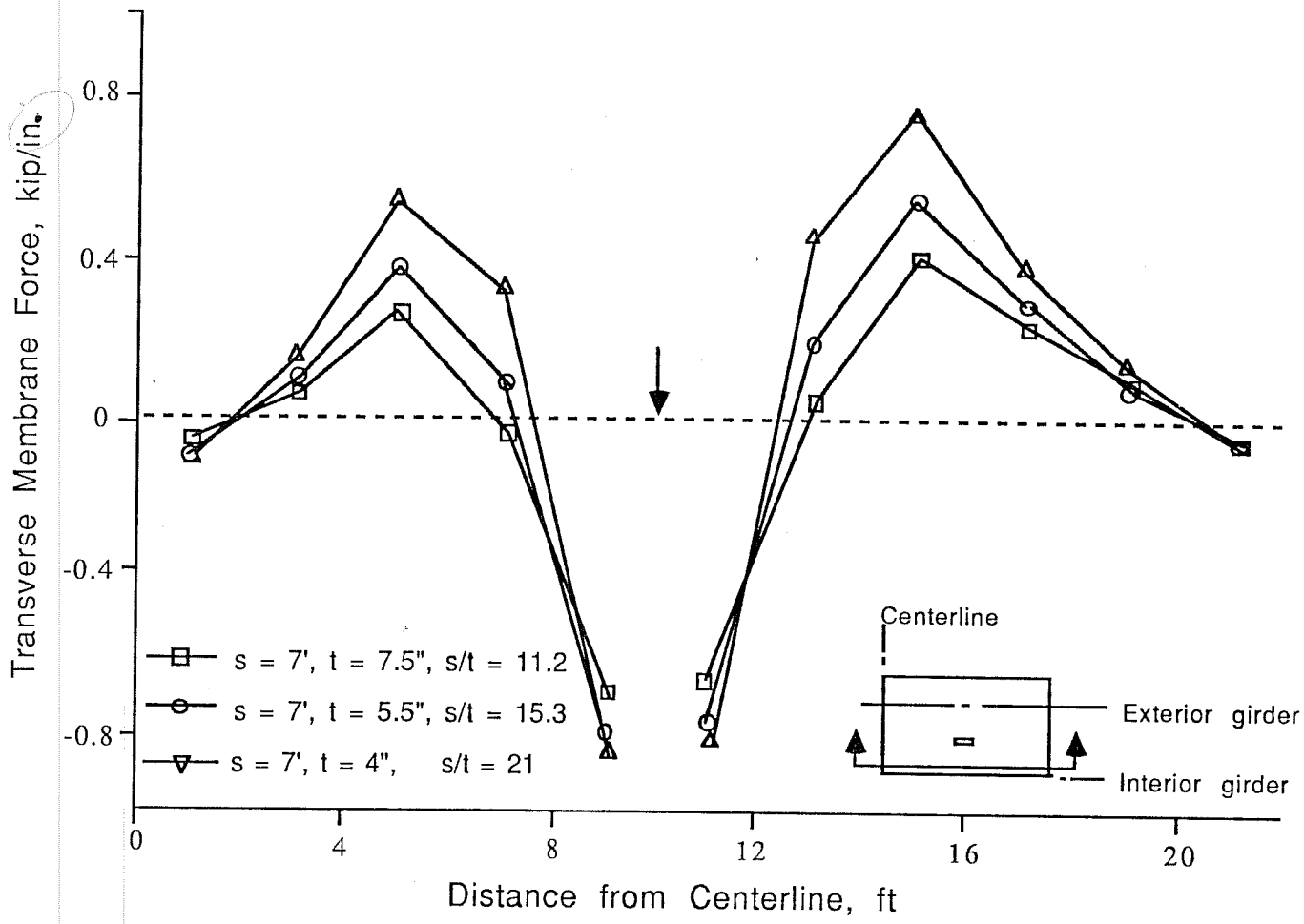

Fig. 9.2 Transverse membrane force at interior girder for different span-to-depth ratio

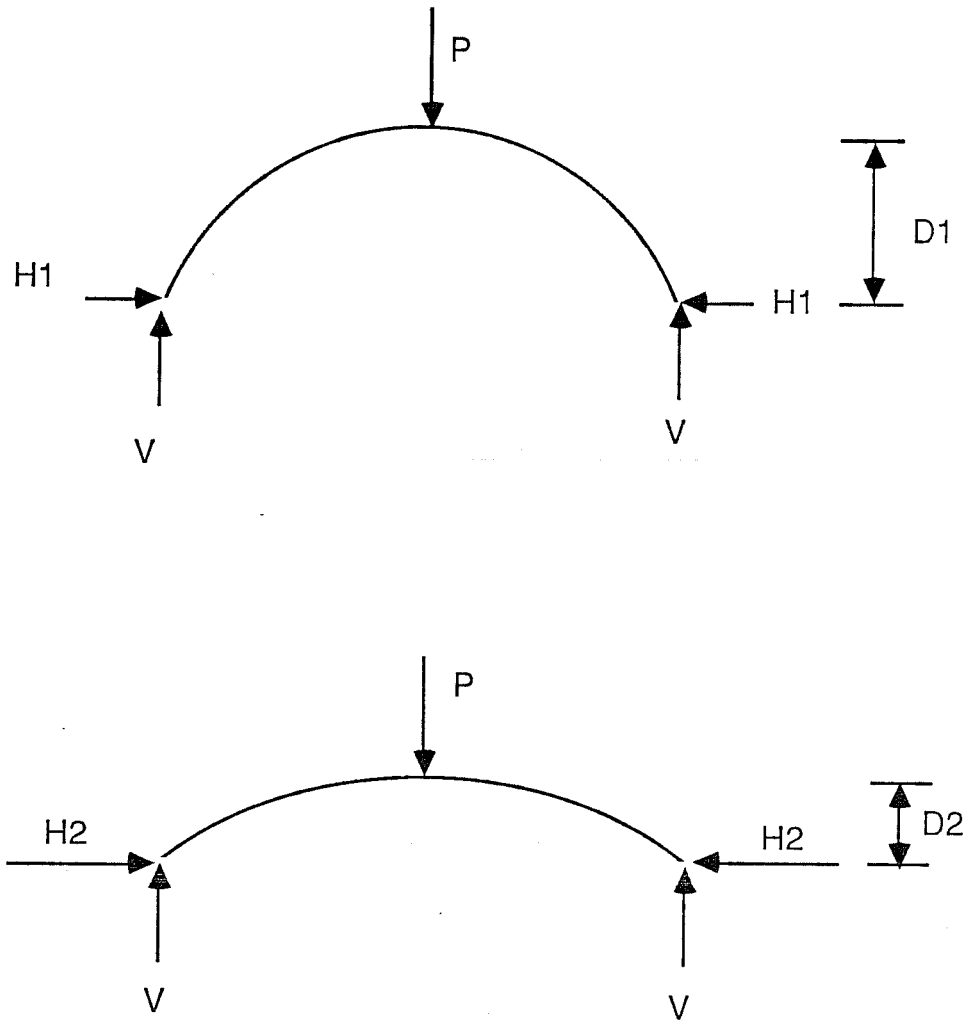

Fig. 9.3 Comparison of lateral reactions

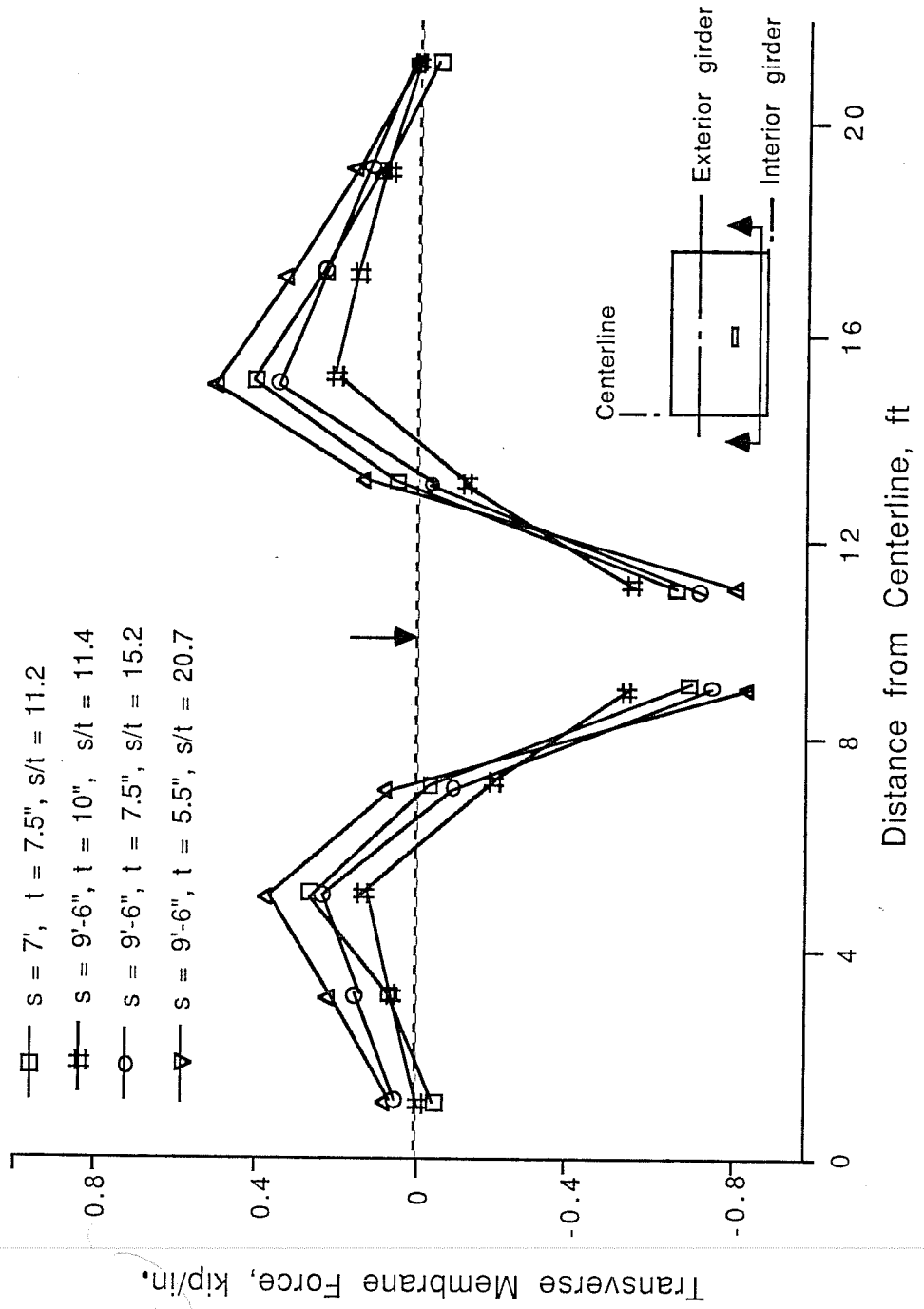

Fig. 9.4 Transverse membrane force at interior girder for different span-to-depth ratio

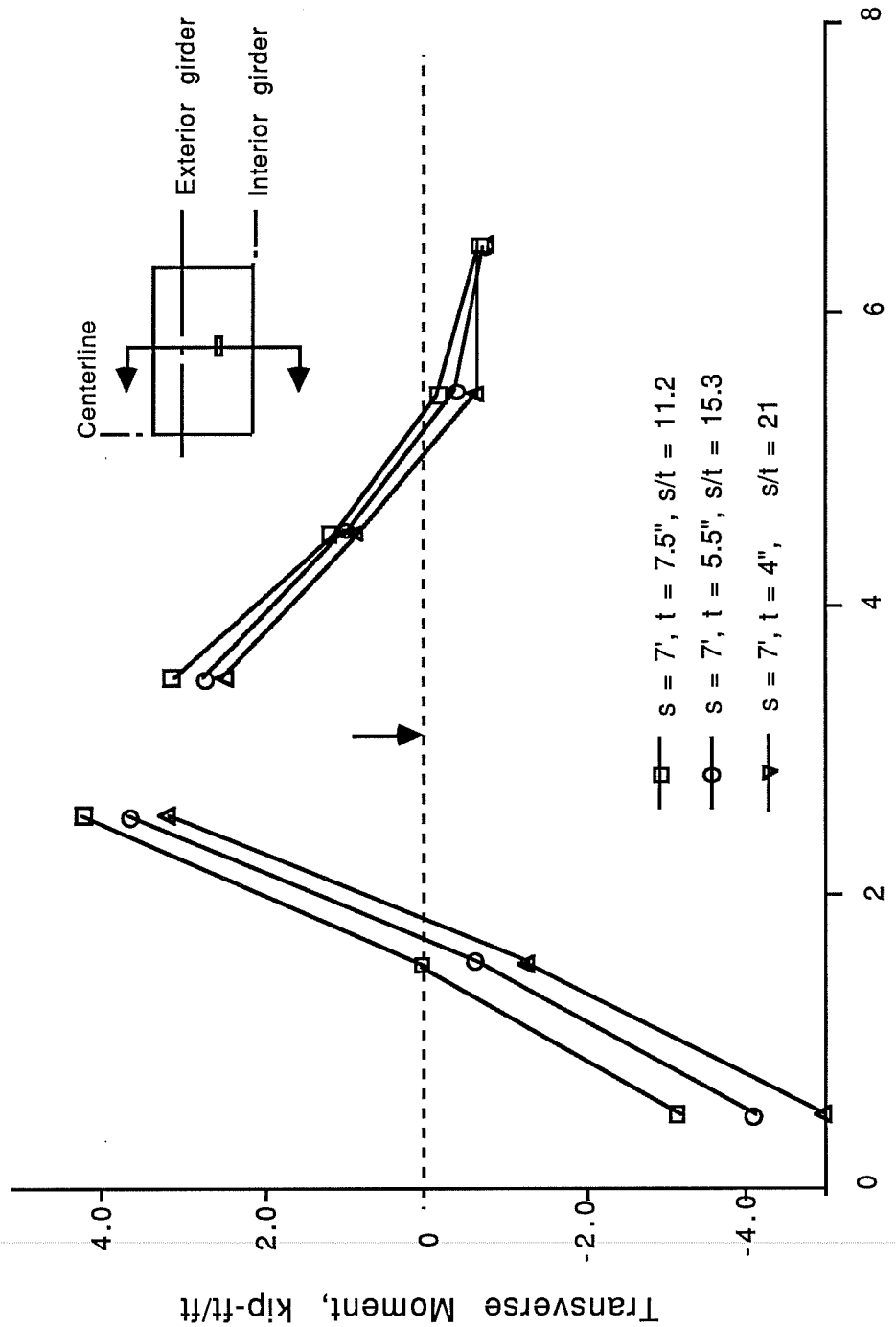

Fig. 9.5 Transverse moment along loaded point for different span-to-depth ratio

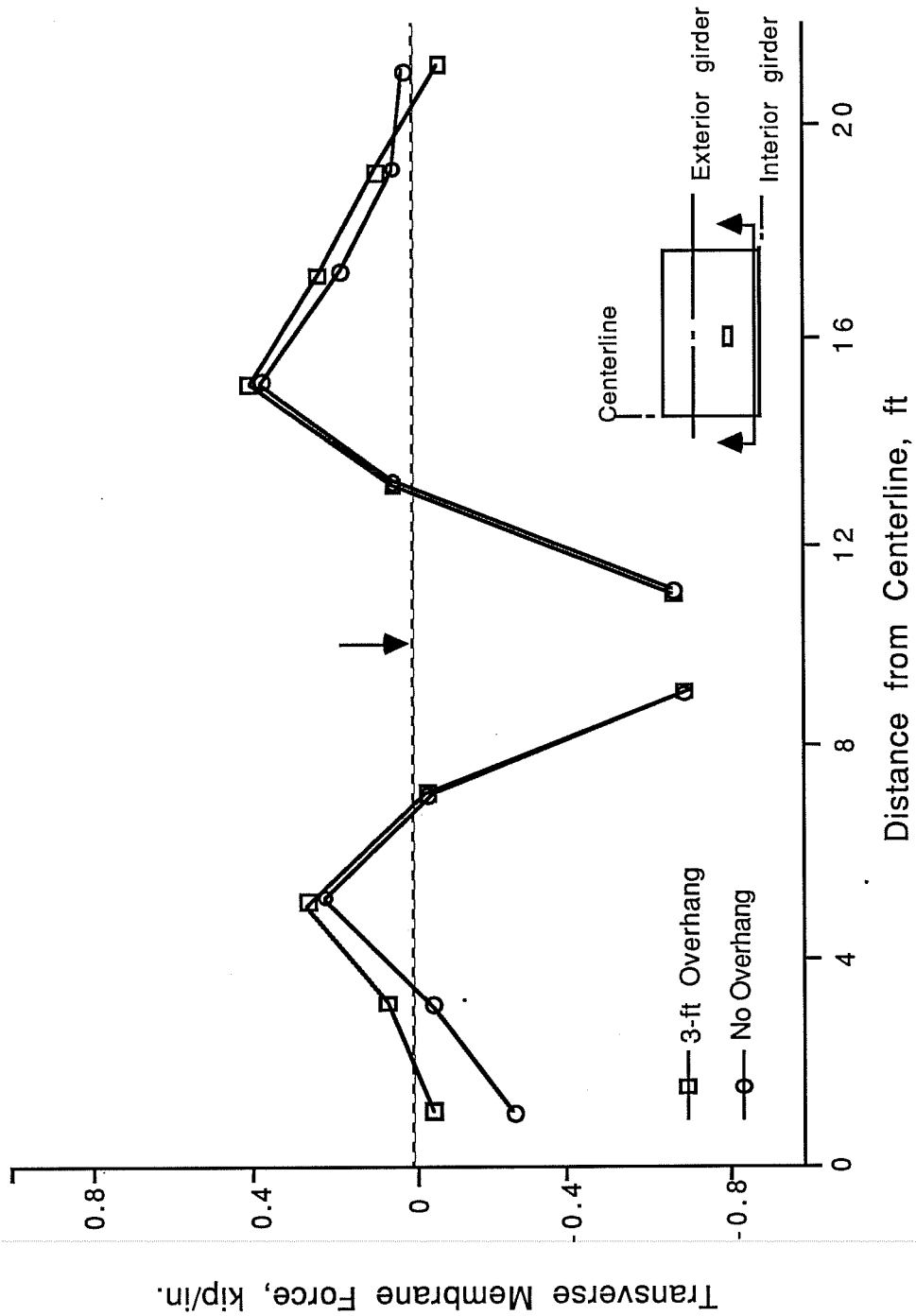

Fig. 9.6 Transverse membrane force at interior girder for different overhang width

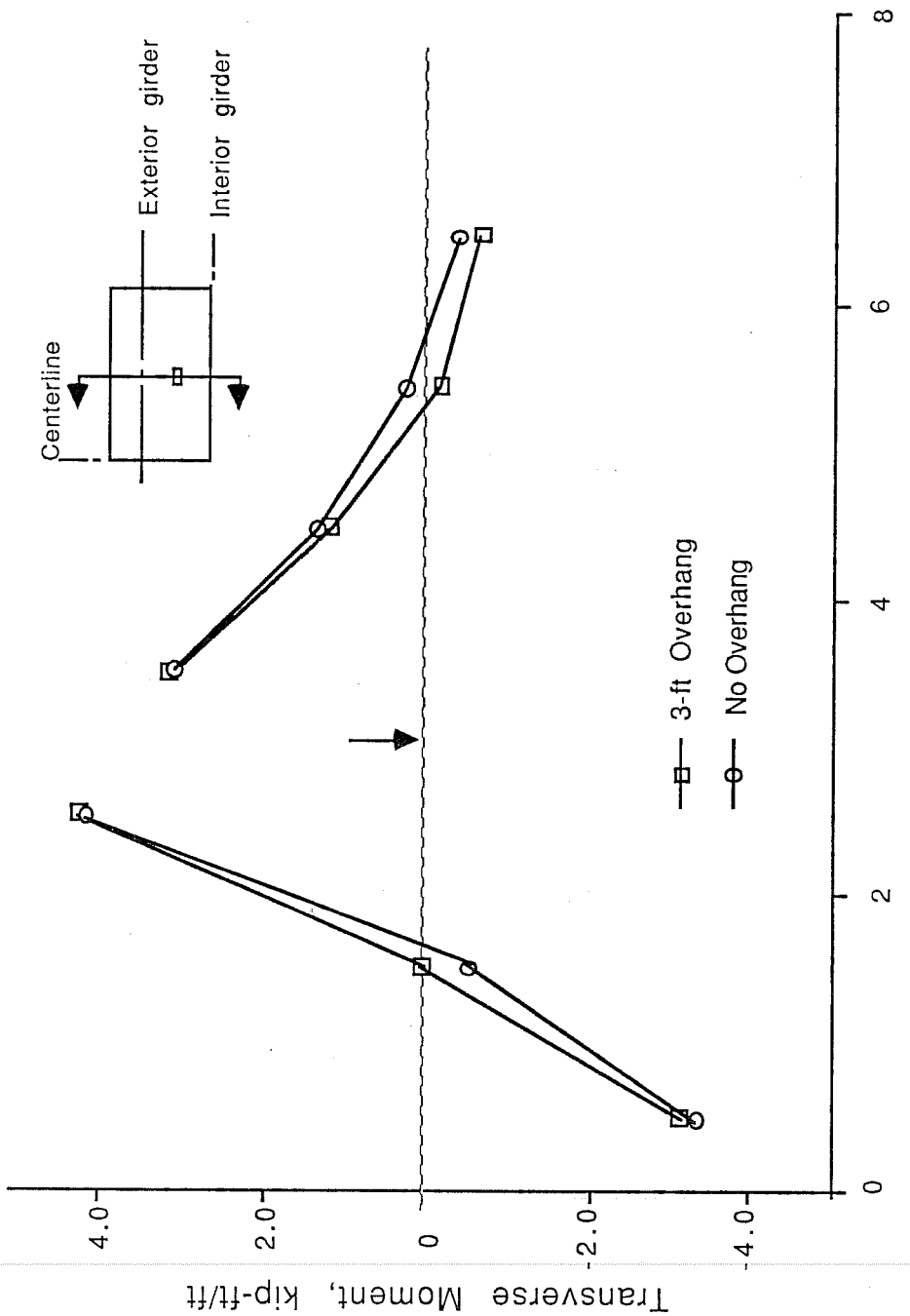

Fig. 9.7 Transverse moment along loaded point for different overhang width

in most practical cases, the overhang is not necessary for arching action.

9.4 Effect of Barrier Stiffness

This parametric study is basically an extension of the above study on overhang effects, since in-plane stiffness increases with increased barrier stiffness as well as increased overhang width. All bridges have some kind of barrier. This bridge model was analyzed for three different cases:

1) no barrier

2) Texas T5 concrete barrier

3) very stiff barrier (three times the stiffness of Texas T5 concrete barrier)

The results are shown in Fig. 9.8. Maximum magnitude and distribution of transverse membrane force did not change with different barrier stiffnesses. As the barrier stiffness increased, the distribution of tensile membrane force changed: larger tensile membrane forces were present near the center of the bridge, and smaller ones, near the edge. However, it can be concluded that variations in barrier stiffness produce little change in response, since the magnitude of the compressive membrane force is the main factor in determining the flexural capacity of the deck. As shown in Fig. 9.9, there was little difference in the flexural behavior as the assumed barrier changed.

9.5 Effect of Line Load

Four cases involving line load were studied:

1) 2 loading points spaced at 20 ft (studied previously)

2) 6 loading points spaced at 8 ft

3) 8 loading points space at 4 ft

4) 12 loading points spaced at 4 ft

Due to the symmetry of the structure, these correspond respectively to 4, 12, 16, and 24 loading points in a real bridge.

The results are shown in Fig. 9.10. With 6 loading points spaced 8 ft apart, compressive membrane forces developed around the loaded points, and tensile membrane forces balancing these compressive

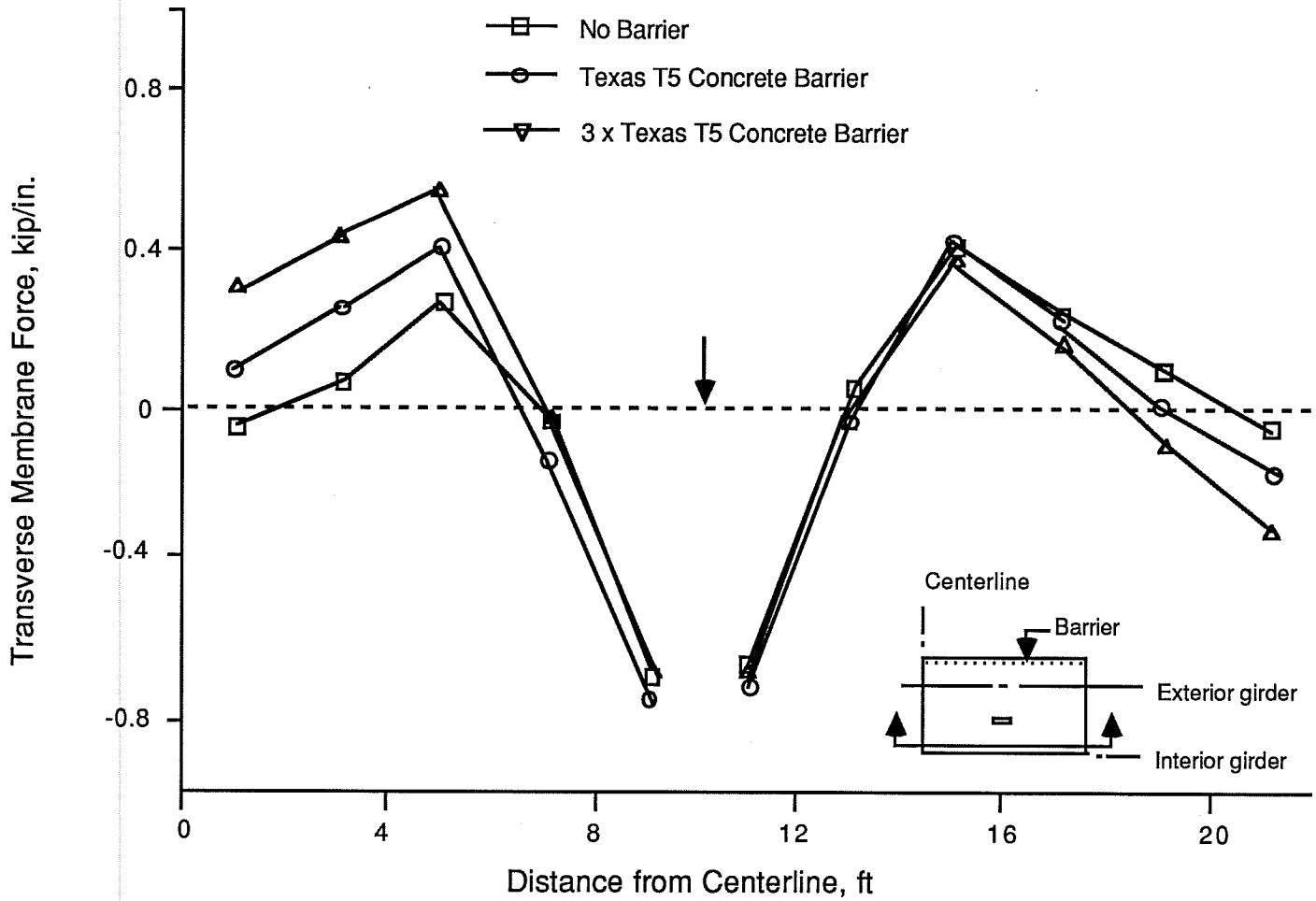

Fig. 9.8 Transverse membrane force at interior girder for different barrier stiffness

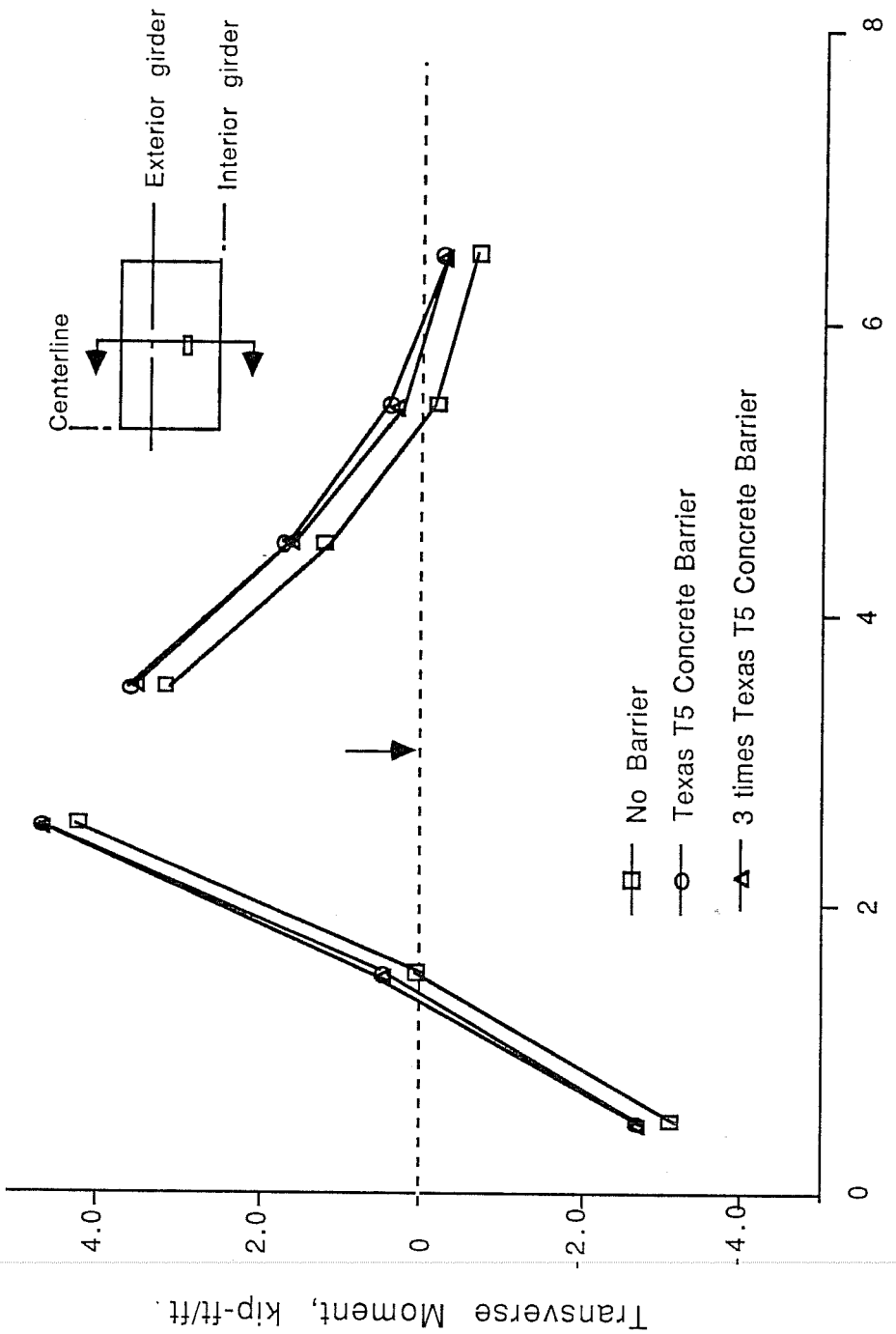

Fig. 9.9 Transverse moment along loaded point for different barrier stiffness

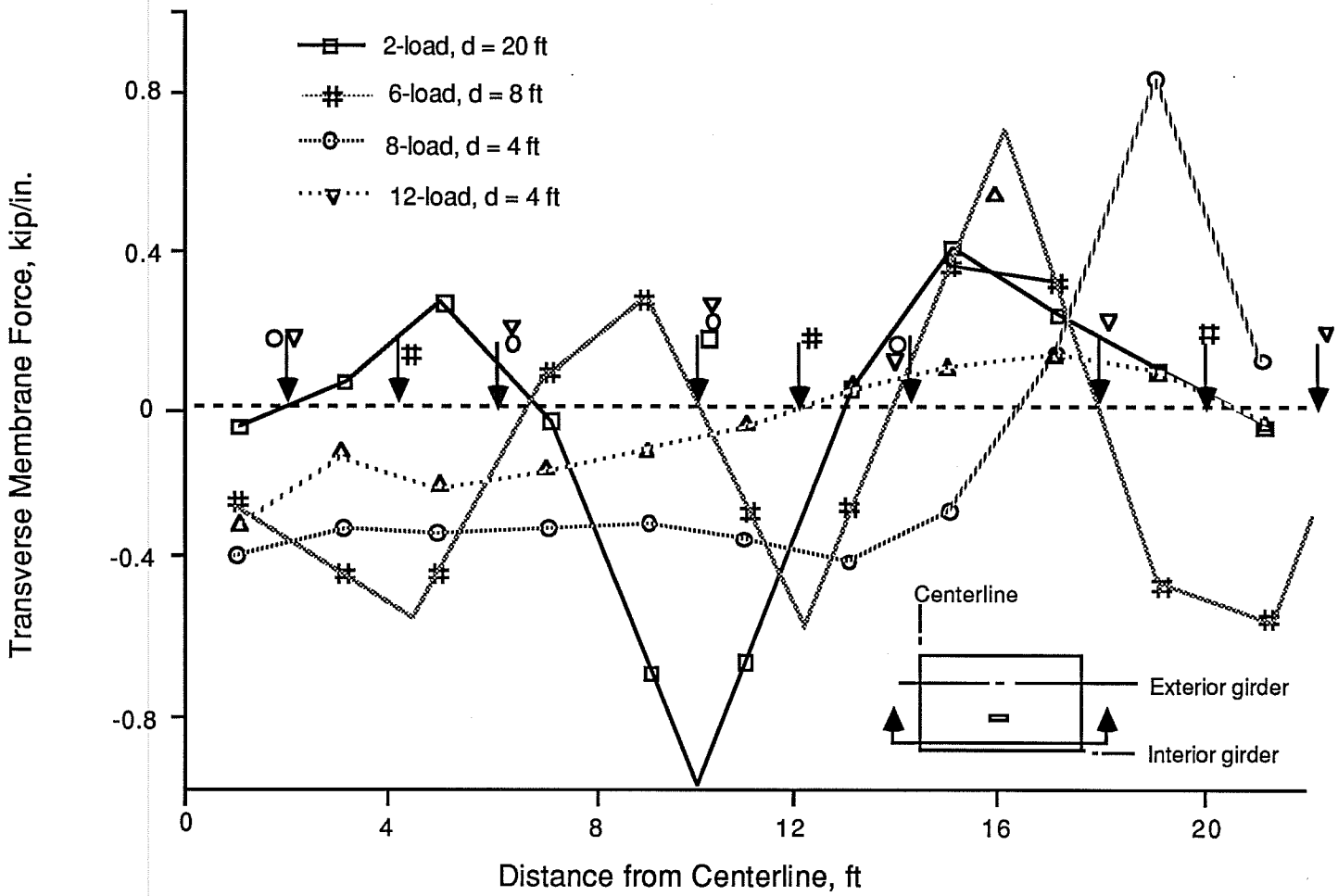

Fig. 9.10 Transverse membrane force at interior girder for different live load arrangment

forces developed between the loaded points. The compressive membrane forces were approximately half as great as those developed in the case involving 2 loading points spaced 20 ft apart. With 8 loading points spaced 4 ft apart, tensile membrane forces did not develop between the loaded points, but only where there were no loads. With 12 loading points spaced 4 ft apart, very little transverse membrane force was developed. The membrane forces decreased in magnitude as the distance between the loading points decreased. Membrane forces could not develop at all in the case involving loads spaced 4 ft apart along the entire bridge span length.

Generally, either the shear or the punching shear capacity controls the failure capacity of a reinforced concrete bridge deck. However, a deck may fail by shear with closely spaced loads. Assuming 4-ft spaced loads along the entire length of the bridge span, the predicted flexure and shear capacities are:

1) Assuming one-way shear failure with the full effective width of 4 ft between each loading point, the calculated shear capacity is 50 kips based on the ACI formula.

2) Assuming one-way flexural failure with the same effective width of 4 ft, the calculated flexural capacity without arching action is 26 kips, about half of the calculated shear capacity. This capacity gives only a factor of safety of 1.25 against the current AASHTO design wheel load of 20.8 kips.

With 6-ft spaced loads, again assuming one-way failure modes and no arching action, the calculated capacities will be 1.5 times the above values, and the factor of safety will be 1.875.

In the case involving 6 loaded points spaced 8 ft apart, transverse membrane forces increased the flexural capacity of the deck by approximately 60 % at the interior support, and 140 % at midspan, based on a load-moment interaction diagram similar to that discussed in Subsection 8.6.4. With the increased moment capacities, again assuming one-way failure, the calculated flexural capacity of 109 kips is larger than the calculated shear capacity of 100 kips. This gives a factor of safety of 4.8 against the current AASHTO design wheel load.

The above results were based on the assumptions of one- way failure and no arching action. Even with closely spaced loads, arching action can be developed if the total length of the loads is short. With 8 loading points spaced 4 ft apart (the total length of the loads was 32 ft, about 60 % of the total length of the bridge span), compressive membrane forces were developed along the loaded length, and tensile membrane forces developed at the unloaded ends. These compressive membrane forces increased the moment capacity of

the deck by approximately 75 % at the interior support and 150 % at the midspan, based on a load-moment interaction diagram similar to that discussed in Subsection 8.6.4. Using this increased moment capacities, and again assuming one-way failure, the calculated flexural capacity was 57 kips, and the calculated shear capacity was 50 kips. This capacity gives the factor of safety of 2.4, close to the implied factor of safety of 2.0 by ACI and 2.5 by AASHTO specification.

The maximum length of the loads to ensure the development of the arching action depends on the length of the bridge span, the length of the deck span, and the in-plane stiffness of the deck. In this studied case, with a total load length of 60 % of the bridge span length, the maximum intensity of the compressive membrane forces was about 40 % of that developed in the case involving 2 loading points spaced 20 ft apart. This magnitude of the compressive membrane forces was barely enough to increase the flexural capacity of the deck to exceed the shear capacity. Thus, it can be concluded that the maximum length of the loads to ensure the development of the arching action is about half of the bridge span length.

If a vehicle is longer than half the length of the bridge span, and arching action is therefore undependable, it is better to use an 8-ft rather than a 4-ft wheel spacing. For the same total load, an 8-ft spacing gives a flexural factor of safety of 2.4, vs. only 1.25 for a 4-ft spacing. If the loaded length is less than half the length of the bridge (in which case arching action is dependable), both wheel spacings result the same factor of safety of 2.4. Consequently, using the 8-ft wheel spacing is preferable to the 4-ft spacing in all cases, except if the single wheel load exceeds the punching shear capacity of the deck. For the same total load, an 8-ft spacing provides at least the same factor of safety as a 4-ft spacing, and always ensures the development of arching action without restrictions on the loaded length or the load location.

In summary, if arching action is depended on in designing bridge decks, the wheel spacing should be large enough, or the total length of the vehicle should be short enough, to permit the development of membrane forces. Based on this study, the maximum spacing is 8 ft, and the maximum loaded length is about half of the bridge span. The 8-ft spacing is preferable to the 4-ft spacing in almost all cases.

9.6 Summary of Parametric Studies

1) Transverse membrane forces increased with increasing span-to-depth ratio of the deck. Limitations on maximum span-to-depth ratios should be based on requirements

other than arching action, such as deflection control, shear strength, and serviceability.

2) Membrane forces were not affected significantly by overhang width, nor by barrier stiffness.

3) To ensure the development of membrane forces, the wheel spacing should be at least 8 ft, or the total loaded length should be shorter than half the length of the bridge span. The 8-ft spacing is better than the 4-ft spacing in practically all cases. The only exception is if a single wheel load exceeds the punching shear capacity of the deck.

CHAPTER 10

SUMMARY, CONCLUSIONS, AND RECOMMENDATIONS

10.1 Summary

10.1.1 General. An experimental and analytical investigation was conducted regarding the behavior of reinforced concrete skew bridge decks with Ontario-type reinforcement.

A series of parametric studies was also conducted to investigate the effect on bridge performance, of some design variables which were not studied experimentally.

10.1.2 Experimental Program. In the experimental part of the investigation, a full-scale model representing the essential behavior of a full-scale skew bridge was built and tested in the Ferguson Structural Engineering Laboratory of The University of Texas at Austin. Using a finite element analysis program, the skew bridge test specimen was developed to behave like the full skew bridge. The test specimen had details similar to those required by the Ontario Highway Bridge Design Code, modified as recommended by the Texas SDHPT. To study the effects of different skew angles in a single test specimen, one edge of the deck had a 45-degree skew angle, and the other, a 20-degree angle.

Three series of tests were conducted: 45-degree skew edge tests, 20-degree skew edge tests, and center tests. At each test location, the skew bridge specimen was first loaded statically until the deck cracks propagated halfway between the loaded point and the adjacent test location. Maximum load levels reached in these overload tests were 51 kips at the 45-degree skew edge, and 60 kips at 20-degree skew edge and the center. These load levels were 2.5 and 3 times the service live load of 20.8 kips respectively (current AASHTO HS20 truck load, including impact factor). The specimen was then tested to failure at each test location, using monotonically increasing load. The 45-degree skew edge failed by shear and torsion at a load of 97 kips; the 20-degree skew edge by shear at 139 kips; and the center by punching shear at 179 kips.

10.1.3 Analytical Program. To check the experimental results and permit their extension to bridge decks other than the one studied experimentally, a detailed finite element model of the specimen was developed using a structural analysis program (SAP4). The reinforced concrete bridge deck was modeled using two layers of 16-node thick

shell elements. The steel girder was modeled by three-dimensional beam elements.

A sequence of linear analyses was used to predict the nonlinear behavior of the deck. Cracking of the deck was followed using a smeared cracking model. This approach was also checked using a nonlinear analysis program, and was found to be accurate and economical.

10.1.4 Overall Behavior of the Skew Bridge Deck. In tests conducted at each skew edge, the first bottom crack occurred at a load of about 25 kips, and the first top crack, at about 35 kips. In the center, first cracking occurred at a load of about 30 kips on the bottom surface of the deck, and on the top, at about 50 kips. Bottom cracks near the 45-degree skew edge were oriented primarily perpendicular to the edge; near the 20-degree edge and in the center, fan-type bottom cracks developed. Top cracks propagated in the form of circular arcs around the loaded point at each edge, but no significant top cracking occurred during the center test. Crack widths were very small at service load levels.

The specimen behaved quite linearly beyond the service live load level. Nonlinear behavior started at about 50 kips at the 45-degree skew edge, and at about 60 kips at the 20-degree skew edge and the center, corresponding to overload factors of 2.4 and 2.9 respectively. More nonlinear behavior was observed in the skew edge tests than in the center test, especially in the 45-degree skew edge. The 45-degree skew edge was most flexible, while the center was stiffest. The center portion of the deck behaved almost linearly to failure.

10.1.5 Bending Moments in the Deck. At every gauged location, three strain gages were installed to measure the strain gradient. Using an assumed linearized strain gradient, the bending moment in the deck were obtained in both the transverse and longitudinal directions.

The negative moment at the interior support was small compared with the positive moment at the midspan of the deck before cracking, and increased after cracking. The longitudinal moment decreased very quickly away from the load. About 5 ft from the loaded point, longitudinal moments were negligible. Analytical and experimental results agreed very well.

10.1.6 Compressive Membrane Forces. The analytically predicted membrane force distribution agreed reasonably well with the experimental results. The magnitude of the compressive membrane forces was not significantly affected by the presence of skew.

10.1.7 Observed versus Calculated Capacities. The 45-degree skew edge failed by shear and torsion at a load of 97 kips, about 4.7 times the AASHTO service live load. The 20- degree skew edge failed by shear at a load of 139 kips, about 6.6 times the AASHTO service live load, and the center, by punching shear at a load of 179 kips, 8.6 times the AASHTO service live load.

Assuming that the diaphragms acting alone support the full design wheel loads, shear capacities calculated according to the provisions of ACI 318-83 (including torsion) were very conservative at both skew edges (about 60 % of the actual failure loads). Neglecting torsion at the 45-degree edge, however, the calculated shear capacity exceeded the actual failure load. It was concluded that edge capacity could be simply and conservatively calculated according to the shear-torsion provisions of ACI 318-83, and considering the thickened portion (diaphragm) to carry all the load.

The punching shear capacity calculated by the ACI formula was again conservative at the center (about 70 % of the actual failure load). The calculated flexural capacity considering arching action always far exceeded the actual failure load by shear or punching shear at each test location. Even without arching action, the calculated flexural capacities exceeded the actual failure loads, except at the 20-degree skew edge.

10.1.8 Parametric Studies. Using a rectangular bridge model, parametric studies were conducted to determine the effects on bridge deck performance of the following design variables:

1) span-to-depth ratio of deck

2) width of cantilever overhang

3) presence of integral barriers

4) longitudinal spacing of live loads

10.2 Conclusions

1) An Ontario-type skew bridge deck, detailed in accordance with Texas SDHPT proposed provisions, performed satisfactorily under the current AASHTO design load levels, with respect to overall behavior of the bridge deck, crack widths, local stiffness of the deck near the loaded points, and bending moments in the deck.

2) Under overload conditions (about three times the current AASHTO design wheel load), the behavior of the deck was fairly linear. More nonlinear behavior was observed in the skew edge with larger skew angle.

3) Compressive membrane forces significantly increased the flexural capacity of the skew bridge deck. The ultimate flexural capacities considering compressive membrane forces of the bridge decks were much larger than the actual failure load.

4) Analytical predictions and the experimental results agreed closely. Results from the sequential linear analyses by SAP4 agreed well with those from the nonlinear analysis by ABAQUS. These proved that the analytical model of the test specimen was satisfactory.

5) After cracking, arching action can be developed, even in a bridge deck whose span-to-depth ratio exceeds the limit of 15 specified in the current Ontario Bridge Design Code.

6) Transverse membrane forces increased with increasing span-to-depth ratio of the deck.

7) Membrane forces were not significantly affected by overhang width, nor by integral barrier stiffness.

8) To ensure the development of membrane forces, the wheel spacing should be at least 8 ft, or the total loaded length should be less than half the length of the bridge span. The 8-ft spacing is preferable to the 4-ft spacing in almost all cases. The only exception is if a single wheel load exceeds the punching shear capacity of the deck.

10.3 Recommendations for Implementation

Skew bridge decks similar to the one tested in this study, and detailed in accordance with the Texas SDHPT recommendations for Ontario-type decks, can perform satisfactorily. Skew bridge decks consisting of precast concrete panels with similar details used in this study also can perform satisfactorily. Such decks should be constructed in the field, and their field performance should be monitored. Flexural capacity of a reinforced bridge deck far exceeds its shear capacity, even at an edge with a large skew angle. Therefore, the factor of safety of a reinforced concrete bridge deck

should be evaluated based on the shear capacity of the edge, considering the skew angle. The precise prediction of the shear capacity at the edge can be obtained by further research as recommended in the following section.

While consideration of compressive membrane forces ("arching action") can lead to increased values for calculated flexural capacity of a bridge deck, flexural capacity is not the only criterion for determining acceptable service loads. Attention must be given to other factors, including shear capacity and serviceability considerations.

10.4 Recommendations for Further Research

The load-carrying capacity of a reinforced concrete bridge deck is controlled by the edge member. Even though stiffened to support the wheel load alone, the edge is the most likely to be damaged or fail. The effects of different stiffening methods on edge stiffness and strength should be examined experimentally.

Flexural design of a reinforced concrete bridge deck is often controlled by the serviceability requirements. This is particularly true when arching action is considered. There is possibility that the amount of nominal reinforcement could be reduced to even less than the value now required for Ontario-type bridge decks, if serviceability is acceptable with the reduced reinforcement. Further study is also recommended to investigate the effects of arching action on the serviceability of minimally reinforced concrete bridge decks.

APPENDIX A

MATERIAL PROPERTIES

Table A.1 Mechanical Characteristics of Concrete

Casting Date: Nov. 25, 1986

Age at Testing	f'c Mix No. 1	Mix No. 2
14 day	3600 psi	4100 psi
28 day	4100 psi	4800 psi
180 day	4100 psi	4900 psi
		7-day Modulus of Rupture
Average	472 psi	499 psi
Standard Deviation	41.2 psi	25.9 psi

REFERENCES

1. American Association of State Highway and Transportation Officials (AASHTO), Standard Specification for Highway Bridges, 13th Edition, 1983.

2. American Concrete Institute, Building Code Requirements for Reinforced Concrete (ACI 318-83), American Concrete Institute, 1983.

3. American Society of Civil Engineers, Finite Element Analysis of Reinforced Concrete, 1982.

4. Bakht, B., "Testing of the Manitou Bridge to Determine Its Safe Load Carrying Capacity," Canadian Journal of Civil Engineering, Vol. 8, No. 1, 1981, pp. 218-229.

5. Bashur, F. K. and Darwin, D., "Nonlinear Model for Reinforced Concrete Slabs," Journal of the Structural Division, ASCE, Vol. 104, No. ST1, Proc. Paper 13495, January 1978, pp. 157-170.

6. Batchelor, B. deV., Hewitt, B. E., and Csagoly, P., "Investigation of the Fatigue Strength of Bridge Deck Slabs of Composite Steel/Concrete Bridges," Transportation Research Record, No. 664, 1978, pp. 153-161.

7. Beal, D. B., "Strength of Concrete Bridge Decks," Research Report 89, New York State Department of Transportation, July 1981.

8. Bieschke, L. A. and Klingner, R. E., "The Effect of Transverse Strand Extensions on the Behavior of Precast Prestressed Panel Bridges," Research Report No. 303-1F, Center for Transportation Research, The University of Texas at Austin, June 1982.

9. Christiansen, K. P., "Experimental Investigation of Rectangular Concrete Slabs with Horizontal Restraints," Materials and Structures, Vol. 16, No. 93, May-June 1982, pp. 178-192.

10. Christiansen, K. P., "The Effect of Membrane Stresses on the Ultimate Strength of the Internal Panel in a Reinforced Concrete Slab," The Structural Engineer, Vol. 41, No. 8, August 1963, pp. 261-265.

11. Csagoly, P., Holowka, M., and Dorton, R. A., "The True Behavior of Thin Concrete Bridge Slabs," Transportation Research Record, No. 664, 1978, pp. 171-179.

12. Dorton, R. A., and Holowka, M., "The Conestogo River Bridge -- Design and Testing," Canadian Journal of Civil Engineering, Vol. 4, No. 1, 1977, pp. 18-39.

13. Elling, C. W., Klingner, R. E., Burns, N. H., "Distribution of Girder Loads in a Composite Highway Bridge," Research Report No. 350-2, Center for Transportation Research, Bereau of Engineering Research, The University of Texas at Austin, December 1985.

14. Fang, I. K., Worley, J. A., Burns, N. H., Klingner,R. E., "Behavior of Ontario-Type Bridge Deck on Steel Girders," Research Report No. 350-1, Center for Transportation Research, Bureau of Engineering Research, The University of Texas at Austin, January 1986.

15. Gamble, W. L., Flug, H., and Sozen, M. A., "Strength of Slabs Subjected to Multiaxial Bending and Compression," Report to the Defense Office of the Secretary of the Army and Office of Civil Defense, October 1970.

16. Girolami, A. G., Sozen, M. A., and Gamble, W. L., "Flexural Strength of Reinforced Concrete Slabs with Externally Applied In-plane Forces," Report to the Defense Office of the Secretary of the Army and Office of Civil Defense, October 1970.

17. Guyon, Y., Prestressed Concrete, Vol 2, New York, John Wiley & Sons, 1962.

18. Hewitt, B. E., "An Investigation of the Punching Shear Strength of Restrained Slabs with Particular Reference to the Deck Slabs of Composite I-beam Bridges," Thesis presented to Queen's University of Kingston, Canada, in 1972, in partial fulfillment of the requirements for the degree of Doctor of Philosophy.

19. Hewitt, B. E., and Batchelor, B. deV., "Punching Shear Strength of Restrained Slabs," Proceedings, ASCE, ST9, September 1975, pp. 1827-1853.

20. Hibbit, Karlson and Sorensen, Inc., "ABAQUS Example Problems Manual," September 1984.

21. Hibbit, Karlson and Sorensen, Inc., "ABAQUS Theory Manual," September 1984.

22. Hibbit, Karlson and Sorensen, Inc., "ABAQUS User's Manual, Version 4.5(a)," July 1985.

23. Kupfer, H., Hilsdorf, H. K., and Rusch, H., "Behavior of Concrete under Biaxial Stresses," Journal of the American Concrete Institute, Vol. 66, No. 8, August 1969, pp. 656-666.

24. Leibenberg, A. C., "Arching Action in Concrete Slabs," National Building Research Institute, Council for Scientific and Industrial Research, Report 234, South Africa, 1966.

25. Lin, C. S. and Scordelis, A., "Nonlinear Analysis of RC Shells of General Form," Journal of the Structural Division, ASCE, No. ST3, Proc. Paper 11164, March 1975, pp. 523-538.

26. Ontario Highway Bridge Design Code, 2nd Edition, Ontario Ministry of Transportation and Communications, 1983.

27. Park, R., "Tensile Membrane Behavior of Uniformly Loaded Rectangular reinforced Concrete Slabs with Fully Restrained Edges," Magazine of Concrete Research, Vol. 16, No. 46, March 1964, pp. 39-44.

28. Park, R., "The Lateral Stiffness and Strength Required to Ensure Membrane Action at the Ultimate Load of a Reinforced Concrete Slab-and-Beam Floor," Magazine of Concrete Research, Vol. 17, No. 50, March 1965, pp. 29-38.

29. Park, R., "The Ultimate Strength and Long-term Behavior of Uniformly Loaded, Two-way Concrete Slabs with Partial Lateral Restraint at All Edges," Magazine of Concrete Research, Vol. 16, No. 48, September 1964, pp. 139-152.

30. Park, R., "Ultimate Strength of Rectangular Concrete Slabs Under Short-Term Uniform Loading with Edges Restrained Against Lateral Movement," Proceedings of the Institute of Civil Engineers, Vol. 28, No. 6705, 1964, pp. 125-145.

31. Park, R., and Gamble, W. L., Reinforced Concrete Slabs, John Wiley and Sons, New York, 1980.

32. Rashid, Y. R., "Analysis of Prestressed Concrete Pressure Vessels," Nuclear Engineering and Design, Vol. 7, No. 4, April, 1968, pp. 334-344.

33. Salem, M. H. and Mohraz, B., "Nonlinear Analysis of Planar Reinforced Concrete Structures," Civil Engineering Studies, Report No. SRS No. 410, University of Illinois at Urbana-Champaign, Urbana, Illinois, July 1974.

34. Texas State Department of Highways and Public Transportation, Standard Specifications for Construction of Highways, Streets, and Bridges, September 1982.

35. Texas State Department of Highways and Public Transportation, Drawing for "Reinforcement of Skew Bridge Deck," Drawing No. Gp DO, 1981.

36. Tsui, K. T., "Behavior of Ontario-Type Bridge Deck on Steel Girders: Negative Moment Region and Load Capacity," Research Report No. 350-3, Center for Transportation Research, Bureau of Engineering Research, The University of Texas at Austin, January 1986.

37. Van Greunen, J., "Nonlinear Geometric, Material and Time Dependent Analysis of Reinforced and Prestressed Concrete Slabs and Panels," UC-SESM Report No. 79-3, University of California at Berkeley, October 1979.

38. Yuzugullu, O. and Schnobrich, W. C., "A Numerical Procedure for the Determination of the behavior of a Shear Wall-Frame System," Journal of the American Concrete Institute, Vol.70, No. 7, July 1973, pp. 474-479.